REDUCTION OF CONVECTIVE HEAT TRANSFER FROM REACTING FLOWS BY APPLICATION OF ELECTRIC FIELDS

by

Brian K. Oakes

Thesis submitted to the Faculty of the

Virginia Polytechnic Institute and State University

in partial fulfillment of the requirements for the degree of

Master of Science

in

Mechanical Engineering

APPROVED:

L. A. Roe, Chairman

U. Vandsburger

C. L. Dancey

May 1993

Blacksburg, Virginia

LD
5655
V855
1993
0354
c.2

c.2

REDUCTION OF CONVECTIVE HEAT TRANSFER FROM REACTING FLOWS BY APPLICATION OF ELECTRIC FIELDS

by

Brian K. Oakes

(ABSTRACT)

The electric field-induced reduction of heat transfer from a rod-stabilized diffusion flame and a step-stabilized premixed flame was investigated. The fuel examined was propane. Inlet velocity for the diffusion mode was a nominal value of 3.4 m/s with nominal air/fuel ratios of 420, 320, and 270. Inlet velocities ranged from 4.5 to 9.9 m/s for the premixed mode with equivalence ratios of 0.65 to 1.03. Maximum applied voltages for the diffusion and premixed modes were 8.0 and 6.6 kVDC, respectively. The field was applied in a direction perpendicular to the flow.

Heat transfer amelioration was quantified using records of temperature versus downstream distance from the stabilizer acquired for the external surface of the heat-loaded electrode which was exposed to the ambient environment. In addition, shadowgraphs and photographs were used to observe any alteration of flame position or of the bulk flowfield. These observations were used to investigate mechanisms potentially responsible for heat transfer reduction.

The rod-stabilized diffusion mode displayed some field-induced reduction in heat transfer. Both bulk flow alteration and reduction in radiation (associated with soot) were concluded to be responsible. Flame impingement on the heat-loaded electrode was

reduced by a field-induced increase in flow along the surface. Flame luminosity was reduced by the electric field (presumably due to a field-induced modification of soot production and/or destruction). This caused a reduction in radiative heat transfer.

No heat-transfer amelioration was noted for the premixed step-stabilized mode. This was attributed primarily to a geometry not accommodating to field-induced heat transfer reduction. Higher velocities and a lower presence of soot than the diffusion mode and problems associated with flame impingement on both electrodes (reduces maximum voltages and distorts field), also contributed to the negative result. Limited displacement of the luminous portion of the reaction zone was noted.

Acknowledgements

The author would like to thank his advisor, Dr. Larry Roe, for his guidance, suggestions, and support during the research work that went into this thesis. He would also like to thank him for his patience and help during the arduous writing process. He would like to thank the members of his advisory committee, Dr. Uri Vandsburger and Dr. C. L. Dancey, for providing their assistance. He would also like to thank Dr. Rick Roby for his help as a committee member earlier in the project. The author extends thanks to the Mechanical Engineering Shop and to Ben Poe in the instrument shop. He would also like to express appreciation to Tom Scattergood, Dave Hamby, and Andy Halsey for hours of enlightening conversation which, though it did preserve his sanity, did not necessarily hasten completion of this project.

The author would also like to thank Tom and Kate for their personal support and very meaningful friendship, without which he would have blown up the lab (just kidding) and left for Utah long ago. He would also like to mention his two long-distance romantic acquaintances. He could have bought a Fender Stratocaster with what he spent on phone calls.

Finally, the author wishes to express sincere appreciation to his mother, Pat Beale, for moral support and excellent advice during some especially dark days. She helped to support a considerable part of the emotional load.

Table of Contents

1 Introduction 1

2 Literature Review 6

3 Description of the Experiment 11

3.1 Overall Description 11

3.2 Equipment 14

3.2.1 Combustor 14

3.2.2 High Voltage Power Supply 19

3.2.3 Air Supply and Metering 19

3.2.4 Fuel Supply and Metering 23

3.3 Optical Instrumentation 26

3.3.1 Thermal Imaging 27

3.3.2 Shadowgraphs 29

3.3.3 Photographs 30

3.4 Experimental Methods 31

3.4.1 Thermal Data Acquisition Procedure 31

3.4.2 Data Reduction 35

4 Results and Discussion 36

4.1 Results for the Rod-stabilized Diffusion Flame 37

4.1.1 Observations for the Highest A/F Ratio 40

4.1.2 Observations for the Lower A/F Ratios 46

4.1.3 Analysis 52

4.2 Results for the Step-Stabilized Premixed Flame 56

4.2.1 Steady State Temperature Data 56

4.2.2 Transient Temperature Data 60

4.2.3 Shadowgraphs 62

4.2.4 Photographs 71

4.2.5 Analysis 74

5 Conclusions and Recommendations 80

5.1 Conclusions 80

5.2 Recommendations 82

References 84

Appendix A. Computer Programs 86

Appendix B. Additional Diffusion Mode Data 91

Appendix C. Additional Premixed Mode Data 98

Vita 121

List of Figures

Figure 1. Step-stabilized Premixed Combustor 3

Figure 2. Rod-stabilized Diffusion Combustor 4

Figure 3. Stable Operating Range for Rod-stabilized Diffusion Mode 13

Figure 4. Injector/Stabilizer for Diffusion Mode 16

Figure 5. Photograph of Combustor showing Use of Ceramic 17

Figure 6. Blower and Piping System 20

Figure 7. Combustor Assembly 22

Figure 8. Distribution of Premixed Injection Ports 25

Figure 9. Optical Instrumentation Schematic 28

Figure 10. Video Output of Thermal Imaging System showing Line Designator . 32

Figure 11. Video Output of Thermal Imaging System showing Area Designator . 34

Figure 12. Heat-loaded Electrode Temperature (external surface) vs. Downstream Distance from the Stabilizer for all Air/Fuel Ratios, V = 0.0 kVDC 41

Figure 13. Heat-loaded Electrode Temperature (external surface) vs. Downstream Distance from the Stabilizer, A/F = 400, U_a = 3.2 m/s 42

Figure 14. Photographs, A/F = 430, U_a = 3.5 m/s 44

Figure 15. Idealized Concept of Flowfield Alteration for the Rod-Stabilized Combustor 45

Figure 16. Composite Shadowgraph, A/F = 420/440, U_a = 3.4/3.6 m/s, V = 0.0 kVDC 47

Figure 17. Composite Shadowgraph, A/F = 420/440, U_a = 3.4/3.6 m/s, V = 4.0 kVDC 48

Figure 18. Composite Shadowgraph, A/F = 420/440, U_a = 3.4/3.6 m/s, V = 8.0 kVDC 49

Figure 19. Heat-loaded Electrode Temperature (external surface) vs. Downstream Distance from the Stabilizer, A/F = 330, U_a = 3.5 m/s 50

Figure 20. Heat-loaded Electrode Temperature (external surface) vs. Downstream Distance from the Stabilizer, A/F = 270, U_a = 3.4 m/s 51

Figure 21. Photographs, A/F = 320, U_a = 3.4 m/s 53

Figure 22. Photographs, A/F = 280, U_a = 3.5 m/s 54

Figure 23. Heat-loaded Electrode Temperature (external surface) vs. Downstream Distance from the Stabilizer, Two Records Separated By 90 Seconds 57

Figure 24. Heat-loaded Electrode Temperature (external surface) vs. Downstream Distance from the Stabilizer 59

Figure 25. Transient Area-averaged Heat-loaded Electrode Temperature (external surface) Histories 61

Figure 26. Shadowgraphs, ϕ = 0.93/0.95, U = 4.8 m/s 66

Figure 27. Upstream Shadowgraph, ϕ = 0.73, U = 5.9 m/s 67

Figure 28. Long Duration Shadowgraphs (1/400 second), ϕ = 0.84, U = 5.1 m/s 69

Figure 29. Multi-exposure Shadowgraphs, ϕ = 0.76, U = 5.7 m/s 70

Figure 30. Photographs, ϕ = 0.74, U = 4.5 m/s 73

Figure 31. Photographs, ϕ = 0.72/0.74, U = 9.5/9.8 m/s 75

Figure 32. Idealized Concept of Flowfield Alteration for the Step Combustor 77

Figure 33. Rough Estimate of Electric Field (Lines of Constant Potential) 78

Figure 34. Composite Shadowgraph, A/F = 320/330, U_a = 3.4/3.5 m/s, V = 0.0 kVDC 92

Figure 35. Composite Shadowgraph, A/F = 320/330, U_a = 3.4/3.5 m/s, V = 4.0 kVDC 93

Figure 36. Composite Shadowgraph, A/F = 320/330, U_a = 3.4/3.5 m/s, V = 8.0 kVDC 94

Figure 37. Composite Shadowgraph, A/F = 270/290, U_a = 3.4/3.6 m/s, V = 0.0 kVDC 95

Figure 38. Composite Shadowgraph, A/F = 270/290, U_a = 3.4/3.6 m/s, V = 4.0 kVDC 96

Figure 39. Composite Shadowgraph, A/F = 270/290, U_a = 3.4/3.6 m/s, V = 8.0 kVDC 97

Figure 40. Shadowgraphs, ϕ = 0.95, U = 4.8 m/s 99

Figure 41. Shadowgraphs, ϕ = 0.66/0.67, U = 6.7 m/s 100

Figure 42. Shadowgraphs, ϕ = 0.66, U = 6.8/6.7 m/s 101

Figure 43. Shadowgraphs, ϕ = 0.81/0.80, U = 6.6/6.7 m/s 102

Figure 44. Shadowgraphs, ϕ = 0.80/0.79, U = 6.7 m/s 103

Figure 45. Shadowgraphs, ϕ = 0.77, U = 5.8 m/s 104

Figure 46. Shadowgraph, ϕ = 0.74, U = 6.0 m/s, V = 4.0 kVDC 105

Figure 47. Shadowgraphs, ϕ = 0.77, U = 6.8 m/s 106

Figure 48. Shadowgraphs, ϕ = 0.77/0.76, U = 6.8/6.9 m/s 107

Figure 49. Upstream Shadowgraphs: (Top) ϕ = 0.83, U = 6.1 m/s, (Bottom) ϕ = 0.96, U = 6.1 m/s 108

Figure 50. Multi-exposure Shadowgraphs, ϕ = 0.61/0.62, U = 8.1 m/s 109

Figure 51. Upstream Multi-exposure Shadowgraph, ϕ = 0.74, U = 5.8 m/s 110

Figure 52. Long Duration Shadowgraphs (1/400 second):
(Top) ϕ = 0.87, U = 4.9 m/s, (Bottom) ϕ = 0.86, U = 5.0 m/s 111

Figure 53. Photographs, ϕ = 0.84, U = 4.7 m/s 112

Figure 54. Photographs, ϕ = 0.92/0.91, U = 4.9 m/s 113

Figure 55. Photographs, ϕ = 0.74/0.75, U = 5.9 m/s 114

Figure 56. Photographs, ϕ = 0.86, U = 6.1 m/s 115

Figure 57. Photographs, ϕ = 1.03/1.01, U = 5.9/6.1 m/s 116

Figure 58. Photographs, ϕ = 0.65, U = 6.8 m/s 117

Figure 59. Photographs, ϕ = 0.76/0.77, U = 6.8 m/s 118

Figure 60. Photographs, ϕ = 0.88, U = 7.1 m/s 119

Figure 61. Photographs, ϕ = 0.82, U = 9.9 m/s 120

List of Tables

Table 1. Diffusion Flame Conditions Investigated Using Temperature Records 38

Table 2. Diffusion Flame Conditions Investigated Using Photographs 39

Table 3. Diffusion Flame Conditions Investigated Using Shadowgraphs 39

Table 4. Premixed Flame Conditions Investigated Using Steady State Temperature Records 58

Table 5. Premixed Flame Conditions Investigated Using Transient Histories 62

Table 6. Premixed Flame Conditions for Downstream Shadowgraphs 63

Table 7. Premixed Flame Conditions for Upstream Shadowgraphs 64

Table 8. Premixed Flame Conditions for Multi-exposure Shadowgraphs 64

Table 9. Premixed Flame Conditions for Long Duration Shadowgraphs (1/400 second exposure) 64

Table 10. Premixed Flame Conditions for Photographs 72

1 Introduction

The importance of combustion systems in modern society can rarely be overstated. These systems currently provide us with the majority of our energy needs. The necessities and conveniences of air conditioning, transportation, electrical appliances, and most of the goods we consume are currently, to a large extent, made possible by combustion systems.

The control of heat transfer in systems utilizing combustion is often of paramount importance. Depending upon the type of device, it may be desirable to either increase or decrease heat transfer near the fuel-oxidizer reaction zone. Heat loading is critical in this region because it often involves the highest system temperatures. The benefits gained from the control of heat transfer in this zone may include higher efficiencies, lower cooling requirements, and lower stresses on materials.

An interesting property of gases undergoing combustion is the presence of charged species. These species generally consist of electrons and positively charged molecules (ions). The net charge is typically near zero, but the mobility distribution is highly skewed among the oppositely charged carriers. If an electric field is applied to the reaction zone, the smaller, low mass electrons are drawn toward the positive electrode but have a relatively small effect on the bulk flow due to their high mobility. Conversely,

the heavier, positively charged species have a considerable effect on the flow through collisions with neutral species. The greater momentum of the positive ions than that of the electrons results in a tendency for bulk movement of the flow towards the negative electrode [1].

The goal of this experimental investigation is to evaluate the effectiveness of applying the asymmetric effect of an applied electric field on a reacting flow in reducing undesirable convective heat transfer. The bulk movement can reduce convective heat transfer by thickening the boundary layer and/or moving the separation and reattachment points. These points often involve the highest levels of convective heat transfer. Simple bulk displacement of the reaction zone and relocation of flame impingement can also reduce heat transfer.

This study will quantify electric field heat transfer amelioration in two phases, first using a step-stabilized premixed propane-air flame and then a rod-stabilized propane-air diffusion flame. The step-stabilized combustor configuration is illustrated in Figure 1. Figure 2 shows the rod-stabilized combustor mode. Two electrodes will comprise the lower and upper surfaces of the combustor, with quartz windows allowing optical access through both sides. In both cases, the lower electrode will be grounded and, as a result of being close to the stabilizer, will be considered the heat-loaded electrode. The upper electrode will be negatively charged. The applied field should reduce convective heat transfer to the lower electrode and also possibly increase heat transfer to the upper electrode. The external surfaces of both electrodes will be exposed to the ambient environment.

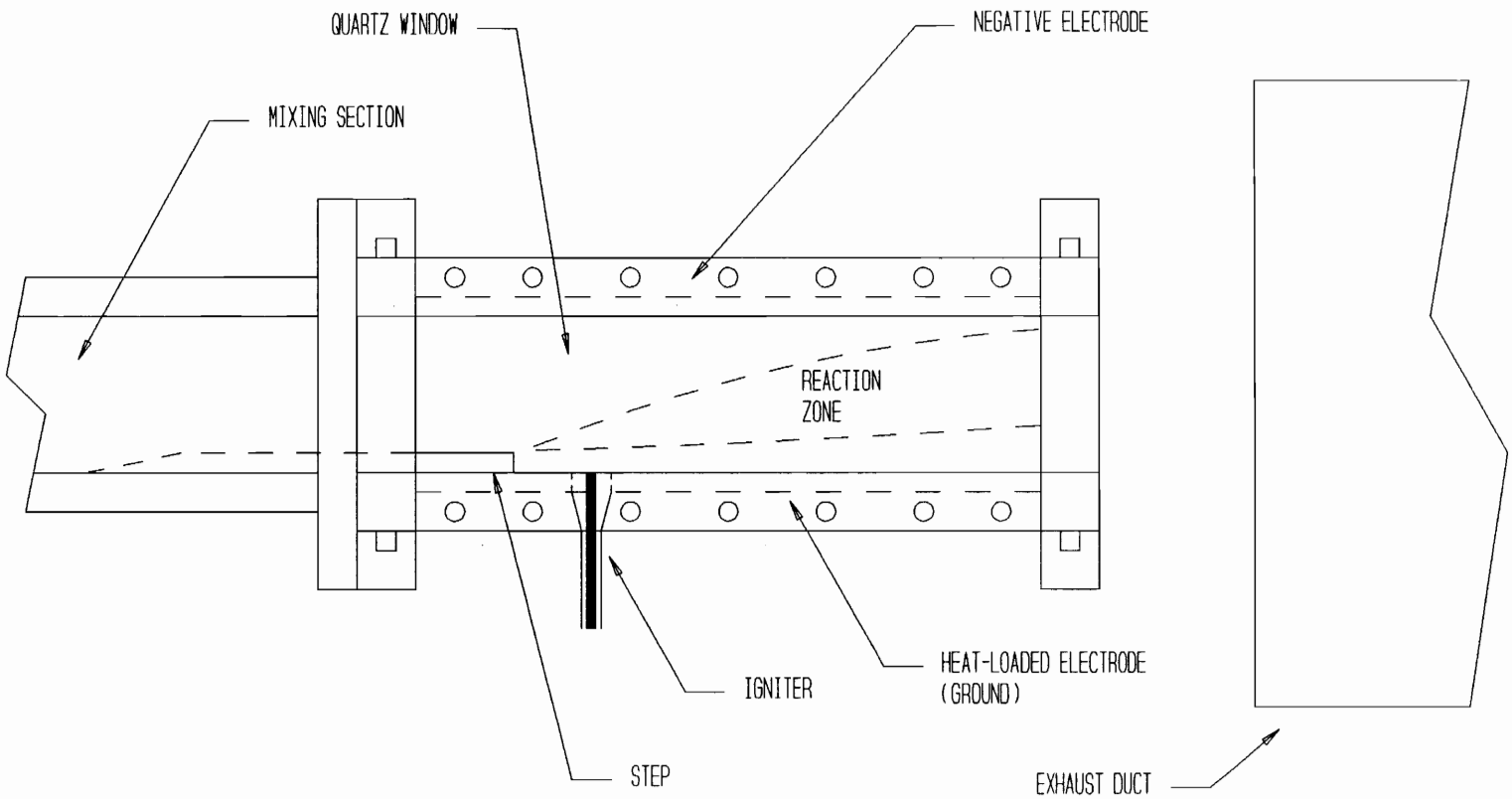

Figure 1. Step-stabilized Premixed Combustor

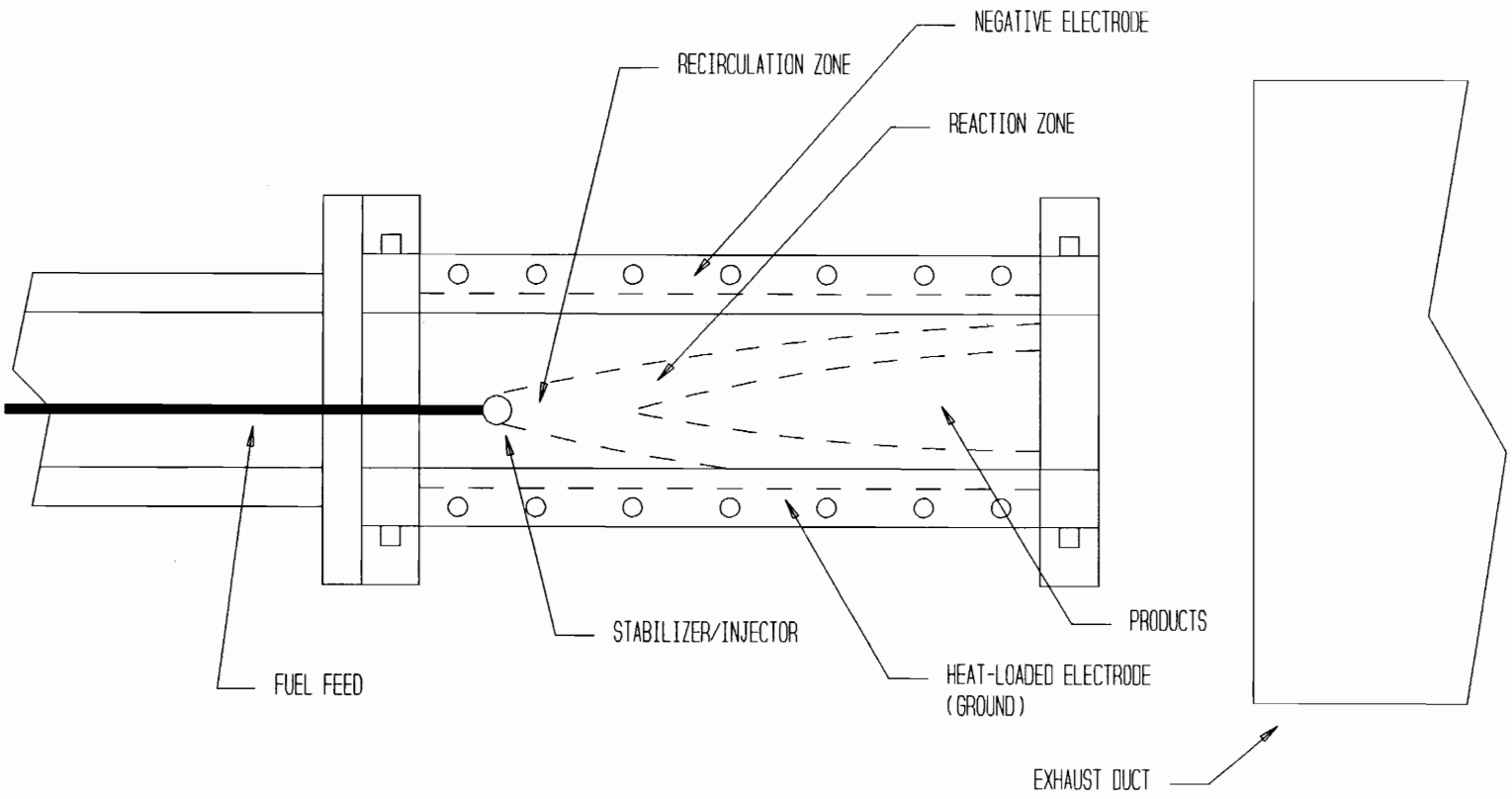

Figure 2. Rod-stabilized Diffusion Combustor

Any reduction in convective heat transfer to the heat-loaded electrode should result in a reduction in the temperature of its free convecting external surface. An infra-red imaging system will be used to obtain temperature contours of this surface as a method of quantification. In addition, shadowgraphs will be used to investigate effects of the electric field on both the flame structure and bulk movements of the reaction zone. Normal photographs will be used to measure the movement of the time-averaged position of the luminous zone of the flame. Both of these flow visualization methods will aid in understanding the fluid mechanical effects behind any reduction in heat transfer.

2 Literature Review

Past works considering the effects of electric fields on flames have covered a multitude of effects and configurations. Some of these include altering blowoff limits, affecting lift-off distance, and increasing and decreasing heat transfer from flame gases. Others include incurring instability in a flame front, affecting flame propagation velocity, and altering luminosity and soot production.

A necessary and excellent source concerning electric field-combustion interaction is provided by Lawton and Weinberg [1]. This work provides a theoretical development and a review of previous related experimentation. It is essentially a thorough textbook and an ideal starting point concerning this field.

A theory of the ionic wind effect was developed by Lawton, Mayo, and Weinberg [2]. It considered flame ions travelling towards electrodes and was used to determine maximum flow parameters that are likely to be encountered in practical devices. These maxima were evaluated experimentally to acquire a feel for possible alterations encountered in real life applications. These experiments confirmed that aeration by entrainment is practical and that combustion intensity can be increased using electric fields without the need for conventional methods (i.e. rod or step stabilizers). They further stated that bulk electric field effects or electro-gas-dynamic effects were almost

entirely responsible for observed experimental results without a consideration of effects on chemical or reaction kinetics. This is the generally accepted thinking, which would indicate that any observed increase in flame propagation velocity must be associated with either bulk movement of the flowfield or an increase in the convolutedness of the flame surface as displayed by Salamandra and Maiorov [3].

Bulk effects on reacting flowfields due to electric fields have been demonstrated using various optical methods. Payne and Weinberg [4] demonstrated the ionic-wind effect on an ethylene diffusion flame. This included the demonstration of the net wind in the direction of motion of the positively-charged carbon particles and a small effect due to the negative ion stream. Lawton and Weinberg [1] reviewed schlieren sequences that also showed the effect of an electric field on an ethylene diffusion flame. The flame was placed between two co-axial ring electrodes. Bulk flow was shown to be strongly affected by the applied field. Further, they reviewed propane flames on Meker burners used to demonstrate transverse field effects. The modification of symmetry caused by mobility differences was clearly shown.

Sandhu and Weinberg [5] found that using an electric field to reduce heat transfer to a solid body seemed to be a promising practical application. They observed reduction in heat transfer to a positively charged plate and attributed this to entrainment of ambient air caused by a displacement of the reaction zone. Their results were found using a laser interferometric technique. Clements and Smy [6] found analogous results in a similar experiment using a calorimetry technique. Oakes [7] demonstrated this effect in a recent investigation during an undergraduate research project. This involved use of the infra-red

system used in the experiment discussed in this thesis.

Payne and Weinberg [4] demonstrated the effect of flame stoichiometry on the potential effect of an applied electric field. They showed that an increase in ethylene concentration in an ethylene-air flame improves field-induced heat transfer reduction. This was attributed to the increased production of soot under fuel-rich conditions. Charged carbon particles are believed to increase the body force on the reaction zone. Calcote and Pease [8] demonstrated the effect of an electric field on an N-butane-air flame. The more pronounced effect on the fuel-rich condition was demonstrated.

Payne and Weinberg [4] used an applied electric field to increase heat transfer to a cylindrical calorimeter. Their flame rose vertically through the inside of the grounded calorimeter with a positively charged nichrome wire placed along the center axis. Premixed ethylene-air, premixed and diffusion coal gas-air, and diffusion hydrogen-air flames were studied. Significant increases were noted. These increases in heat transfer were two orders of magnitude larger than the electrical power expended.

Mitchell and Wright [9] did work using a similar experimental setup applying radial electric fields to a lifted propane diffusion flame. A lifted flame is stabilized some distance away from the burner mouth. Their primary intention was to study the displacement of the point at which burning commences on the fuel jet. They also studied flame length and luminosity effects. They noted an increase in off-port height for an increase in potential difference (r.m.s) regardless of the type of field applied, namely AC, negative DC, or positive DC. Flame radiation and flame length decreased as a function of potential difference (r.m.s.), also regardless of field type.

Heinsohn, Wilhelm, and Becker [10] have studied ducted ethane-air diffusion flames. They looked at the effect of DC electric fields on such parameters as heat transfer, luminosity, and velocity field. The field was applied along the flame axis. It was found that for either field polarity, the flame responded as if the fuel and air flow rates had been reduced. Air and fuel flow rates were found for which the electric field had an effect. It was also indicated that the recirculation zone between the duct and the flame was reduced in size and moved downstream by an applied field.

Payne and Weinberg [4] investigated the effect of an electric field on carbon agglomeration. They concluded that carbon particles behave as positive charge carriers and can be confined to the negative electrode. In another investigation, Place and Weinberg [11] concluded that electric fields can govern soot particle size by controlling residence time in the pyrolysis zone.

Mayo, Watermeier, and Weinberg [12] also used an applied electric field to both accelerate and brake propagation of flame spread on a solid propellant surface. The acceleration usage was found to be significant and more effective than the latter.

Both Salamandra and Maiorov [3] and Noorani and Holmes [13] investigated flame propagation speed for a premixed methane-air flame with differing results. The former found that a transverse field of 12 kVDC increased the propagation speed by a factor of 5, presumably caused by an expansion of the flame front area. This expansion was produced by instability instilled in the flame front by the applied field. The latter researchers saw small changes in speed and found their results unconvincing.

Recently, Kishi, Xie, and Kono [14] studied the effect of electric fields on flame

propagation using two electrode configurations of a conical laminar methane-air flame. For one electrode geometry, an increase in burning velocity was noted for either polarity. For a second geometry, a positive voltage increased observed flame velocity while a negative polarity had the opposite effect. Also, a premixed propane-air porous cylindrical burner was investigated. For this configuration, an increase in flame velocity was noticed for both polarities.

3 Description of the Experiment

3.1 Overall Description

The purpose of this experiment is to quantify the effect of an applied electric field on the convective heat transfer from a reacting flow. This is done by operating a premixed propane-air step-stabilized flame and a propane-air rod-stabilized diffusion flame. The combustor used (Figures 1 and 2 in Section 1) is constructed with two electrically isolated electrodes configured to apply an electric field in a direction perpendicular to the flow direction. The lower electrode is electrically grounded, positioned downstream of the stabilizer, and significantly heat-loaded. The outer surface of this electrode is undergoing free convective and radiative heat transfer to the ambient surroundings. The upper electrode is negatively charged.

It is intended to use the "ionic wind" produced by the applied electric field to thicken the boundary layer or otherwise affect the combustor flowfield in such a way as to reduce heat transfer to the heat-loaded electrode from the flame reaction zone. Any reduction in heat transfer from the flame should correspondingly result in a decrease in the temperature of the exposed surface of the heat-loaded electrode. This decrease can be monitored and recorded using an infra-red camera.

In addition, shadowgraphs will be used to examine the effect of the electric fields on the flowfield. It is hoped that they will aid in understanding the fluid mechanics behind any reduction in heat transfer. Further, normal long duration photographs will be used with the same general purpose. These photos document any effect on the time-averaged luminous zone of the flowfield.

The primary controllable variables are the applied voltage (V), the mean combustor inlet velocity, the equivalence ratio (ϕ), for the premixed mode, and the volumetric air/fuel ratio (A/F), for the non-premixed flame. The latter three are controlled by metering air and fuel flow rates. For the premixed flame investigation, the mean inlet velocity (U), is considered to be the sum of the volumetric flow rates of both fuel and air divided by the cross-sectional area of the combustor just upstream of the step. For the diffusion mode, the mean inlet air velocity (U_a), is based on the cross-sectional area of the combustor upstream of the injector/stabilizer.

Non-premixed testing is for a nominal air velocity of 3.4 m/s and nominal volumetric air/fuel ratios of 420, 320, and 270. These represent mean fuel inlet velocities of 1.2, 1.5, and 1.8 m/s respectively. Applied voltages studied are 0.0, 4.0 and 8.0 kVDC. Details of conditions investigated are included in Section 5.1. The crosshatched area in Figure 3 represents combinations of mean inlet air velocity and air/fuel ratio that allow stable flame operation. Operating conditions were chosen to allow operation well within these stability limits.

Premixed testing involves inlet velocities ranging from 5 to 10 m/s and equivalence ratios ranging from approximately 0.65 to 1.00. Applied voltages will range

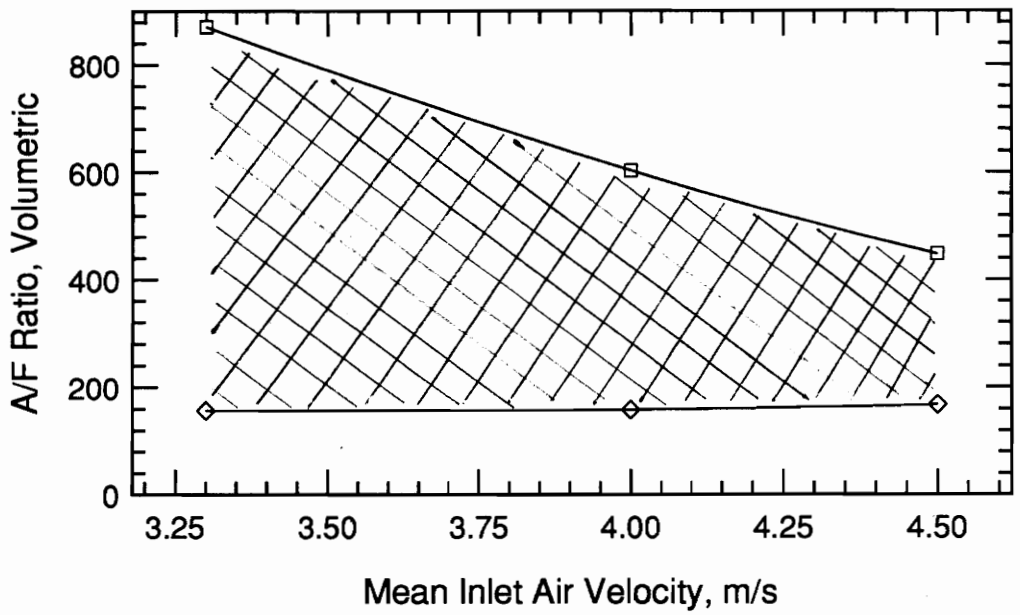

Figure 3. Stable Operating Range for Rod-stabilized Diffusion Mode

up to approximately 7 kVDC. Details of test conditions are given in Section 5.2.

Premixed operating limits are controlled both by the dimension of the step and limitations of the fuel supply. The observed lower limit of equivalence ratio is about 0.65. Fuel supply limitations are of prime importance to operation of the premixed flame mode. High fuel flow rates cannot be maintained because of extreme tank cooling encountered with the use of liquified fuels. A tank heating system was employed, but with limited success. The high power output of the flame during this type of operation produces high temperatures in the heat-loaded electrode and requires long warm-up periods. The combination of long run times and high fuel flow rates hamper operation at high air inlet velocities.

3.2 Equipment

3.2.1 Combustor

The electrical nature of this experiment requires that the combustor design be unique. A machinable ceramic (Aremcolox 502-1200) was chosen to facilitate the electrical insulating capability necessary to allow application of voltage maximums reaching 8 kVDC or more. The high thermal insulating capability and high temperature survivability of ceramics are also beneficial. Lower heat loss afforded by the use of ceramics is also helpful in reaching steady state conditions.

The general design of the combustor is flexible, allowing the use of either a

reverse-facing step or a rod for flame stabilization. Figure 1 (Section 1) shows the step combustor mode. The step produces a recirculation zone which acts as a stabilizer for a premixed combination of propane and air. The step height used is 6.4 mm. The rod-stabilizer doubles as a fuel injector in the non-premixed combustor mode. This configuration is shown in Figure 2 (Section 1). The dimensions of the combustor body include a height of 51 mm, a width of 102 mm, and a length of 203 mm. A rod with a diameter of 9.5 mm is used to stabilize the diffusion flame. A drawing of the injector/stabilizer is included as Figure 4. This is positioned 5 mm above the lower heat-loaded electrode. Fuel is injected from the downstream side of the stabilizer in a direction parallel to the air flow. The fuel emerges from twenty ports having a diameter of 1.5 mm and a center separation of 5.1 mm.

The insulating ceramic in the combustor was used in such a way as to electrically isolate the electrodes. A photograph in Figure 5 displays the combustor and shows how the ceramic is employed. The electrodes comprise the upper and lower surface of the combustor. Quartz windows act as sides and also insulate the high voltage electrodes. The electrodes are machined from stainless steel because of the high temperature and corrosive environment of the combustor. Stainless steel threaded fasteners are also used in assembly.

Both electrodes are identical as initially constructed. The center of the electrodes, which is the primary area exposed to the flame, has a thickness of 3.2 mm, which is small in comparison to the width and length. This should allow the assumption of one-dimensional heat conduction perpendicular to the plane of the electrode to be made. With

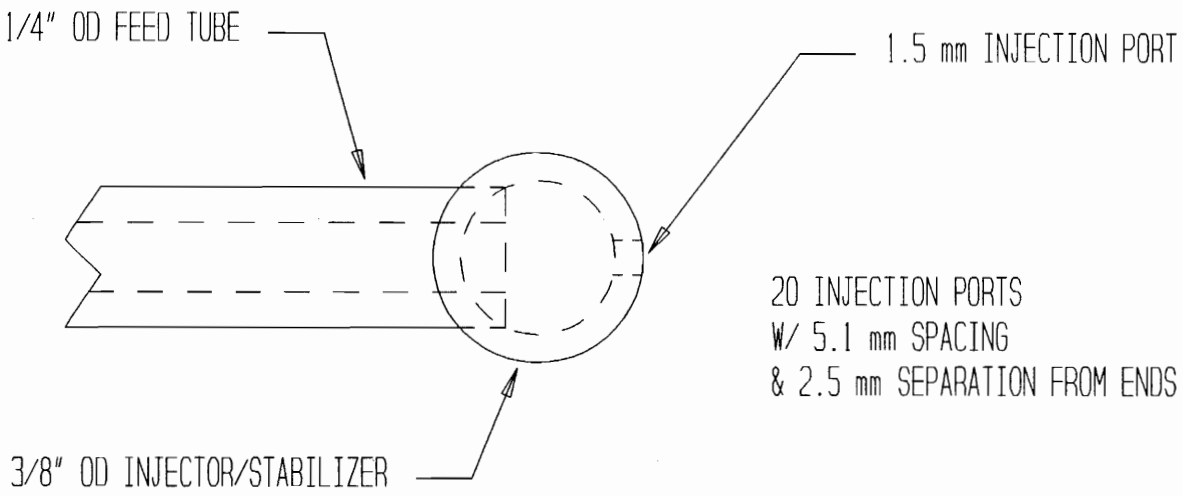

Figure 4. Injector/Stabilizer for Diffusion Mode

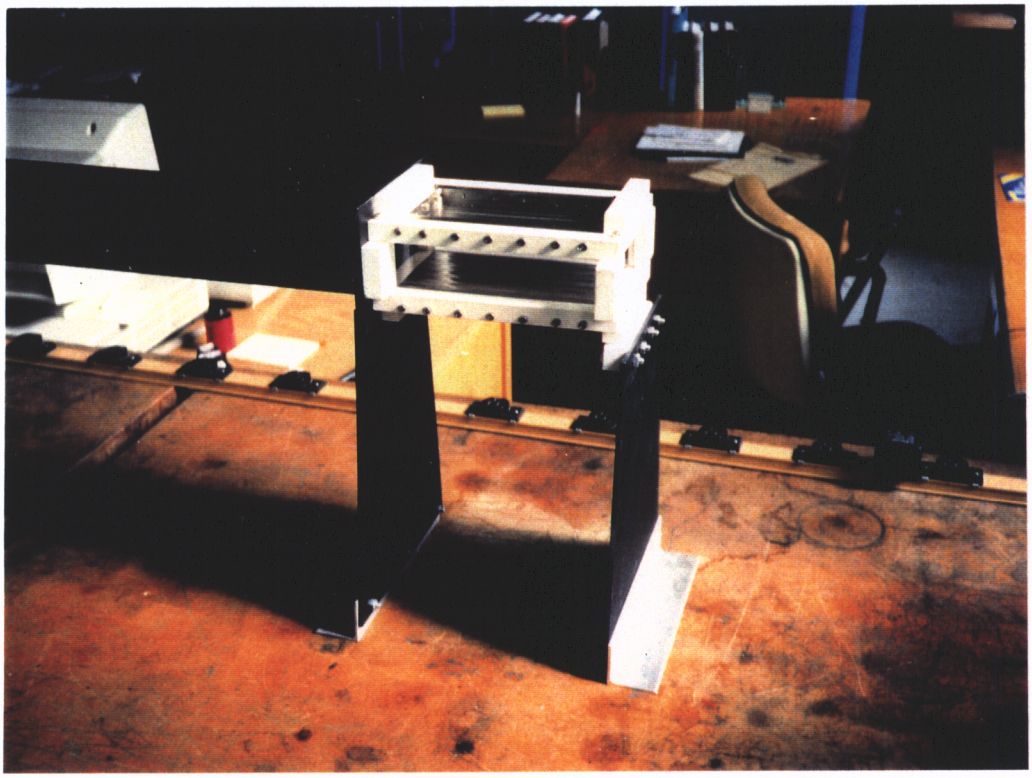

Figure 5. Photograph of Combustor showing Use of Ceramic

this assumption, examination of the temperature contour of the lower surface of the heat-loaded electrode allows estimation of the change in local convective heat transfer. The lower heat-loaded electrode was modified, in service, to reduce heat loss to surrounding material. This was done by milling a small groove around the heat-loaded area.

The poor electrical insulating performance of the machinable ceramic under actual service lead to the removal of all of this material which bridged the negative and positive electrodes. The structural integrity of the combustor was not compromised. In addition, a plexiglass spacer was machined and used to insulate the negative electrode from a remaining piece of ceramic. Fortunately, this involved a low temperature region. It was later determined that a critical ceramic part could be heated using a Bunsen burner with a corresponding increase in insulation capability. The heating may drive out moisture caught in the porous material. This allowed operation without the before-mentioned spacer during later testing.

The diffusion flame is ignited using a steel probe mounted with electrical insulation to a ring stand. It is extended into the combustor so as to create a spark gap on the downstream side of the injector/stabilizer. This allows for optimum ignition location. The same high voltage power supply (described in Section 3.2.2) used for providing the electrical field is used to produce ignition energy. The probe is removed after ignition and thus presents no flow obstruction.

Ignition in the step combustor mode is accomplished using a specially fabricated surface-gap spark plug. This is mounted through a threaded hole in the lower electrode slightly downstream of the step. Spark energy is supplied using a source utilizing

components of an electronic automobile ignition. This provides a continuous ignition spark, easing combustor start-up. The surface-gap plug also has the advantage of not interfering with the flowfield.

3.2.2 High Voltage Power Supply

A Hipotronics model 830B high voltage DC power supply is used to provide the electric fields required. It has both negative and positive polarity capability. This selection is made by removing the supply's back cover and switching the high voltage leads. The supply is also current limited and shuts off instantly in case of accidental contact with the high voltage leads. The voltage output is limited to 36 kV with current limited to 5 mA. The supply includes a voltage meter having a smallest graduation of 0.2 kV and a current meter having a smallest division of 0.02 mA. All current and voltage values reported are read from these meters.

3.2.3 Air Supply and Metering

The air supply system includes a lobe-type blower, a piping system, a circular-to-rectangular transition, and a rectangular pre-combustor section. The blower and piping system are shown in Figure 6. Air is supplied by a 550 CFM Roots blower with a 25-HP drive motor and delivered using a 4-inch PVC piping system which includes a combustor supply line and a bypass line to handle excess air. A pressure relief valve is present just downstream of the blower. Flow is controlled by a combination of butterfly valves, one in the main combustor supply line and another in the bypass line. The main line valve

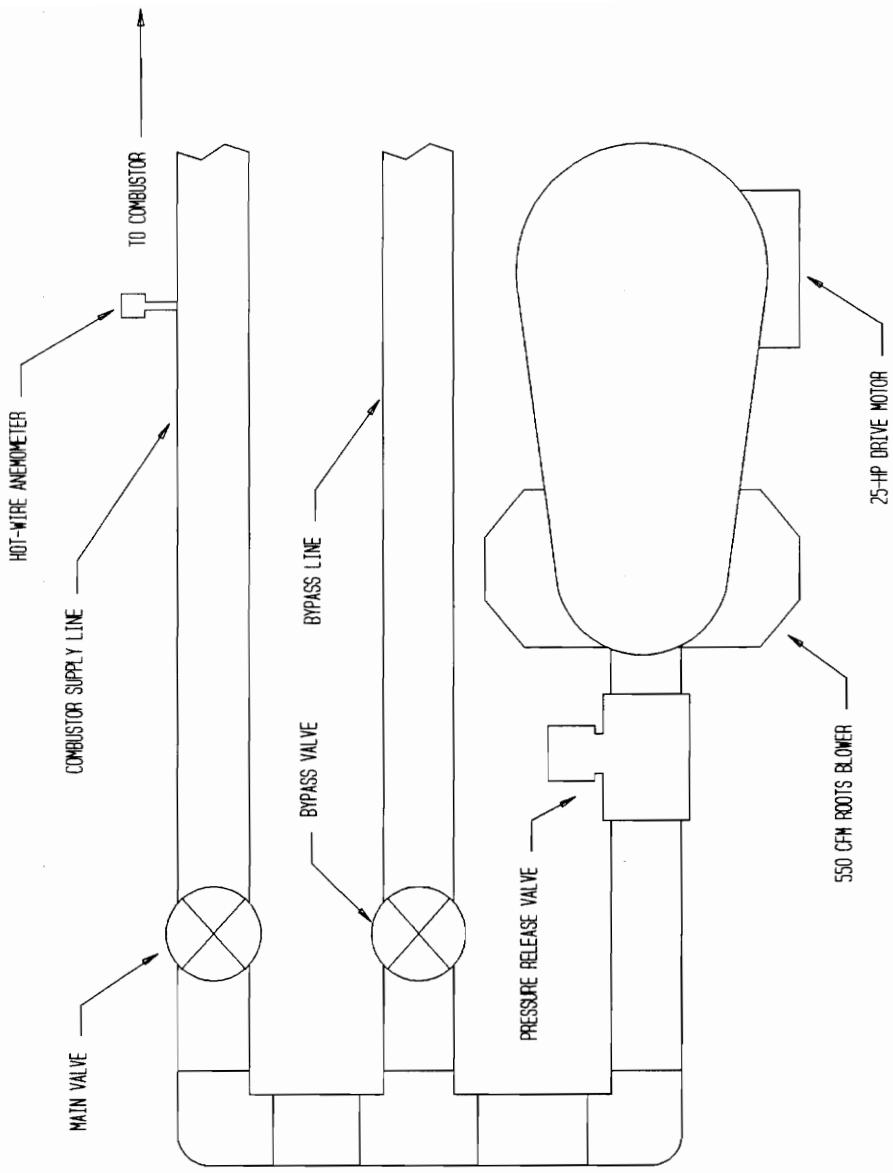

Figure 6. Blower and Piping System

has been specially fabricated to allow precise flow control and reduce drift to a minimum. The system is constructed to allow installation of a hot-wire anemometer in a location with significant straight pipe length upstream to allow accurate flow measurement and also provide more settled flow to the combustor. The separation distance between the anemometer and the valve is approximately 20 pipe diameters.

The aluminum circular-to-rectangular transition consists of two welded assemblies connected at a flanged joint. The first section is a circular-to-square transition with the second being a square-to-rectangular transition. These are shown in Figure 7 along with the rectangular pre-combustor section which is positioned between the transition and the combustor and acts to provide sufficient length for fuel-air mixing in the premixed mode of combustion. The pre-combustor section is 914 mm long with a 102 mm by 51 mm cross-section matching that of the combustor. This length is comparable to that of the pre-combustor section used by Ganji and Sawyer [15]. In addition, this section acts as an anchor for both the step and rod stabilizers.

The air supply is fitted with a Sierra Model 661 hot-wire anemometer upstream of the combustor assembly. This allows measurement of air velocity and, consequently, the volumetric air flow. The output of the anemometer is a voltage signal which is monitored by a voltmeter, and recorded using a Hewlett-Packard model 7045A X-Y plotter. The flowmeter output fluctuates due to flow turbulence and noise. This makes it difficult to determine a mean voltage value when adjusting the metering valve. The plotter allows a readout that is easily averaged visually by the operator. This ease is not possible when the flowrate is monitored using a common digital voltmeter. The use of

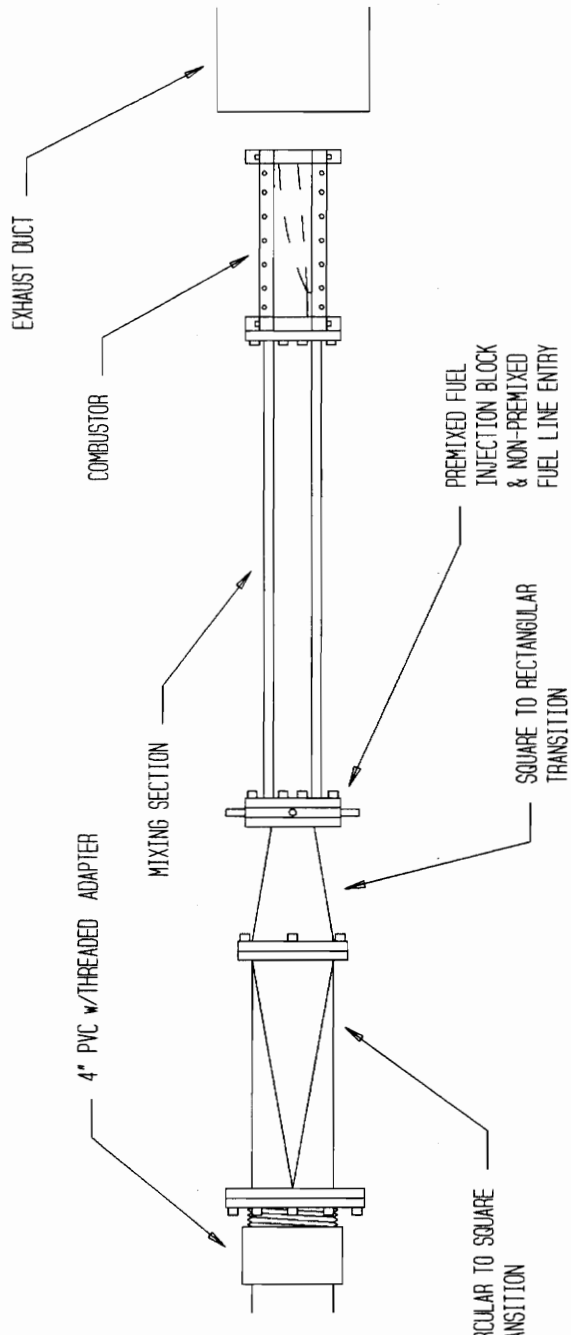

Figure 7. Combustor Assembly

the plotter also allows confirmation of flowrate constancy and notation of pertinent events during experimental operation.

The voltage output of the flowmeter is converted to a velocity (SFPM) using a curve fit developed based on factory calibration data. This value is converted from a centerline value to a mean value by assuming a 1/7 power velocity profile. This profile can be integrated to yield a ratio of mean to centerline velocity. Using this method, a volumetric air flow rate can be determined based on the pipe cross-sectional area.

3.2.4 Fuel Supply and Metering

The fuel used throughout this investigation is commonly available liquified petroleum gas or LPG. This type of fuel is generally known to contain approximately 90% propane with the remaining composition being made up of butane and other gases. This type of fuel was chosen because of ease of acquisition and availability in small manageable quantities (30 lb tanks).

A distinctly different fuel system is used for each combustor configuration. The diffusion flame setup requires much lower fuel flow rates and pressures than that of the premixed portion of the experiment.

Fuel for the diffusion flame is provided to the injector/stabilizer from a single LPG tank. The system operates at low pressure because of low flow rates. A pressure gage and thermocouple were initially used to allow correction for temperature and pressure. This was found to be unnecessary because these parameters did not vary significantly from ambient conditions. Flow is both measured and metered using a Cole Parmer

Instrument Co. rotameter (18 l/min air at STP capacity). The flow is delivered to the injector supply lines using two nylon tubes connected with compression fittings. Other connections are made using threaded piping.

A calibration curve for the rotameter was developed using a dry gas meter under standard conditions. Volumetric flow rates are found based on a the curve developed for the meter. These rates are used to calculate air/fuel ratios and to estimate the mean exit velocity of the fuel from the injector based on the total area of the circular injection ports.

Fuel for the premixed mode is supplied by a pair of LPG tanks. A threaded piping manifold directs the flow to a non-vented regulator. The output of this regulator is delivered through a solenoid valve to a Brooks rotameter and then to an injection manifold via tubing. The manifold distributes fuel to four stainless steel tubes containing a total of sixteen injection ports. These ports are identical in size (0.76 mm diameter) and arranged in a manner that is expected to facilitate thorough mixing. The distribution of injection ports is detailed in Figure 8. The injector tubes are mounted in an injector block having a cross section matching that of the pre-combustor section. The block is positioned at the upstream end of this section. The port size was chosen to allow choked flow operation of the fuel system over the normal operating range of the combustor. A choked-flow delivery design is used to take advantage of resulting stability and safety characteristics.

The use of propane fuel for the step-stabilized premixed flame requires the use of a tank heating system in order to allow sustained high output without "freeze-up". This is a result of the large amount of heat required to vaporize the liquid fuel in the tank. This

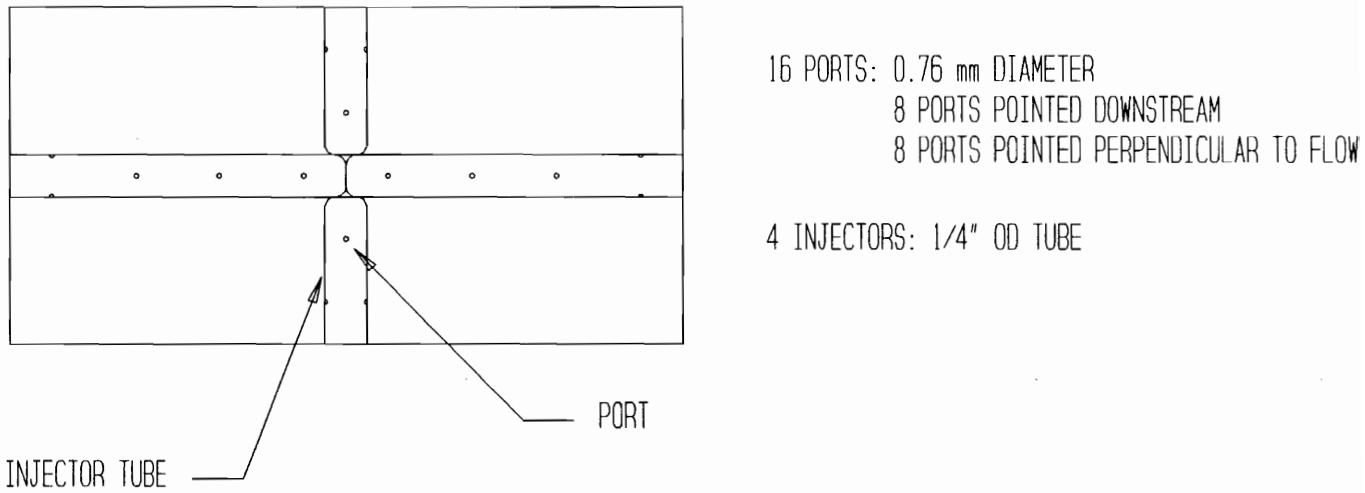

Figure 8. Distribution of Premixed Injection Ports

system uses a pair of thermostatically controlled resistive heaters.

Premixed fuel supply measurement is accomplished using a Brooks rotameter (278 l/min air at STP capacity). Flow is controlled using a ventless pressure regulator and shutoff is accomplished using a solenoid valve. The regulator allows operation of the fuel injection system with little or no drift in flow rates. Fuel flow drift will occur as a result of tank cooling if a throttling valve is used alone.

Both the pressure and temperature of the fuel within the flowmeter are monitored. A pressure gage is connected at the exit of the rotameter with the connecting line being attached at a right angle to the fuel flow direction. The pressure gage being used has been calibrated using a dead weight tester. The resulting error correction is applied to raw pressure readings. Fuel flow temperature is determined using a type-K (Chromel-Alumel) thermocouple inserted into the flow via a teflon seal at the input of the flowmeter. The standard pressure and temperature corrections are applied to the direct reading of the rotameter. The entire fuel injection system for the premixed mode was calibrated using propane (LPG) under operating pressures using a dry gas meter.

3.3 Optical Instrumentation

Data acquisition involves three types of thermal and flow visualization: shadowgraphs, photographs, and temperatures derived from a thermal imaging system. The nature of shadowgraphs reveals the instantaneous location of flame fronts and other flow characteristics. Photographs are used to examine the time-averaged location of the

luminous components of the reaction zone. Thermal contours allow an indirect quantification of heat transfer from the flame to the heat-loaded electrode. A schematic in Figure 9 illustrates the optical instrumentation systems.

3.3.1 Thermal Imaging

Thermal images are acquired using an Inframetrics thermal imaging system. This system includes an infra-red scanner, a control electronics unit, a primary monitor, a remote monitor, and a VHS video cassette recorder. In addition, an IBM PC is used for remote control of the unit and to facilitate the acquisition of records of heat-loaded electrode temperature (external surface) versus downstream distance from the stabilizer and subsequent disk storage. Area-averaged temperature data is also acquired and stored using the PC. It is necessary for operation that the scanner contain a small amount of liquid nitrogen. This severely limits available angles at which the scanner can be used. This difficulty has been resolved by the employment of a gold plated infra-red mirror. The underside of the combustor can be imaged through the use of this mirror.

An Omega model HH-26K digital thermometer which employs a Type-K (Chromel-Alumel) thermocouple is used for redundant temperature measurement. Actual temperatures are not of specific interest because the primary focus is on the field-induced reduction of electrode temperature. Accurate temperatures are available using this system for values below 200°C. Some inaccuracy is present beyond this value because of variations in the emissivity of the electrode surface and the use of the infra-red mirror.

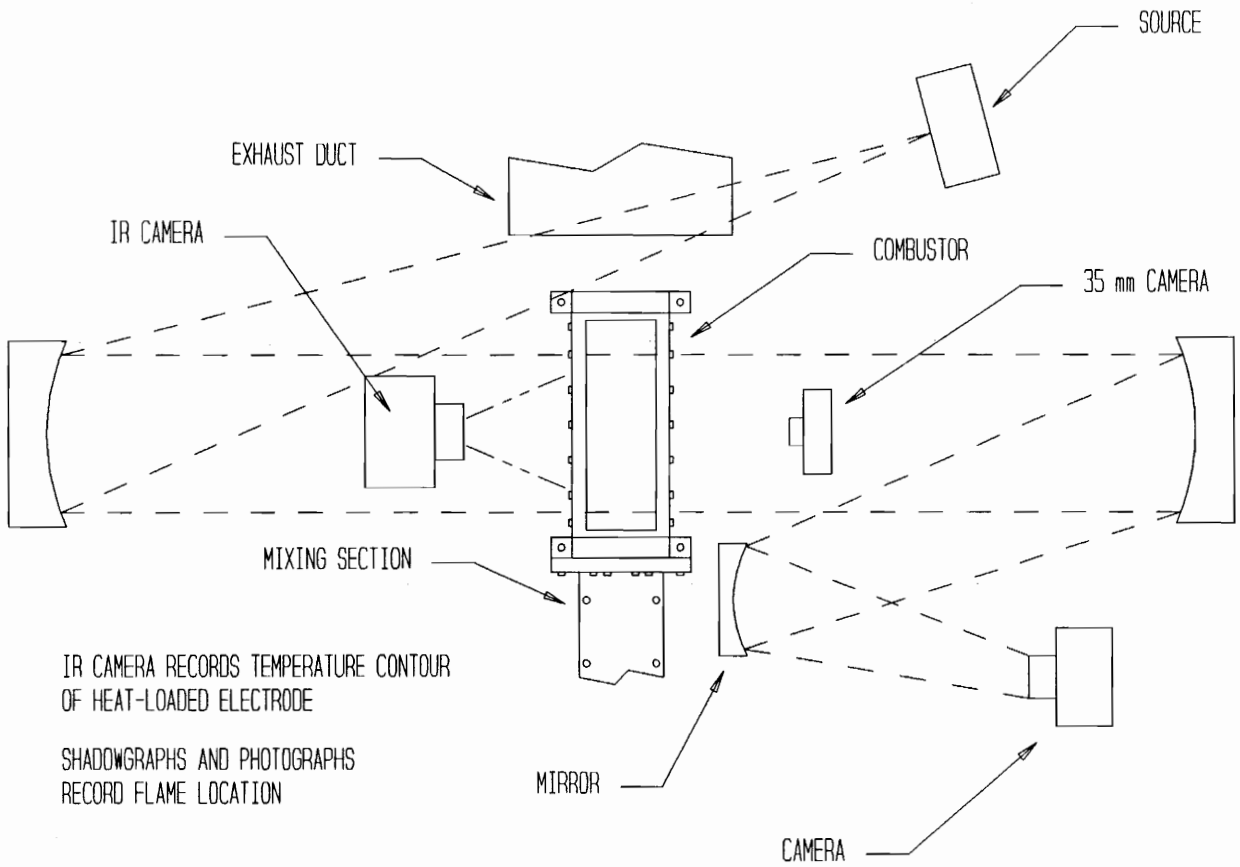

Figure 9. Optical Instrumentation Schematic

Real-time thermal images acquired by the scanner are stored using the video recorder. Video images can be recalled from tape and either transferred directly as a color image or processed using an appropriate image processing system.

3.3.2 Shadowgraphs

Shadowgraph images are produced using a point light source collimated by a J. Unertl Optical Co. 10-inch parabolic mirror. The collimated light is passed through the test section and then focused using two 6-inch Edmund Scientific parabolic mirrors. The image is made using a Calumet 4x5-inch format camera. The light sources used are an Oriel xenon arc-lamp for a continuous light supply and a triggered strobe for short duration shadowgraphs. Long duration exposures are made using the continuous source and an appropriate shutter. Durations used are as short as 1/400 second. A shutter is also used with short exposures to limit extraneous light and acts as the strobe trigger. Films used include Polaroid types 52, 54, and 57 with speeds of 400 ASA, 100 ISO, and 3000 ISO, respectively.

The length of the combustor in combination with the smaller size of the focusing mirrors prevents full combustor length shadowgraphs from being taken. Although two images must be made for complete coverage, this has the advantage of a higher magnification factor and better resolution.

Several types of shadowgraphs are available using this system. They include long exposure shadowgraphs which are intended to give a time-averaged flame front position, short duration shadowgraphs which give an instantaneous image, and multi-exposure

shadowgraphs which give an overlapped sequence of flame front progression.

It is not generally possible to acquire shadowgraphs and thermal data concurrently due to time and space limitations. As a result, shadowgraphs are taken during separate tests and typically before steady state conditions are reached. The temperature of the electrode is monitored and whenever possible, attempts are made to make shadowgraphs in a common temperature range.

3.3.3 Photographs

Normal photographs are made using a 35 mm camera and color film. The films used include ISO 100, 200, and 400 speed films. Exposure times range from 1/64 to 1 second. These photographs reveal the time-averaged position of the luminous components of the flame. The flame position can be roughly scaled from a given photograph and compared case to case to reveal the effect of the applied electric field.

Normal photographs are not taken concurrently with thermal data acquisition (as with the shadowgraphs) due to operational difficulties. A dark background is placed behind the combustor to provide suitable contrast. As with shadowgraphs, where possible, photographs are made when the heat-loaded electrode reaches a common temperature range.

3.4 Experimental Methods

3.4.1 Thermal Data Acquisition Procedure

Temperature data is obtained in three forms. These are records of heat-loaded electrode temperature (external surface) versus downstream distance along the combustor centerline, area-averaged temperature-time histories, and temperature contours recorded on videotape. All data are for the exposed surface of the heat-loaded lower electrode.

Records of temperature versus downstream distance along the combustor centerline are taken at steady state conditions and are also used to determine when steady state conditions have been reached. Steady state in this context is defined to be when the temperature of the exposed surface of the electrode has stabilized around a mean value. The thermal inertia of the electrode prevents measurement of any rapid fluctuation of heat transfer due to the turbulent nature of the flames studied. A photograph of the video output of the thermal imaging system is included as Figure 10. It displays the line designating the pixels for which temperature data are transferred to an IBM PC for storage. This line is located along the combustor centerline, with the stabilizer located to the right and the combustor exit to the left. These records are used to evaluate heat transfer reduction. Local information along the axis of the combustor is provided, allowing spatial resolution of the heat reduction effect.

Two strategies are used to obtain temperature records. It is generally preferable to use the first method, in which records are obtained for all values of applied voltage during one continuous operation of the experimental apparatus. This method should be

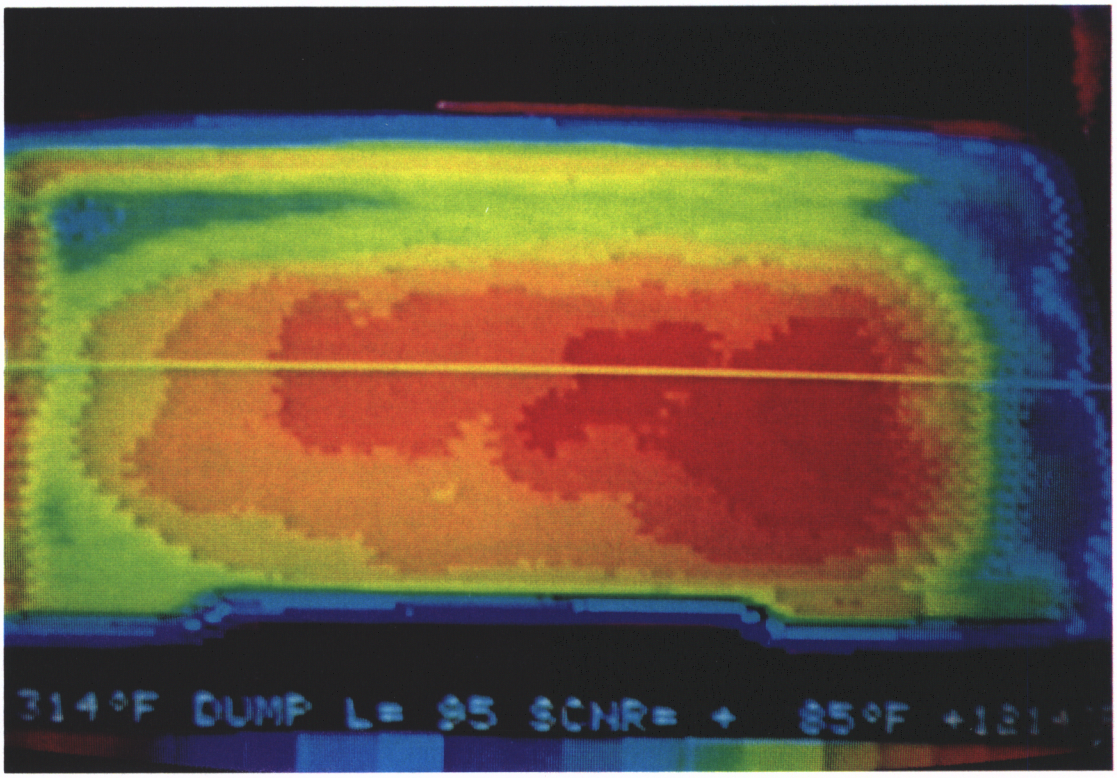

Figure 10. Video Output of Thermal Imaging System showing Line Designator

less dependent on experimental repeatability. In practice, experimental difficulties precluded the use of this method for certain segments of testing. The second method is to acquire contours for the null voltage condition and then shut off the apparatus, wait for ambient conditions and equipment to return to initial conditions. Afterwards, the test is repeated with voltage applied. This method reduces test duration.

When the first method is used, temperature records are generally taken in sets of four. These sets are taken after a voltage is selected and a predetermined amount of time is allowed for steady state to be reached. The time period used is based on experience with the apparatus. Steady state is further confirmed by the analysis of the records. The individual acquisitions are separated by two minutes. Two minutes allows proper monitoring of the experiment and an acceptable rate of data collection. Operation would consist of igniting the combustor and then allowing steady state conditions to be reached with no applied voltage. A set of records would now be taken and then the electric field applied. Another set of records would be made and then the process would be repeated. This provides four record sets that could later be averaged and/or normalized. This method was more applicable to the non-premixed mode of this investigation. This was because of the extended operation time possible with the low power diffusion flame.

Area-averaged temperature-time histories are a secondary method of evaluating the effect of the electric field. The image in Figure 11 shows a typical averaging block. Temperatures for all of the pixels located within the block are averaged internally by the control unit of the thermal imaging system. The averaged value is periodically transferred (typically every 1 to 2 seconds) to a computer for storage. The histories are transient and

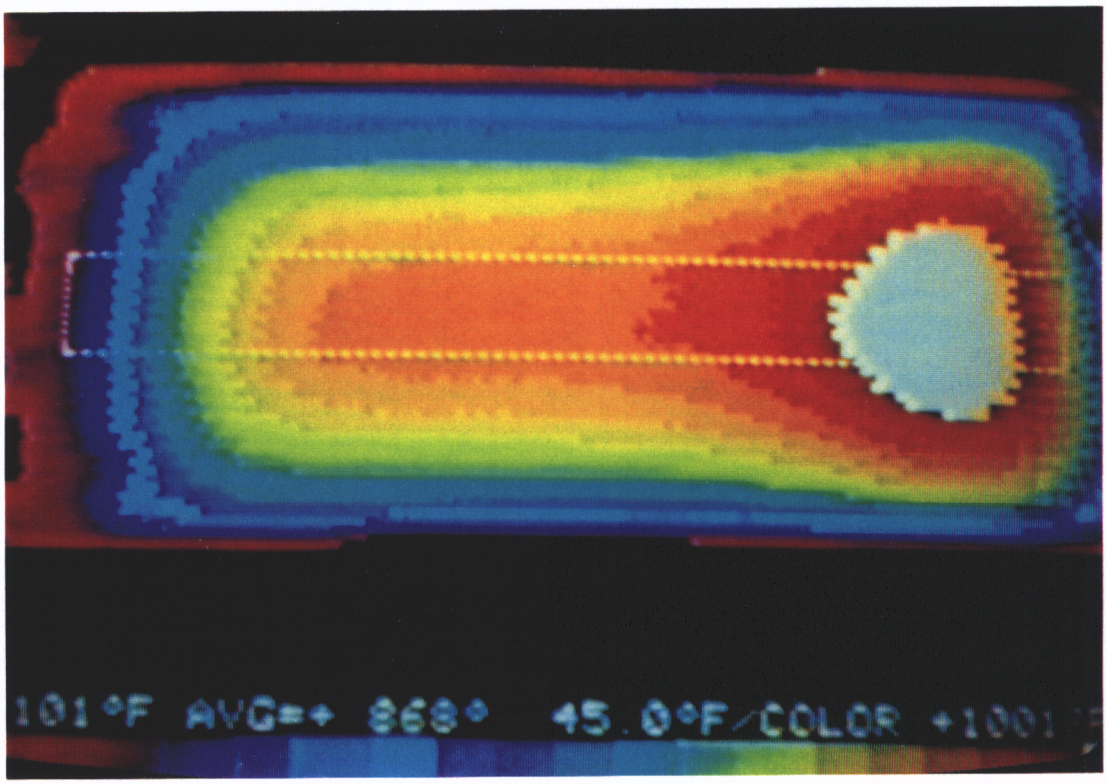

Figure 11. Video Output of Thermal Imaging System showing Area Designator

can be used to allow short duration operation, thereby avoiding extensive fuel use and the highest electrode temperatures associated with steady state operation. The electric field, if any, is applied at a time near that of ignition and remains on for the duration of the test. Therefore, two separate operations of the apparatus are necessary for a quantification of the effect of the electric field on heat transfer.

3.4.2 Data Reduction

Thermal data is primarily in the form of records of heat-loaded electrode temperature (external surface) versus downstream distance along the combustor centerline. These records are dumped from the imaging system to an IBM PC in blocks of 256 values in hexadecimal form. The low character 00 represents the low end of the currently selected temperature scale with FF representing the high value. A FORTRAN program is used to make the conversion to decimal values. This FORTRAN code is included in Appendix A. The high and low scale temperatures must be recorded at the time of record acquisition. This code also adds a coordinate base representing the distance downstream of the stabilizer (x), which is divided by the stabilizer dimension. The stabilizer dimension is the diameter of the rod (D), or the height of the step (H). The base is produced using the fact that the leftmost pixel is the first dumped. The position of the stabilizer is located on the thermal image. The center of the rod stabilizer is used for the diffusion mode and the step location is used for the premixed phase of the study. Also, a dimension of known length is taken from the image to give a ratio of pixels to actual distance.

4 Results and Discussion

Test data were gathered for both a rod-stabilized diffusion flame and for a step-stabilized premixed flame. Both flame types used propane as fuel and air as the oxidizer. The primary data type collected was records of temperature versus downstream distance along the combustor centerline. All temperature data are for the exposed surface of the heat-loaded electrode. A high voltage negative potential was applied to the upper electrode. The lower heat-loaded electrode was grounded.

Shadowgraphs and photographs were used to investigate movements of the flowfield and the luminous portion of the flame. They proved helpful, but somewhat difficult to interpret, especially for the step-stabilized premixed flame.

The rod-stabilized diffusion flame provided the best results, both in data quality and observed effects. These results are discussed in Section 4.1. The fact that this mode of operation is immune to flashback allowed operation at lower inlet air velocities. Also, because operation is both at low air flow rates and is overall lean, the power output is low. This allowed operation at lower wall temperatures and for longer periods. Additionally, the reaction zone for this mode of operation did not impinge on both electrodes which allowed higher applied voltages. Reaction zone contact with both electrodes provides a path for higher current flow. Maximum applied voltage is therefore

limited as a result of the current limit of the power supply.

The step-stabilized premixed mode was much more difficult to implement. Results are addressed in Section 4.2. Potential flashback requires operation at velocities somewhat greater than the flame speed. For premixed operation, the overall ratio of fuel to air is much closer to stoichiometric. These two factors combine to provide power output at levels more than two orders of magnitude greater than that of the diffusion flame mode. Increased heat loading resulted in much higher electrode temperatures. This caused high stress on the combustor and required extremely long warm up periods. This (combined with difficulty in maintaining fuel flow) made reaching steady state conditions arduous. Additionally, the flame was generally in contact with both electrodes which, due to the earlier discussed mechanism, limited applied voltages.

4.1 Results for the Rod-stabilized Diffusion Flame

All temperature data presented in this Section was obtained at a nominal inlet velocity of 3.4 m/s. This value was chosen because it allowed stable operation without flame contact with both electrodes (reduces maximum applied voltage). This velocity is a mean value based on the area of the 102 mm by 51 mm cross section of the combustor. Nominal volumetric air/fuel ratios of 420, 320, and 270 were investigated with applied voltages of 0.0 and 8.0 kVDC.

The procedure described in Section 3.4.1 was used to produce temperature records for the nominal test conditions. Actual experimental conditions for thermal data are given

in Table 1. There is some divergence from the nominal values due to problems selecting precise air flow rates.

Table 1. Diffusion Flame Conditions Investigated Using Temperature Records

Air/Fuel Ratio	Mean Inlet Air Velocity, m/s	Voltage, kVDC	Current, mA
270	3.4	0.0	0.0
270	3.4	8.0	0.1
330	3.5	0.0	0.0
330	3.5	8.0	0.5
400	3.2	0.0	0.0
400	3.2	8.0	0.7

Shadowgraphs and photographs were made at the same primary conditions with the addition of an applied voltage value of 4.0 kVDC. Composite shadowgraphs were made and cover the length of the combustor including some distance past the exit. Photographs also cover a similar area.

Photographs were made using a one second exposure, an aperture setting of 16, and a film speed of 100 ASA. They represent a time-averaged image of the luminous zone of the flame. Experimental conditions for the photos are given in Table 2.

Test conditions for the shadowgraphs are included in Table 3. Conditions for the upstream shadowgraphs are separated by a slash from those for the downstream half. The composites cover the entire combustor including a limited area past the exit. The

Table 2. Diffusion Flame Conditions Investigated Using Photographs

Air/Fuel Ratio	Mean Inlet Air Velocity, m/s	Voltage, kVDC	Current, mA
280	3.5	0.0	0.0
280	3.5	4.0	0.5
280	3.5	8.0	1.8
320	3.4	0.0	0.0
320	3.4	4.0	0.4
320	3.4	8.0	1.4
430	3.5	0.0	0.0
430	3.5	4.0	0.4
430	3.5	8.0	1.5

Table 3. Diffusion Flame Conditions Investigated Using Shadowgraphs

Air/Fuel Ratio	Mean Inlet Air Velocity, m/s	Voltage, kVDC	Current, mA
270/290	3.4/3.6	0.0	0.0
270/290	3.4/3.6	4.0	0.4
270/290	3.4/3.6	8.0	2.0/2.1
320/330	3.4/3.5	0.0	0.0
320/330	3.4/3.5	4.0	0.5
320/330	3.4/3.5	8.0	1.7
420/440	3.4/3.6	0.0	0.0
420/440	3.4/3.6	4.0	0.4
420/440	3.4/3.6	8.0	1.7/1.6

extremely turbulent nature of the diffusion flame which is undergoing both mixing and combustion simultaneously allows comparison of shadowgraphs under different applied electric field strengths.

The thermal data taken for the non-premixed phase of the investigation proved encouraging. The much lower power output of the rod stabilized diffusion flame provided for operation at lower electrode temperatures. Steady state conditions were reachable and maintainable.

Figure 12 shows mean curves for the three air/fuel ratios taken with no applied voltage. The peak temperature is located about six diameters downstream of the stabilizer. Another peak is noted upstream of this point and most likely represents the upstream limit of flame impingement. The location of the peaks does not change with air/fuel ratio.

The greatest heat transfer reduction was seen for the highest air/fuel ratio and is discussed first in Section 4.1.1. The less obvious results for the lower air/fuel ratios are presented later in Section 4.1.2. Analysis of the former allowed the development of an explanation for the difference in results.

4.1.1 Observations for the Highest A/F Ratio

Figure 13 displays mean curves taken for an inlet velocity of 3.2 m/s and an air/fuel ratio of 400. This represents the lowest fuel flow rate. The applied voltages are 0.0 and 8.0 kVDC. The curves are averages of several records. Maximum standard deviation for the records is 10°C. The maximum temperature difference is approximately

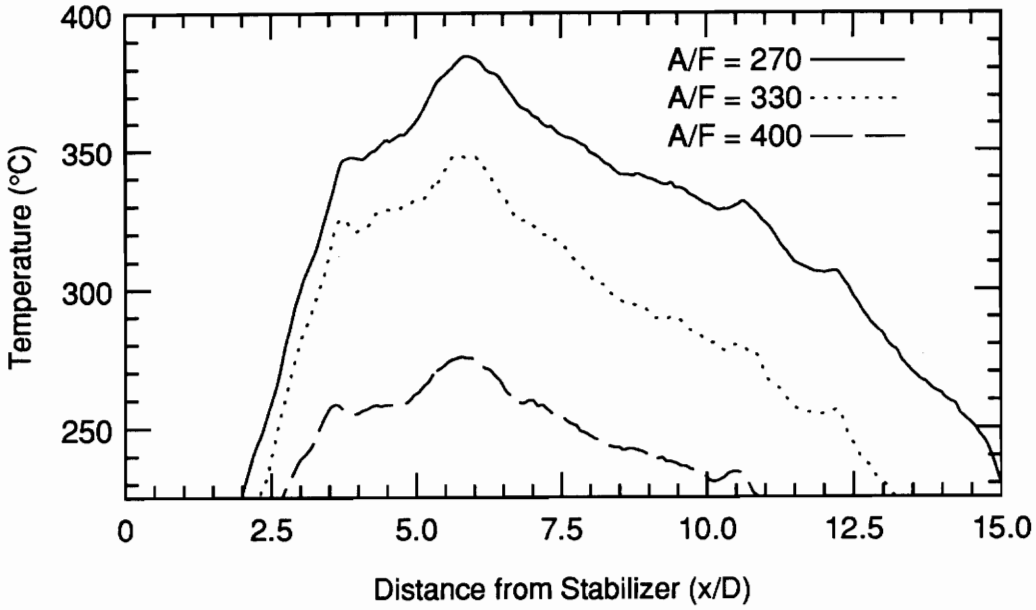

Figure 12. Heat-loaded Electrode Temperature (external surface) vs. Downstream Distance from the Stabilizer for all Air/Fuel Ratios, V = 0.0 kVDC

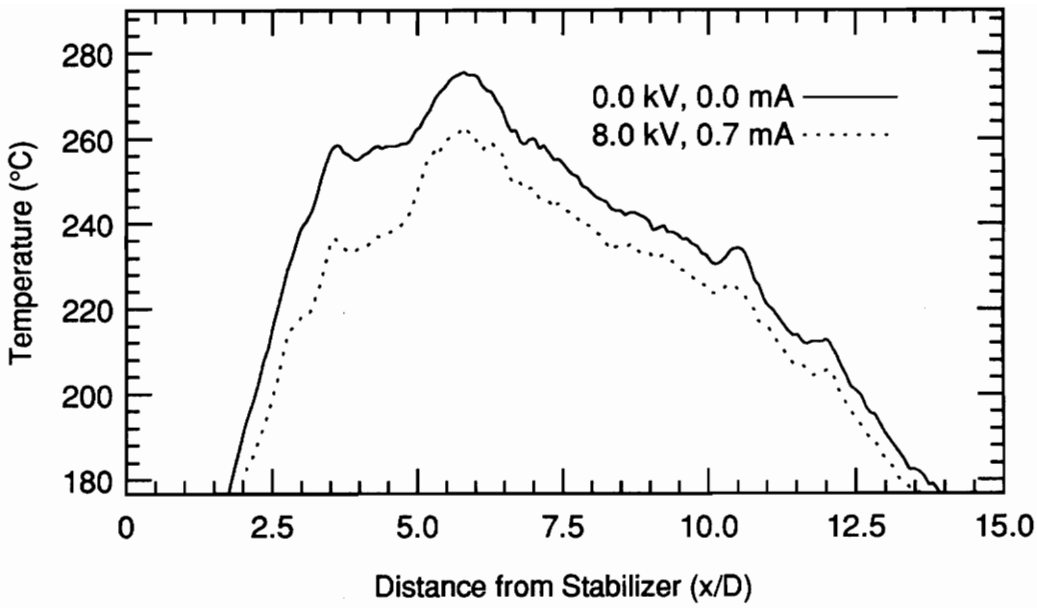

Figure 13. Heat-loaded Electrode Temperature (external surface) vs. Downstream Distance from the Stabilizer, A/F = 400, U_a = 3.2 m/s

20°C. This case represents the greatest temperature reduction for the test conditions presented in Table 1. For each voltage condition, the standard deviation was calculated for various points along the length of the curve. The deviation is larger where the temperature difference between the two mean curves is larger. The records gathered with voltage applied have the highest deviation.

Two photographs are presented in Figure 14. A disturbance of the yellow-orange luminous zone of the flame is noted. This is especially apparent in the downstream half of the combustor. The luminous zone is shortened and deflected upwards by the applied field. This could be attributed to an alteration of the bulk flow and/or a field-induced reduction in the amount of soot.

The observed effects noticed for this geometry are partially attributable to bulk effects on the flowfield. The effect of the applied field in this case may be as illustrated in Figure 15. The figure shows how an applied field would have the effect of redirecting some inlet air flow from above the stabilizer to under it. The direct effect of the electric field would be to impart an upwards component of velocity to the gas in the reaction zone. This would cause displacement of flow towards the upper electrode which would be replaced by an increase in flow under the stabilizer. A displacement of the flame upward would occur as displayed in the previously discussed photographs. The replacement of hot products with cool reactants caused by the displacement downstream of the flame along the heat-loaded electrode would reduce heat transfer. This is different from boundary layer thickening, although that may also take place. The two mechanisms will combine to reduce heat transfer to the lower electrode.

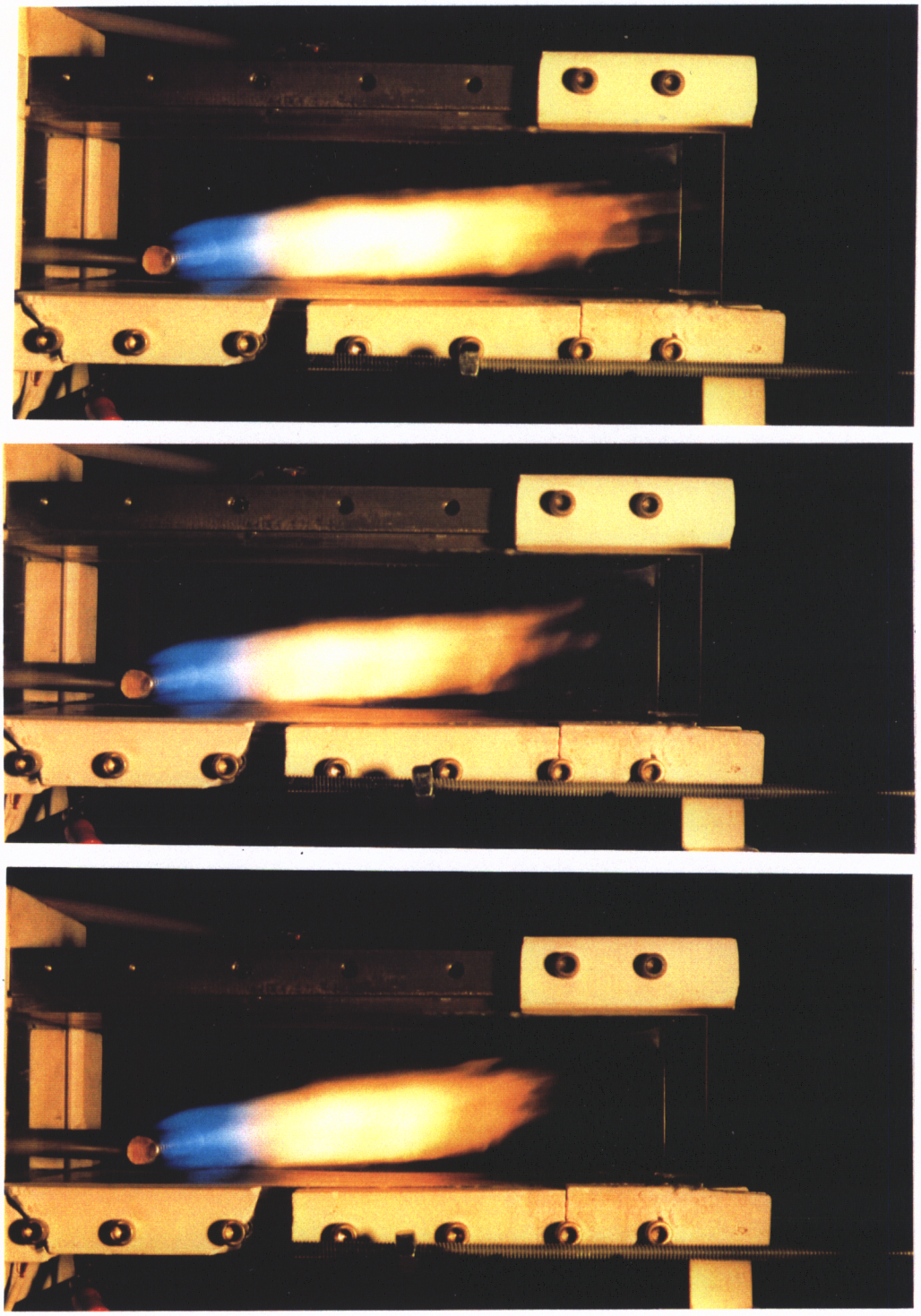

Figure 14. **Photographs, A/F = 430, U_a = 3.5 m/s: (Top) V = 0.0 kVDC, (Middle) V = 4.0 kVDC, (Bottom) V = 8.0. kVDC**

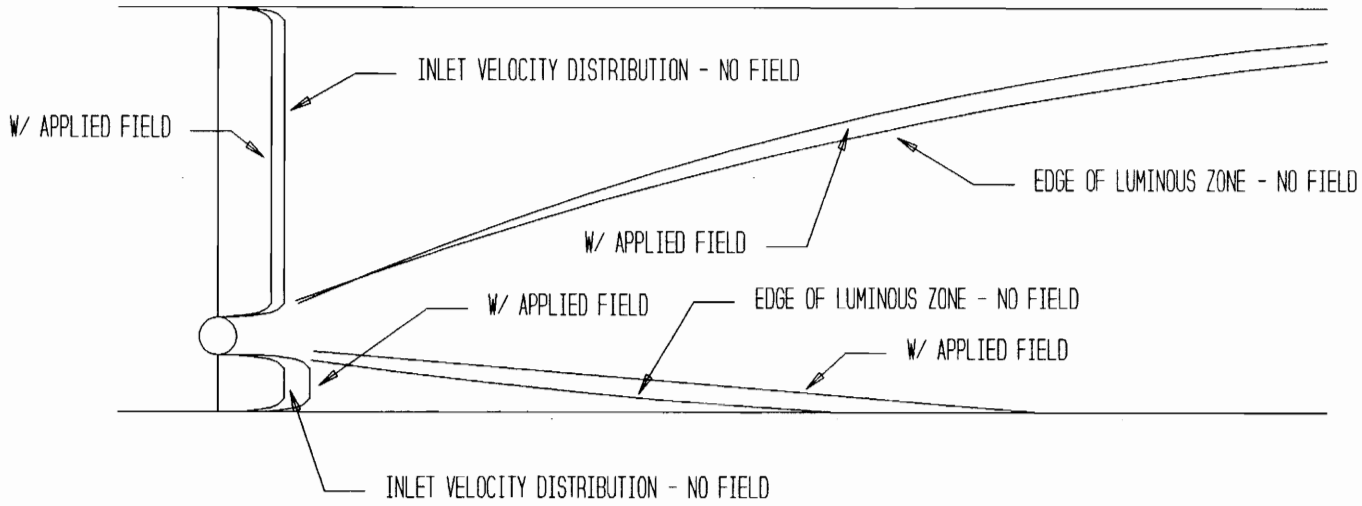

Figure 15. Idealized Concept of Flowfield Alteration For the Rod-Stabilized Combustor

Another possible contributor to heat transfer reduction may be a decrease in radiative transfer due to a reduction in flame soot. Radiation can contribute considerably to wall heating. Photographs show a significant decrease in the yellow-orange luminous portion of the flame. It may be that this causes a reduction in radiative heat transfer to the downstream half of the combustor with a limited effect on heat transfer for the upstream portion.

Shadowgraphs in Figures 16, 17, and 18 demonstrate the electric field effect on the bulk flow. They are for the highest air/fuel ratio of 420 and represent the least pronounced case observed with shadowgraphs. Displacement of the flowfield is apparent in the downstream half of the combustor. The thin light and dark lines primarily represent boundaries between cold reactants and hot reaction products. Disturbance of the flowfield in the downstream half of the combustor is somewhat more noticeable for the other air/fuel ratios, being most pronounced for the nominal air/fuel ratio of 270. The shadowgraphs made for these conditions are included in Appendix B.

4.1.2 Observations for the Lower A/F Ratios

The effect of an increase in fuel rates on potential heat transfer amelioration is illustrated in Figures 19 and 20. The field-induced temperature reduction is 10°C for and air/fuel ratio of 330 with a maximum standard deviation of 3°C. Decline in temperature is fairly uniform along most of the electrode. The reduction is approximately 5°C for an air/fuel ratio of 270 with a standard deviation of 1°C in the area showing a field-induced decrease. The change in temperature is noticed primarily for the downstream half of the

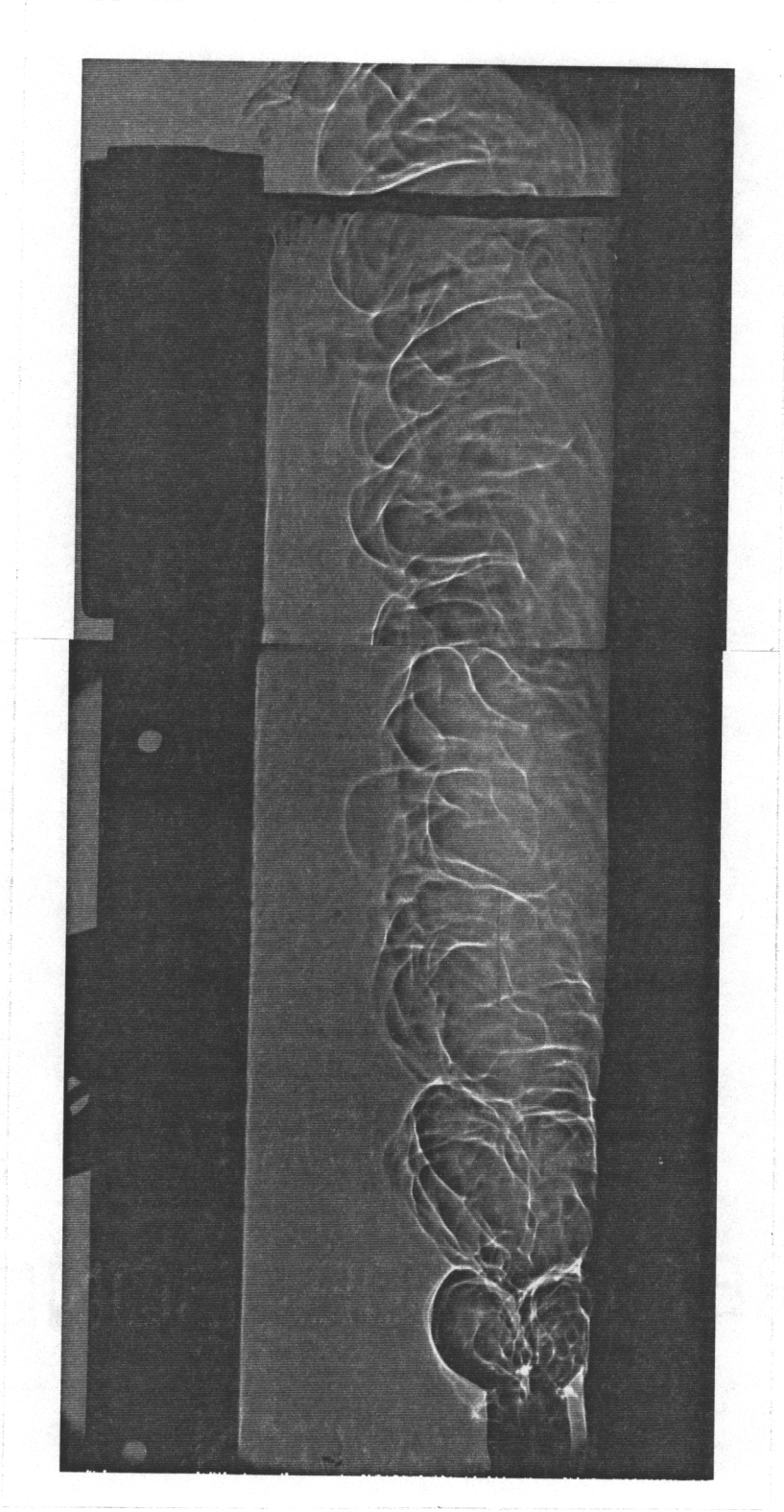

Figure 16. Composite Shadowgraph, A/F = 420/440, U_a = 3.4/3.6 m/s, V = 0.0 kVDC

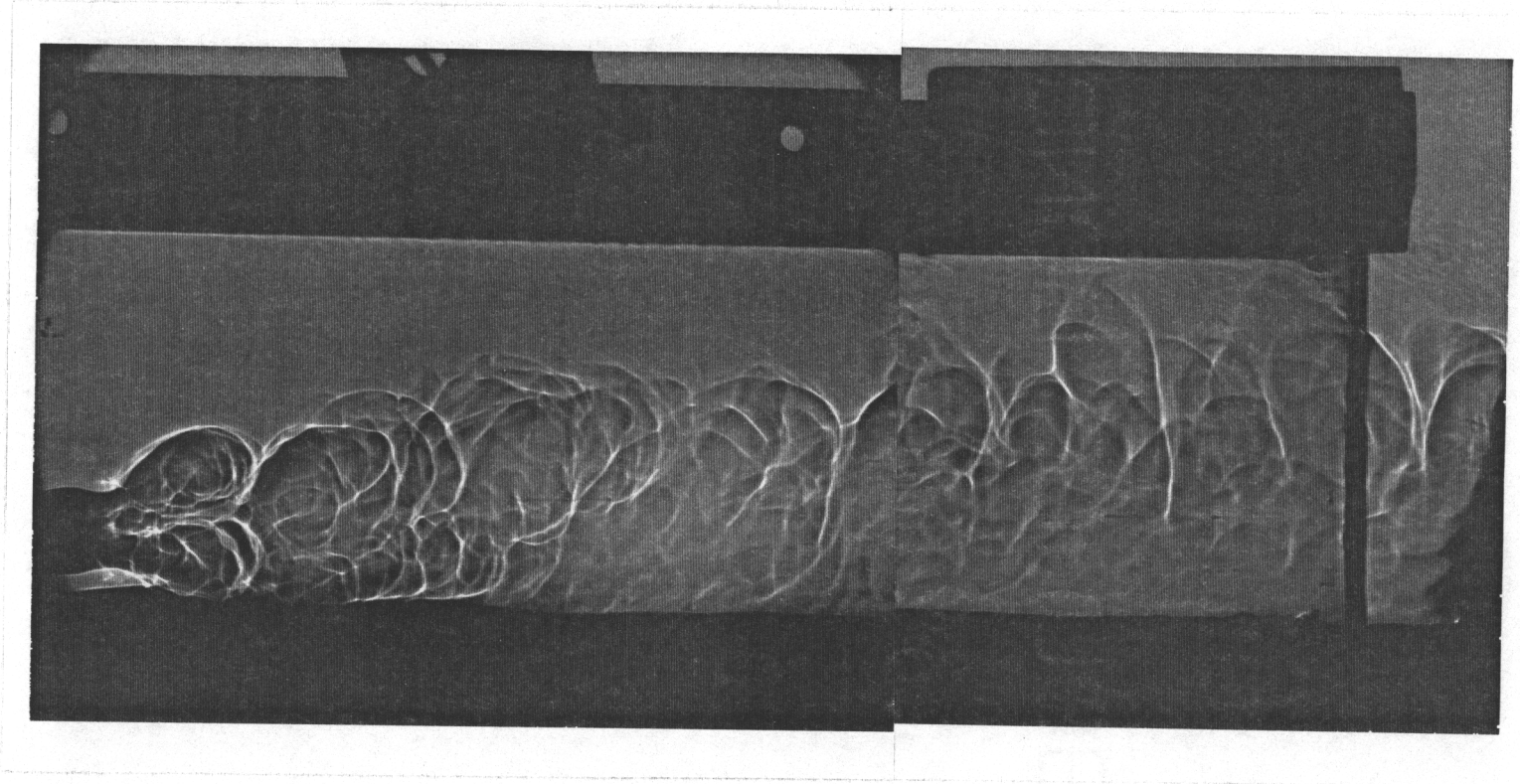

Figure 17. **Composite Shadowgraph, A/F = 420/440, U_a = 3.4/3.6 m/s, V = 4.0 kVDC**

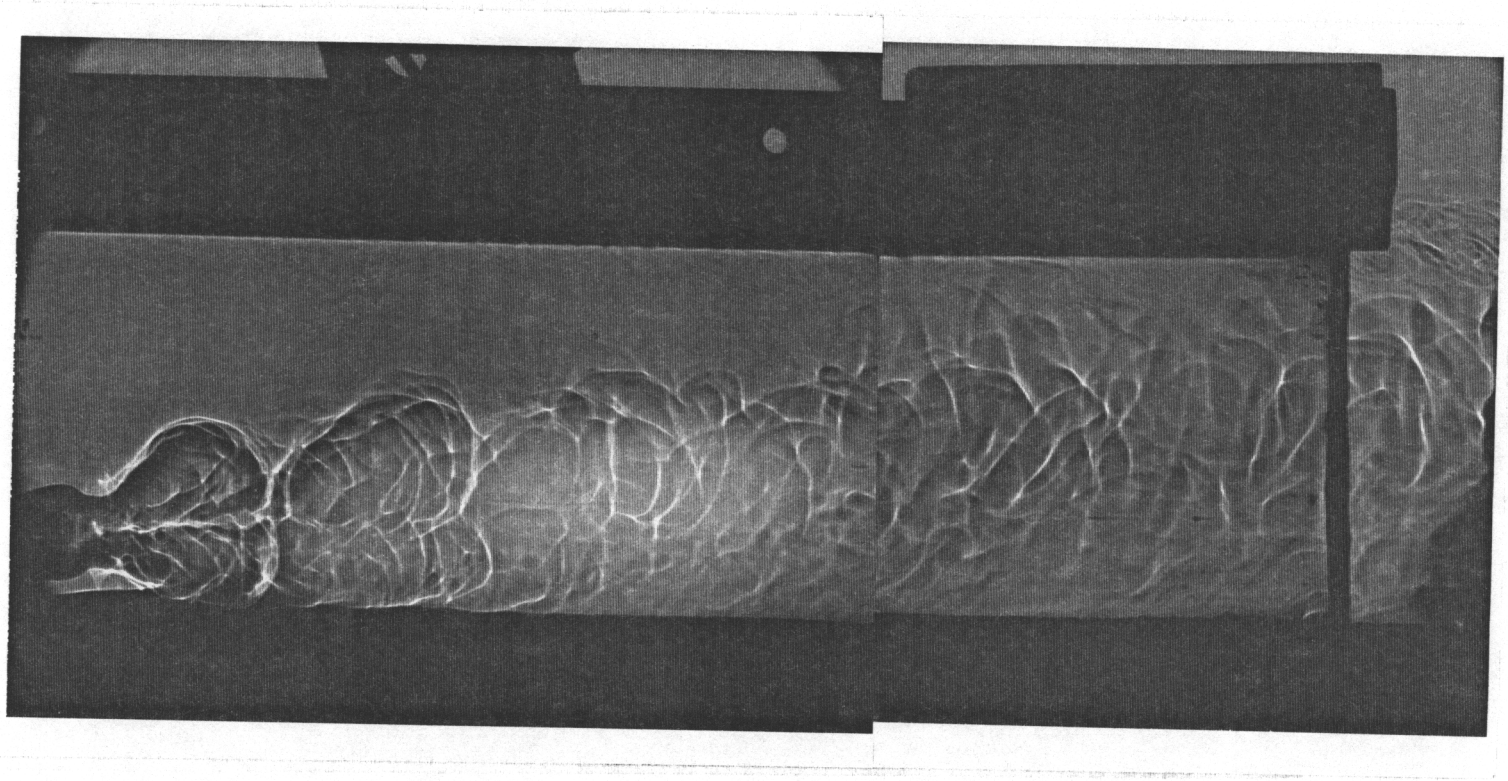

Figure 18. Composite Shadowgraph, A/F = 420/440, U_a = 3.4/3.6 m/s, V = 8.0 kVDC

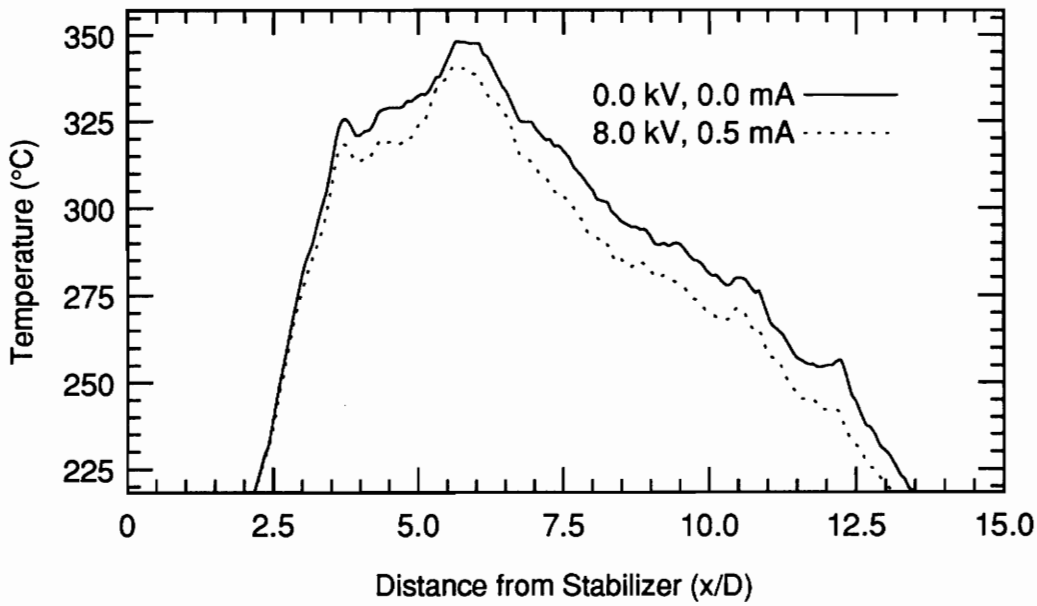

Figure 19. **Heat-loaded Electrode Temperature (external surface) vs. Downstream Distance from the Stabilizer, A/F = 330, U_a = 3.5 m/s**

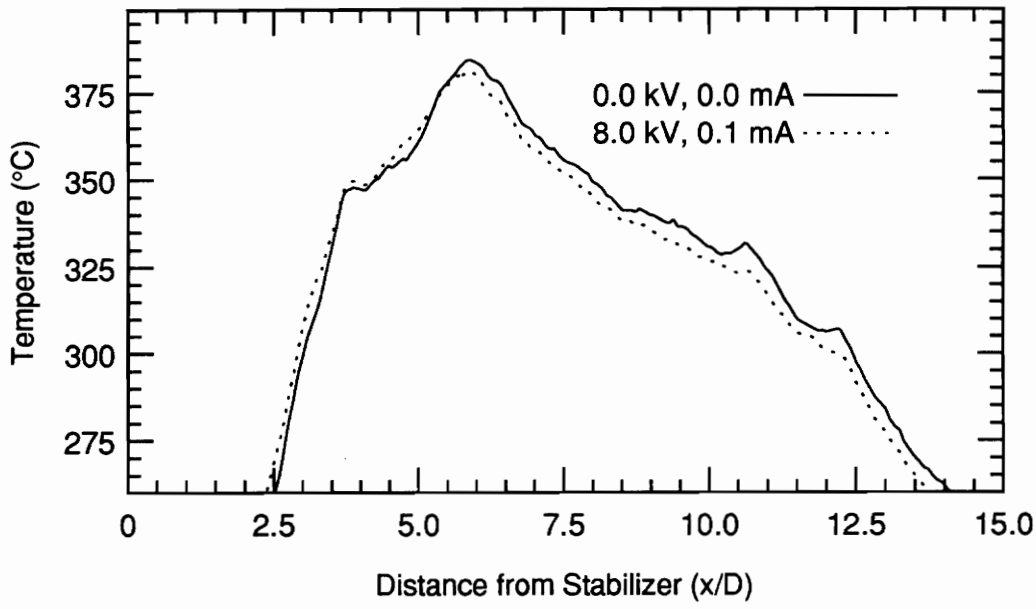

Figure 20. Heat-loaded Electrode Temperature (external surface) vs. Downstream Distance from the Stabilizer, A/F = 270, U_a = 3.4 m/s

combustor. Standard deviation for the curves was greater for higher temperatures.

The photographs in Figure 21 are for an inlet air velocity of 3.4 m/s and an air/fuel ratio of 320. Applied voltages are 0.0, 4.0 kVDC, and 8.0 kVDC. In this sequence, the yellow-orange zone extends out of the combustor for the zero-field condition but is shortened by an applied field so that is almost entirely contained within the combustor. The flame appears to be both shortened and deflected upwards. Figure 22 is for an air/fuel ratio of 280 for which the yellow-orange zone extends well out of the combustor. The applied field reduces the amount of this zone apparent beyond the exit. No noticeable effect on the blue portion of the luminous zone is apparent in any of the photo sequences. The yellow-orange zone is indicative of the presence of soot.

4.1.3 Analysis

Two distinct mechanisms are suspected of having an effect on heat transfer. The first is the field-induced bulk effect on the flowfield. This was discussed using Figure 15. The second involves a reduction in soot due to interference by the electric field with production and/or destruction of carbon particles. The first mechanism has two effects. One is that air flow under the stabilizer is increased and the flame is displaced away from the heat-loaded electrode, reducing heat transfer. The other is that the slowing of flow over the stabilizer would cause the flame to move upstream which would then increase heat transfer by increasing gas temperatures in the combustor. The second mechanism, a reduction in soot, should decrease heat transfer by decreasing radiative heat transfer to the combustor walls. Soot acts as a radiation source (especially strong

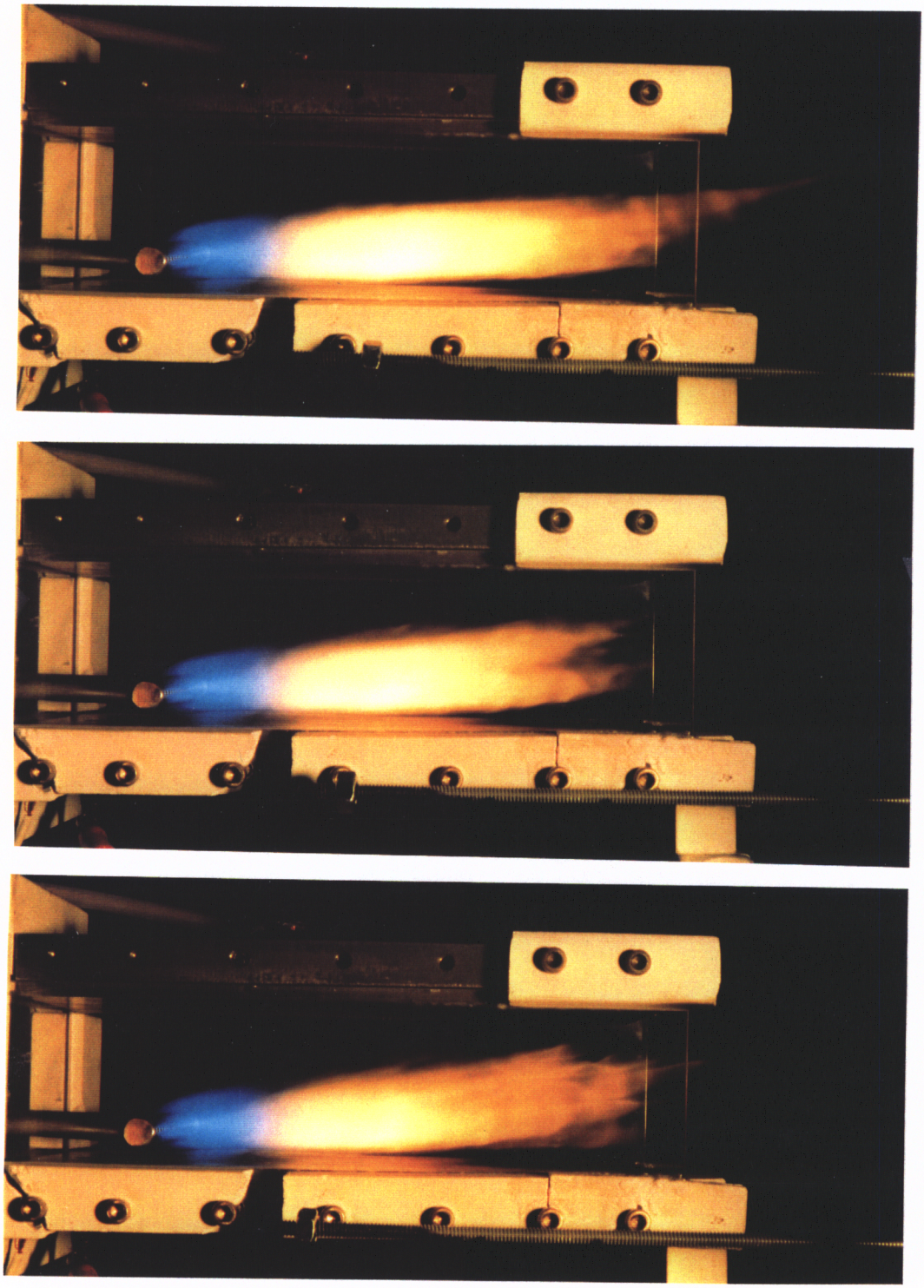

Figure 21. **Photographs, A/F = 320, U_a = 3.4 m/s: (Top) V = 0.0 kVDC, (Middle) V = 4.0 kVDC, (Bottom) V = 8.0 kVDC**

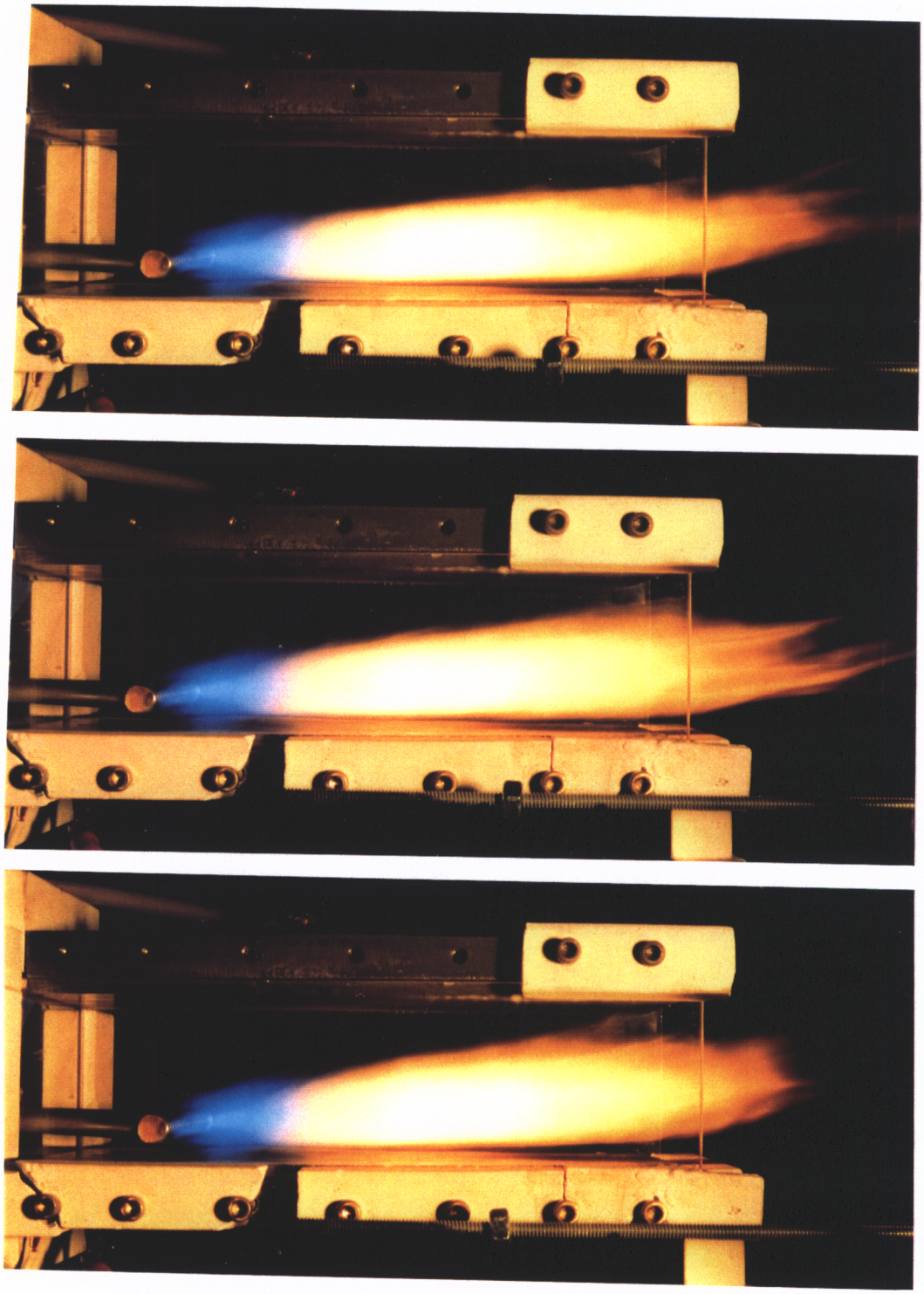

Figure 22. Photographs, A/F = 280, U_a = 3.5 m/s: (Top) V = 0.0 kVDC, (Middle) V = 4.0 kVDC, (Bottom) V = 8.0 kVDC

in the infra-red range) and contributes to heat transfer from the high temperature combustion gas to the combustor walls.

The effect of an increase in flow under the stabilizer is difficult to observe using photographs and shadowgraphs. The point of flame impingement on the lower electrode is not clearly discernable. The intense nature of the flame near the stabilizer and the site of impingement causes this difficulty. A reduction in heat transfer to the heat-loaded electrode and/or a displacement of the flowfield in the upper half of the combustor are indirect methods of confirming this effect. Both of these were observed.

The displacement of the reaction zone in the upper half of the combustor upstream is observable using visual methods. Photographs and shadowgraphs indicate an upward and upstream displacement of the flame. If bulk effects alone and not an increase in flame speed are responsible for this displacement, then a redirecting of the flow past the stabilizer is indicated.

The presence of the second mechanism is supported by the observed shortening of the yellow-orange luminous portion of the flame under an applied field. Also, it is noted that the lower air/fuel ratios display less field-induced heat transfer amelioration. These cases have luminous zones which extend beyond the combustor exit. The only significant reduction in the yellow-orange zone occurs outside the combustor. It may be that no notable reduction in radiative heat transfer to the inner surface of the combustor is taking place for these ratios as was postulated for the highest air/fuel ratio. This may explain the reduced field effect on heat transfer for the lower air/fuel ratios.

4.2 Results for the Step-stabilized Premixed Flame

Temperature data was collected for inlet air velocities ranging from 4.6 to 9.0 m/s. These velocities are mean values based on the area of the 102 mm by 44.5 mm cross section of the combustor upstream of the step. Equivalence ratios of 0.72 to 0.94 were investigated. Applied voltages ranged up to 3.5 kVDC.

Shadowgraphs and photographs were made for equivalence ratios of 0.65 to 1.03 and for inlet velocities ranging from 4.5 to 9.9 m/s. Maximum applied voltage was 6.6 kVDC. The bulk of the shadowgraphs cover the downstream half of the combustor. Photographs cover the entire combustor including some length past the exit.

4.2.1 Steady State Temperature Data

Although steady state conditions were difficult to attain, modifications to the heat-loaded electrode have allowed some reasonable data to be acquired. Examination of centerline temperature plots indicates no effect induced by the electric field greater than experimental uncertainty. Experimental uncertainty is fairly high with an estimated value of ± 10°C due to the problems associated with reaching steady state electrode temperatures. Test conditions investigated are listed in Table 4. Centerline records were taken at or near steady state conditions.

Figure 23 is indicative of problems reaching steady state. This figure depicts two centerline records that were taken separated by approximately 90 seconds. Upward temperature drift is especially noticeable in the peak region just downstream of the step. This problem was persistent even for extended test periods and is the reason for the high

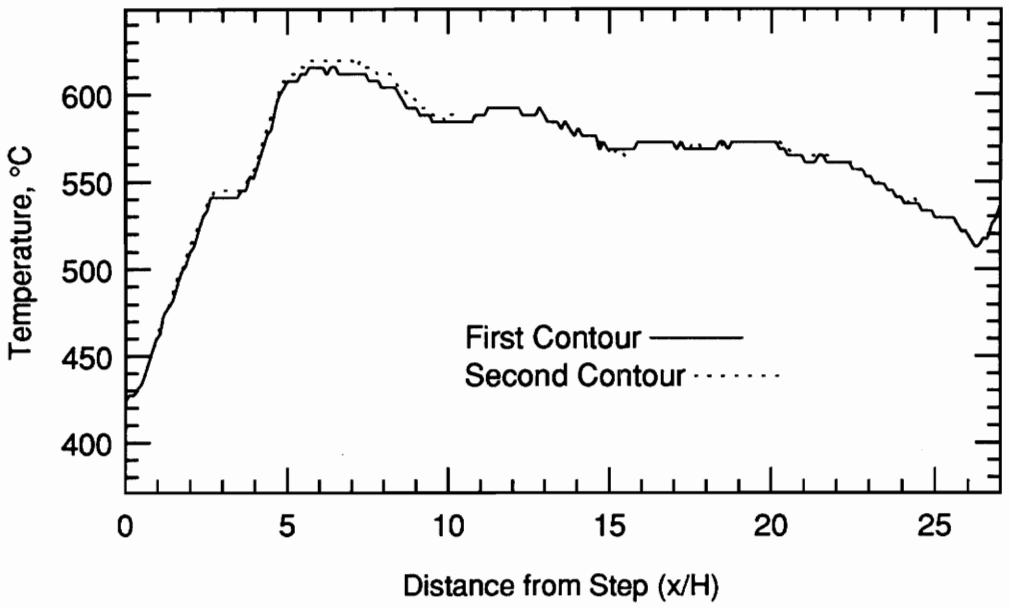

Figure 23. **Heat-loaded Electrode Temperature (external surface) vs. Downstream Distance from the Stabilizer, Two Records Separated by 90 Seconds: ϕ = 0.78, U = 5.8 m/s, V = 3.3 kVDC**

Table 4. Premixed Flame Conditions Investigated Using Steady State Temperature Records

Equivalence Ratio, ϕ	Inlet Velocity, m/s	Voltage, kVDC	Current, mA
0.73	4.6	0.0	0.0
0.73	4.6	2.6	1.0
0.89	4.6	0.0	0.0
0.85	6.1	0.0	0.0
0.85	6.1	2.1	3.5
0.76	5.7	0.0	0.0
0.78	5.8	0.0	0.0
0.78	5.8	3.3	3.1
0.75	6.1	3.5	2.9

estimated experimental uncertainty.

Figure 24 is representative of the null effect of the electric field. These records are taken under similar operating conditions with no applied voltage and a voltage of 3.5 kVDC. Maximum temperature differences are approximately 6°C with the applied voltage curve being the coolest. Differences would need to be greater than twice the experimental uncertainty in order to confirm the presence of a field-induced temperature reduction. This temperature difference is less than the estimated experimental uncertainty of ± 10°C and significantly less than twice that value.

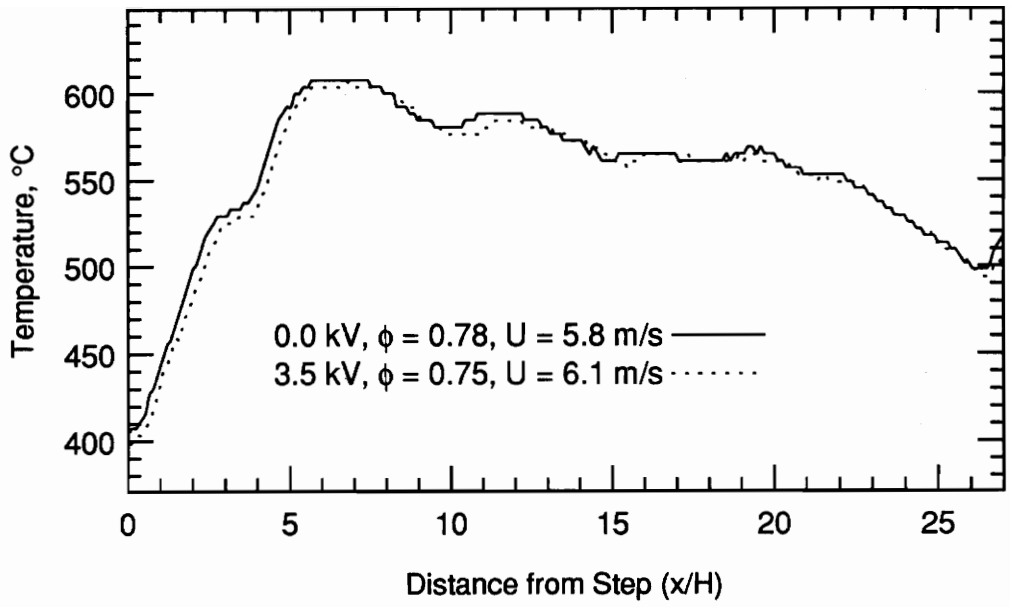

Figure 24. **Heat-loaded Electrode Temperature (external surface) vs. Downstream Distance from the Stabilizer**

4.2.2 Transient Temperature Data

The difficulties encountered in attaining good steady-state temperature data lead to the use of transient temperature histories. Any reduction in heat transfer to the heat-loaded electrode should slow the transient temperature increase. These histories are not useful in determining differences in steady state convective heat transfer. However, these tests can be of shorter duration and are not dependent upon reaching the steady state condition. Transient histories are generally made in pairs, one with voltage and one without. Table 5 shows the test conditions investigated using transient histories.

Transient run temperatures are area-averaged values. Blocks denoting the area to be averaged are typically located at the downstream end of the combustor, near the step, or bordering a thin strip along the combustor length.

Figure 25 displays transient run histories made with an averaging block covering a thin strip along the length of the electrode centerline. The histories are plotted versus time beginning at a common temperature of 201°C. The histories display very similar behavior. This plot further supports earlier discussed steady state temperature records. Transient and steady state data indicate very limited field-induced heat transfer reduction in the premixed mode of operation. Possible causes for the lack of a positive result are provided by analysis of the flowfield using shadowgraphs and photographs which are now presented.

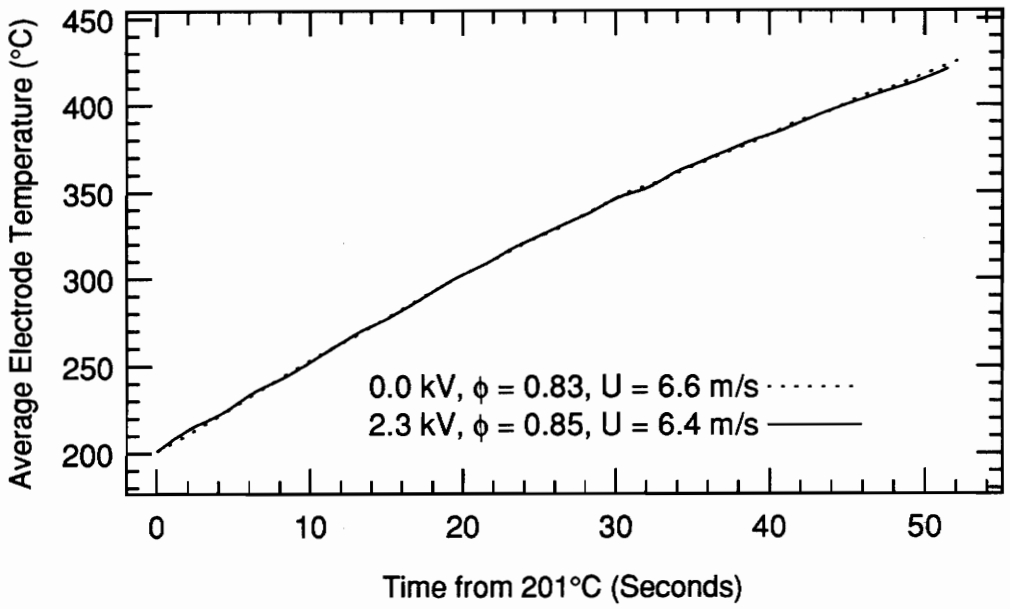

Figure 25. Transient Area-averaged Heat-loaded Electrode Temperature (external surface) Histories

Table 5. Premixed Flame Conditions Investigated using Transient Histories

Equivalence Ratio, ϕ	Inlet Velocity, m/s	Voltage, kVDC	Current, mA	Average Block Location
0.83	6.6	0.0	0.0	Thin Strip Along Length
0.85	6.4	2.3	4.5	
0.94	4.8	0.0	0.0	Near Step
0.94	4.7	2.0	2.6	
0.73	6.0	0.0	0.0	Downstream
0.72	6.0	2.6	0.6	

4.2.3 Shadowgraphs

Three types of shadowgraphs are made. These include long duration shadowgraphs, short duration shadowgraphs, and multiple exposure shadowgraphs. Table 6 lists the short duration shadowgraphs of the downstream half of the combustor. Table 7 lists the short duration shadowgraphs made of the upstream half of the combustor. Table 8 lists the multiple exposure shadowgraphs, which, with the exception of one, were acquired for the downstream portion of the combustor. Table 9 lists the long duration (1/400 second) shadowgraphs, which are only made for the downstream half of the combustor. The majority of these shadowgraphs are included in Appendix C with the remainder presented in this section. Some shadowgraphs are presented in pairs taken at slightly different values of velocity and equivalence ratio. The values are given separated by a slash, with the first value being for the upper shadowgraph and the second value being for the lower one.

Table 6. Premixed Flame Conditions for Downstream Shadowgraphs

Equivalence Ratio, ϕ	Inlet Velocity, m/s	Voltage, kVDC	Current, mA
0.93	4.8	0.0	0.0
0.95	4.8	2.4	3.0
0.95	4.8	0.0	0.0
0.95	4.8	2.4	3.0
0.66	6.7	0.0	0.0
0.67	6.7	6.6	3.0
0.66	6.7	5.6	1.0
0.66	6.8	0.0	0.0
0.81	6.6	0.0	0.0
0.80	6.7	3.2	3.0
0.79	6.7	3.6	3.0
0.80	6.7	0.0	0.0
0.77	5.8	0.0	0.0
0.77	5.8	4.0	4.0
0.74	6.0	4.0	3.0
0.77	6.8	0.0	0.0
0.77	6.8	3.4	3.0
0.77	6.8	0.0	0.0
0.76	6.9	3.2	3.0

Table 7. Premixed Flame Conditions for Upstream Shadowgraphs

Equivalence Ratio, ϕ	Inlet Velocity, m/s	Voltage, kVDC	Current, mA
0.73	5.9	0.0	0.0
0.83	6.1	0.0	0.0
0.96	6.1	0.0	0.0

Table 8. Premixed Flame Conditions for Multi-exposure Shadowgraphs

Equivalence Ratio, ϕ	Inlet Velocity, m/s	Voltage, kVDC	Current, mA
0.76	5.7	0.0	0.0
0.76	5.7	1.2	1.0
0.74	5.8	0.0	0.0
0.61	8.1	0.0	0.0
0.62	8.1	5.2	1.3

Table 9. Premixed Flame Conditions for Long Duration Shadowgraphs (1/400 second exposure)

Equivalence Ratio, ϕ	Inlet Velocity, m/s	Voltage, kVDC	Current, mA
0.87	4.9	0.0	0.0
0.86	5.0	0.0	0.0
0.84	5.1	0.0	0.0
0.84	5.1	2.0	2.2

Short duration shadowgraphs indicate movement of the flame front structures that can be attributed to the applied electric field when many examples are examined. Observations concerning this phenomenon are difficult to make due to the random nature of flame front movements. A statistically substantial survey would require a great many shadowgraphs. This is both costly and time consuming. Scaled measurements of the shadowgraphs are also difficult.

Particular cases demonstrate the trends observed in the shadowgraphs. A comparison of the shadowgraphs in Figure 26 shows to some degree a flame front displacement near the upper electrode. Experience with numerous shadowgraphs helps in their analysis. It may not be apparent, but the author believes, based on an examination of all shadowgraphs, that some displacement is occurring.

Effects due to the electric field are visible in the flowfield close to the upper negatively charged electrode. Little or no effect is apparent in other areas of the reaction area, especially near the recirculation zone. The separation distance between the upper electrode and the reaction zone decreases with increasing downstream distance. At some point, the cold reactant layer may become thin enough to allow some diversion of the ion stream through this area. The ion stream consisting of electrons and positively charged molecules is generally confined to the reaction zone. Discussion of the ion stream is given by Lawton and Weinberg [1]. This effect will later be more clearly demonstrated with photographs.

A representative upstream shadowgraph is included as Figure 27. It was taken at an inlet velocity of 5.9 m/s and an equivalence ratio of 0.73 with no applied voltage

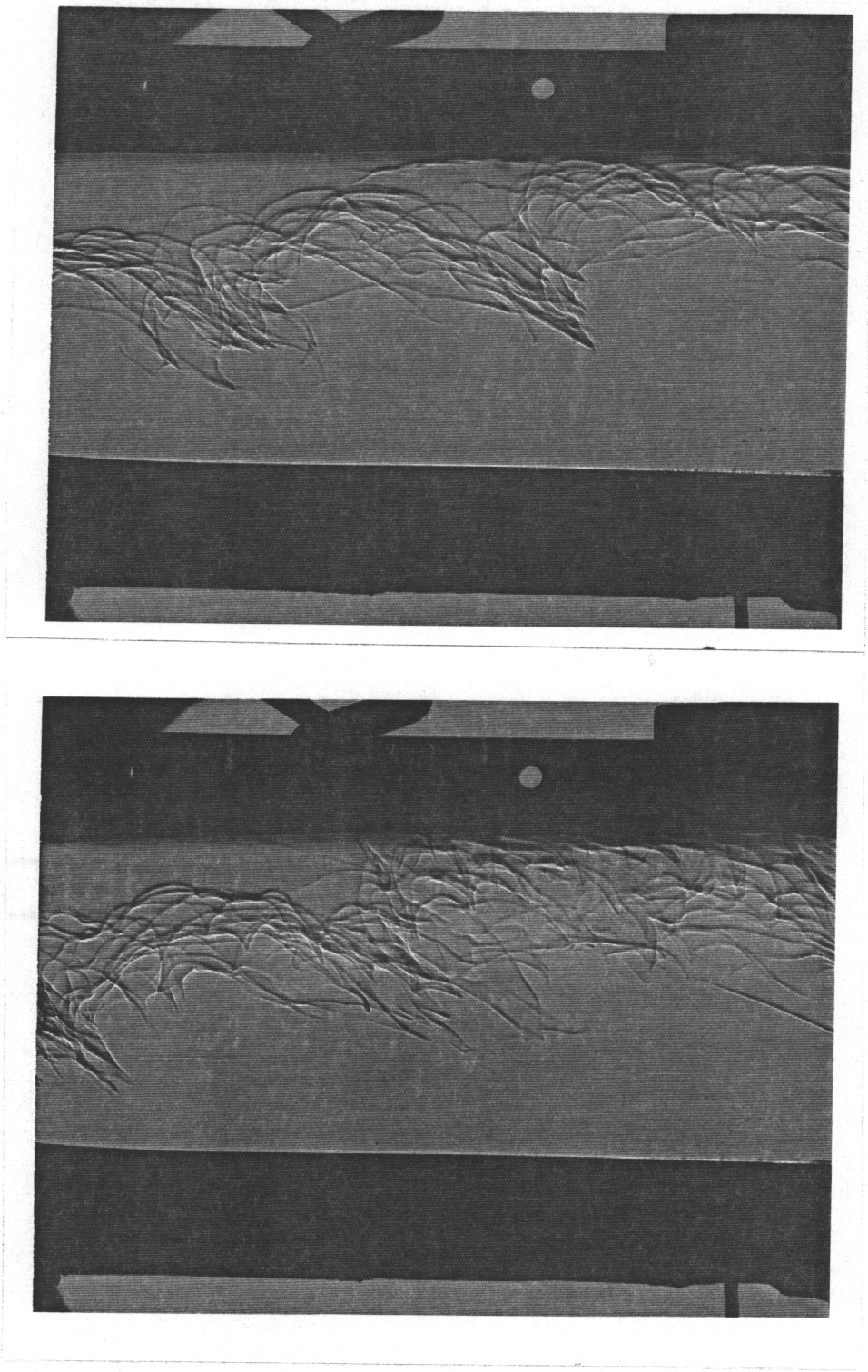

Figure 26. **Shadowgraphs, ϕ = 0.93/0.95, U = 4.8 m/s: (Top) V = 0.0 kVDC, (Bottom) V = 2.4 kVDC**

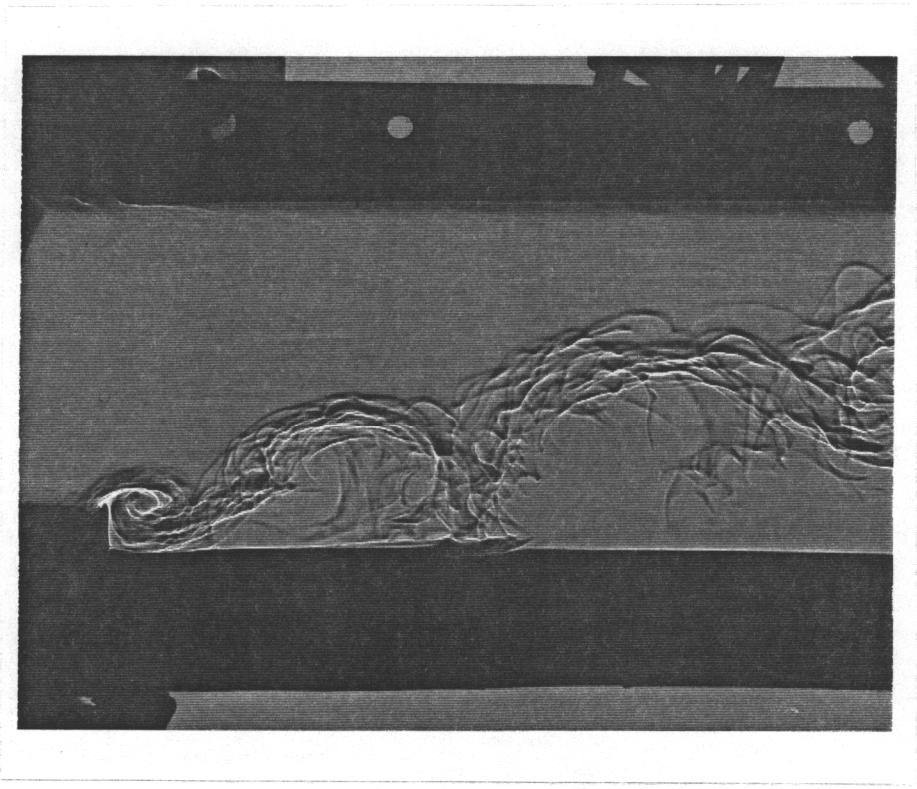

Figure 27. Upstream Shadowgraph, ϕ = 0.73, U = 5.9 m/s

and clearly displays a vortical structure beginning at the step.

Figure 28 includes two long duration shadowgraphs. They represent an inlet velocity of 5.1 m/s and an equivalence ratio of 0.84 with applied voltages of 0.0 and 2.0 kVDC. The images give a smeared average of the flame front progression. Exposure duration is 1/400 second. No clear difference is noticeable.

Included as Figure 29 are two multiple exposure shadowgraphs. They are comprised of approximately five overlapping exposures and can give fair indications of flame front progression without obscuring particular areas of the flowfield. This is in contrast to the long duration shadowgraphs which can overlook some flame front paths entirely. Flow conditions for these exposures include an inlet velocity of 5.7 m/s, an equivalence ratio of 0.76, and applied voltages of 0.0 and 1.2 kVDC. Some limited displacement may be apparent, but an effect is not clearly present.

Analysis of shadowgraphs demonstrates that the applied voltage has a small effect on the bulk flame front motion. Long exposure shadowgraphs and multiple exposure shadowgraphs also support this conclusion. Some effect is noted near the upper electrode and may be due to redirection of the ion stream made possible because of the small distance to the electrode. The nature of a turbulent step-stabilized reaction zone requires qualitative (as opposed to quantitative) analysis. Full investigation would require very numerous exposures or a shadowgraph movie relating the progression of the strongly fluctuating flowfield. The methods used are not sensitive enough to detect small changes which still may be significant.

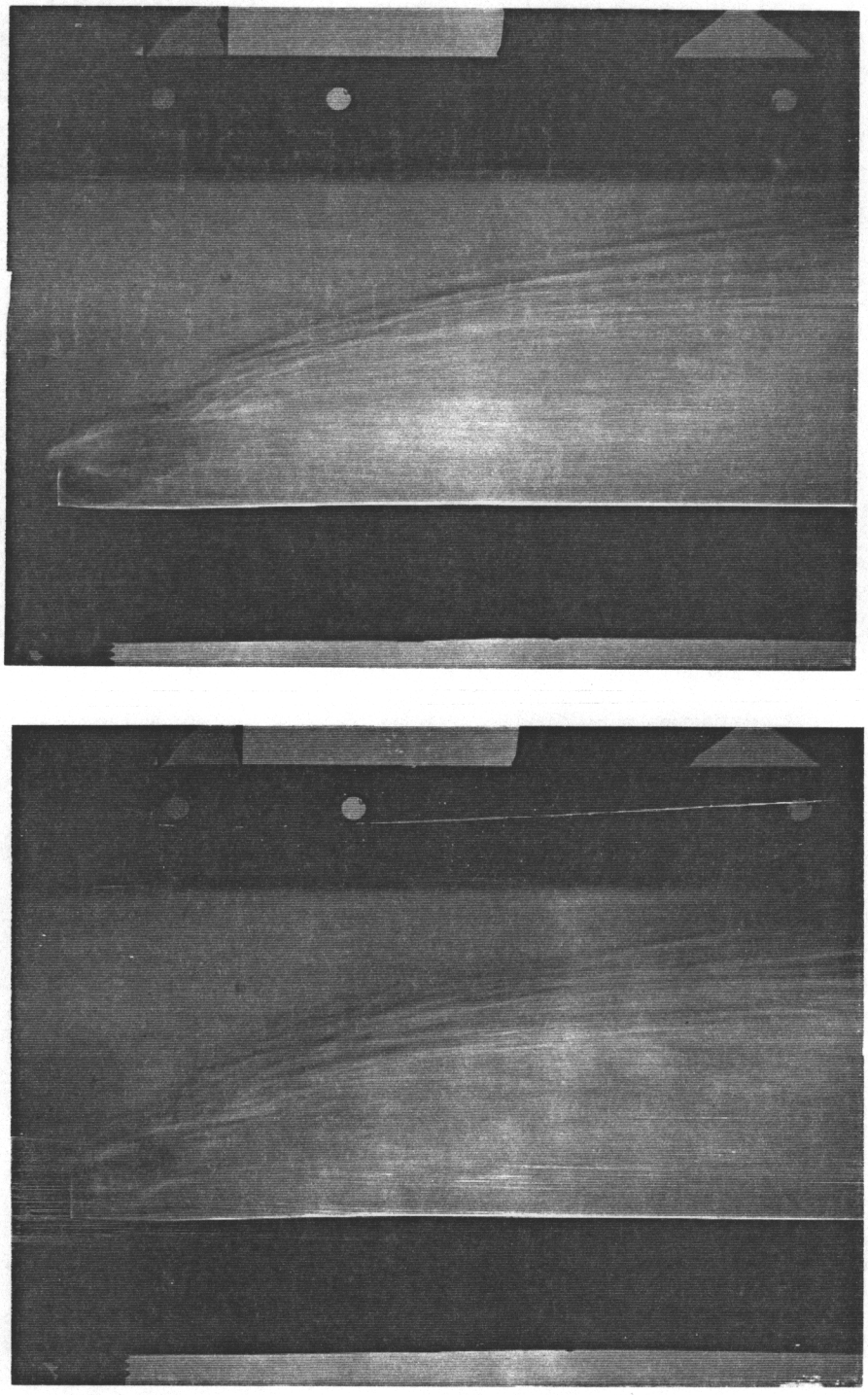

Figure 28. Long Duration Shadowgraphs (1/400 second), ϕ = 0.84, U = 5.1 m/s: (Top) V = 0.0 kVDC, (Bottom) V = 2.0 kVDC

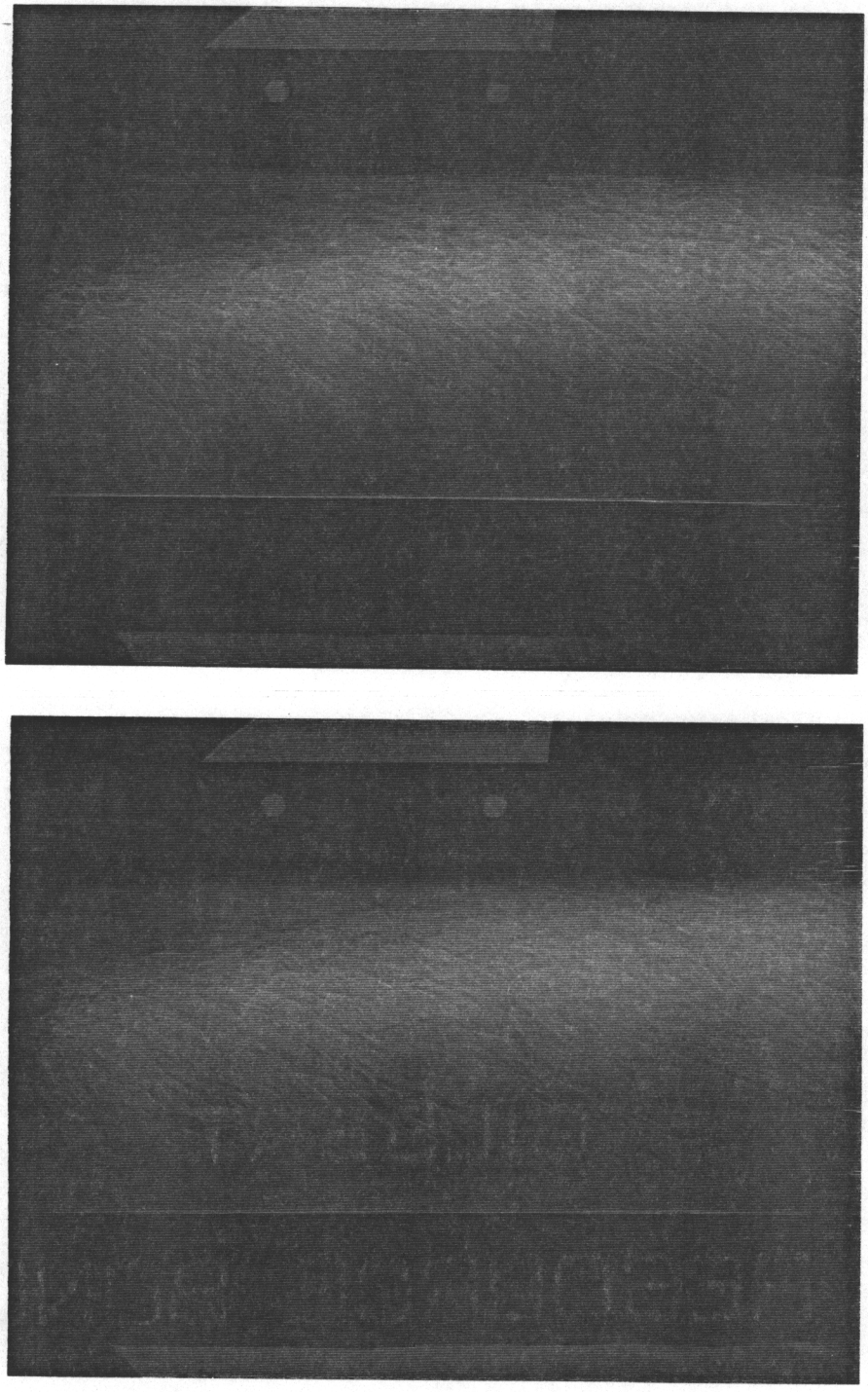

Figure 29. **Multi-exposure Shadowgraphs, ϕ = 0.76, U = 5.7 m/s: (Top) V = 0.0 kVDC, (Bottom) V = 1.2 kVDC**

4.2.4 Photographs

An initial set of photographs was made to determine the most appropriate camera settings. These were determined to be an exposure duration of 1 second with an F-stop value of 16. These values are used for all test conditions. Photographs are made when the heat-loaded electrode reaches a predetermined temperature range. Conditions investigated are included in Table 10. Representative photographs are presented with the remainder being in Appendix C. Some photographs (as with shadowgraphs) are presented in pairs taken at slightly different values of velocity and equivalence ratio. The values are given separated by a slash, with the first value being for the upper photograph and the second value being for the lower one.

Two photographs are shown in Figure 30. The main body of the luminous zone does not appear to be displaced by the applied field although a diffuse luminous area is apparent above it and near the upper electrode for the applied voltage of 3.6 kVDC. As discussed concerning the shadowgraphs, it may be the ion stream can flow across the smaller distances between the upper electrode and the reaction zone in this area. This effect is apparent in all photographs which contact the upper electrode. It could also be said that due to this action at least some percentage of fuel consumption is taking place farther upstream. This would act to increase gas temperatures in the combustor to at least some degree.

Displacement of the lower boundary of the reaction zone is not as apparent as with the upper boundary. This disparity between movement of the upper and lower boundaries of the reaction zone is noticed somewhat for all conditions investigated. The higher inlet

Table 10. Premixed Flame Conditions for Photographs

Equivalence Ratio, ϕ	Inlet Velocity, m/s	Voltage, kVDC	Current, mA
0.74	4.5	0.0	0.0
0.74	4.5	3.6	4.0
0.84	4.7	0.0	0.0
0.84	4.7	2.6	4.0
0.92	4.9	0.0	0.0
0.91	4.9	2.3	4.0
0.74	5.9	0.0	0.0
0.75	5.9	3.6	4.0
0.86	6.1	0.0	0.0
0.86	6.1	2.4	4.0
1.03	5.9	0.0	0.0
1.01	6.1	2.1	4.0
0.65	6.8	0.0	0.0
0.65	6.8	4.6	1.0
0.76	6.8	0.0	0.0
0.77	6.8	2.8	3.0
0.88	7.1	0.0	0.0
0.88	7.1	2.4	4.0
0.74	9.5	0.0	0.0
0.72	9.8	5.2	1.0
0.82	9.9	0.0	0.0
0.82	9.9	3.2	3.0

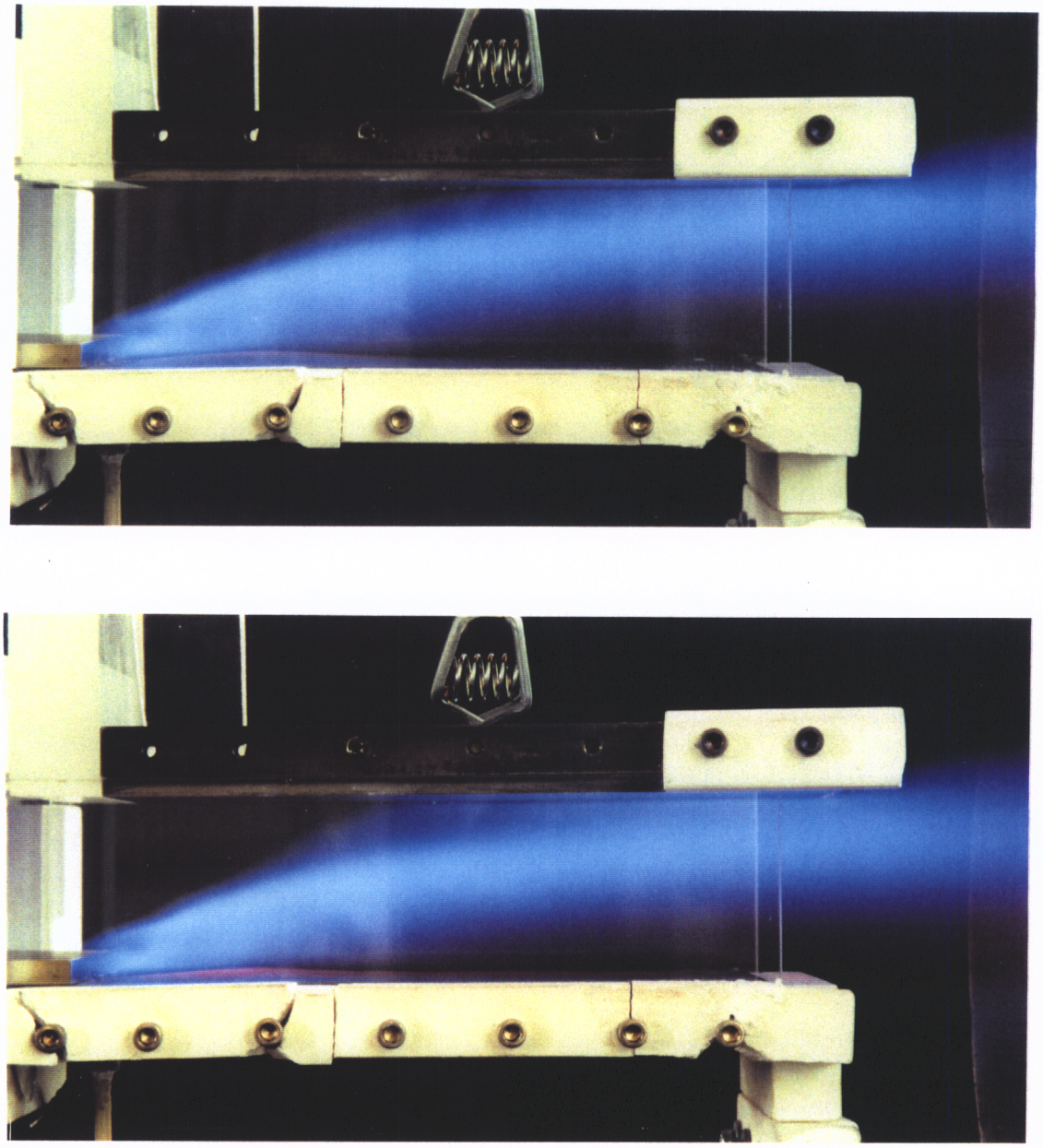

Figure 30. Photographs, ϕ = 0.74, U = 4.5 m/s: (Top) V = 0.0 kVDC, (Bottom) V = 3.6 kVDC

velocity cases do display the greatest movement of the lower boundary. This can be seen by comparing Figure 31 with Figure 30. It is noted that for this case the reaction zone is not in contact with the upper electrode. This may cause the electric field to be more uniform because the ion stream must flow more perpendicular to the flow. Applied voltages are 0.0 and 5.2 kVDC. The higher applied voltage than in Figure 30 is possible because the flame does not contact the upper electrode. Some displacement of the entire luminous zone is apparent, especially near the downstream end of the combustor. The lower boundary of the luminous zone is displaced roughly the same as the upper boundary.

Higher equivalence ratios would be expected to increase the electric field effect because of the presence of more charged species. This is somewhat apparent in the photographs but not appreciably demonstrated by any particular case. The geometry impedes a comparison of this type, because the increase in flame angle associated with an increase in equivalence ratio advances the flame into contact with the upper electrode. This reduces the applicable voltage and may distort the electric field. Analysis would be aided if cases could be compared with a significant separation of the flame from the upper electrode.

4.2.5 Analysis

Photographs of the luminous zone of the flame indicate some field-induced displacement. Consideration of this and the shadowgraph analysis suggest that in some cases the electric field does not significantly affect the bulk flow, but it may cause the

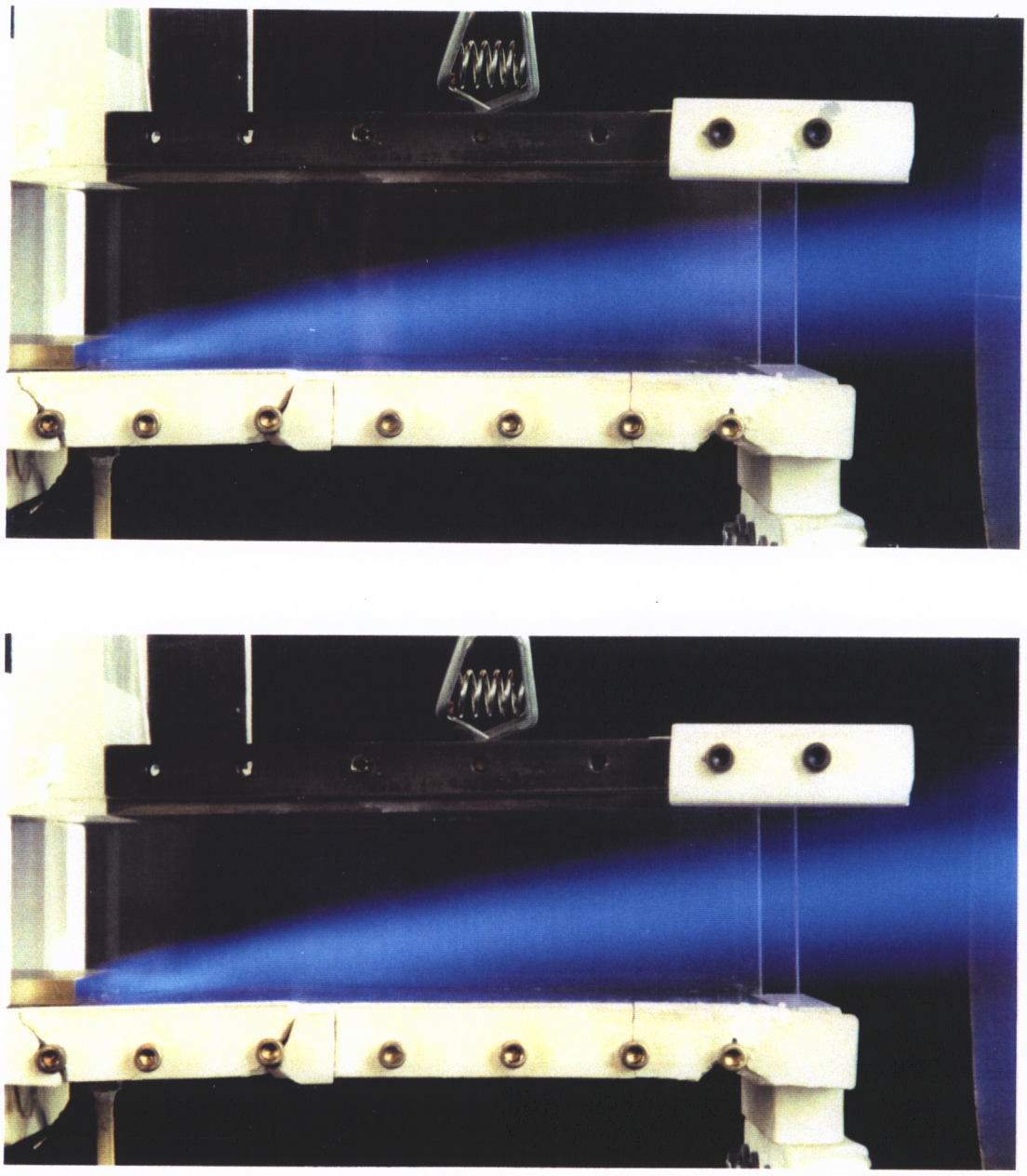

Figure 31. Photographs, ϕ = 0.72/0.74, U = 9.5/9.8 m/s: (Top) V = 0.0 kVDC, (Bottom) V = 5.2 kVDC

positively charged radicals or carbon particles to migrate a limited distance through the unreacted mixture toward the negative electrode. The luminous zone expansion may be a result of this action. Some distortion of the flame fronts may also be occurring, effectively increasing apparent flame speed by increasing the flame surface area. This effect is similar to that investigated by Salamandra and Maiorov [3].

The step stabilizer configuration does not allow for replacement of hot products with cool reactants as with the rod-stabilized diffusion mode. The reduction in heat transfer must occur by a thickening of the boundary layer or a shifting of the post-step reattachment point. The boundary layer thickening concept is illustrated in Figure 32. The idealized velocity distribution downstream shows how flow is redirected by an applied body force towards the upper electrode.

The fact that the reaction zone is in contact with the ground electrode just downstream of the step and with the upper electrode further downstream may cause significant field distortion. That is, resulting body forces may not be acting perpendicular to the flow. This is supported indirectly by the limited displacement of the luminous zone near the upper electrode demonstrated by photographic data. It is possible that the positive ion stream flows diagonally from the grounded lower electrode to the negatively charged upper electrode. A distribution of electric potential can be inferred from this and is displayed in Figure 33. This shows how the body force acting on the flow may be directed significantly downstream. The effect of this would be diminished results compared to those caused by a perpendicular field.

Another possible contributor to lack of heat transfer amelioration may be an

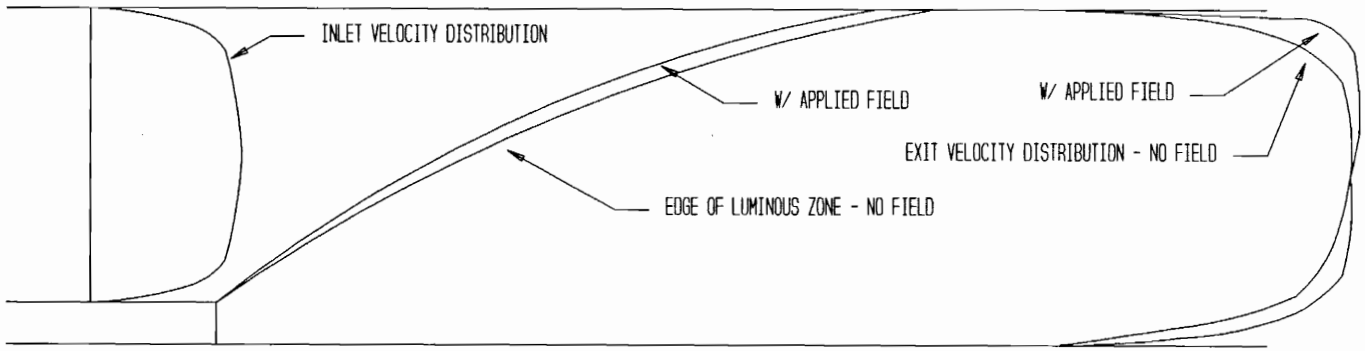

Figure 32. Idealized Concept of Flowfield Alteration for the Step Combustor

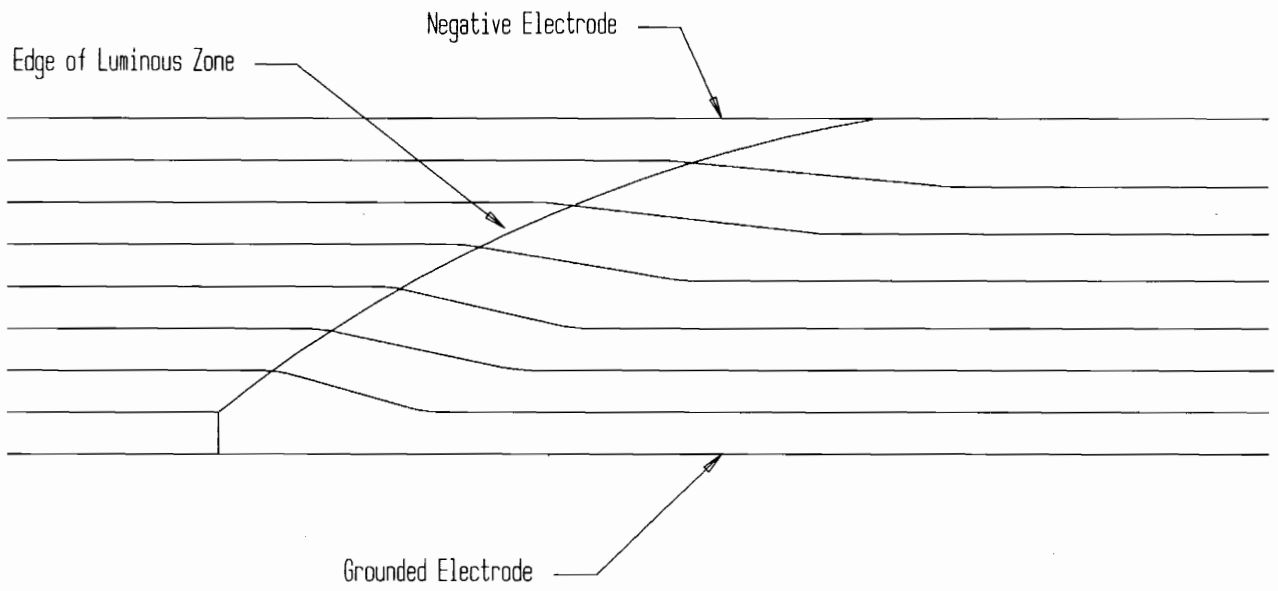

Figure 33. Rough Estimate of Electric Field (Lines of Constant Potential)

increase in the combustor gas temperatures caused by a displacement of the reaction zone upstream. The displacement of the luminous zone observed in photographic analysis supports this to some extent. The increase in gas temperature may primarily occur near the upper electrode. This would not directly increase the temperature of the reactants passing near the wall through conduction, but may do so through mixing and increased radiation. This phenomenon, if it is occurring, would increase heat transfer rates and negate any decrease due to boundary layer thickening or reattachment point displacement.

5 Conclusions and Recommendations

5.1 Conclusions

A small field-induced decrease in the temperature of the exposed surface of the heat-loaded electrode was noted for the diffusion flame. The yellow-orange portion of the luminous zone was shortened significantly and displaced away from the heat-loaded electrode. Downstream flow features apparent in shadowgraphs were similarly displaced.

Two mechanisms are concluded to be responsible for observed effects on heat transfer. The first involves bulk alteration of the flowfield and has two effects. One effect reduces heat transfer from the flame and involves an increase in flow under the stabilizer. This reduces heat transfer by displacing the reaction zone away from the heat-loaded electrode. The other effect increases heat-loaded electrode temperatures by displacing the flame upstream. This increases heat transfer to some degree by increasing gas temperatures in the combustor. The second mechanism decreases heat transfer through a reduction in soot (reduced luminosity). The applied electric field intervenes in soot production and/or soot destruction. Decreased soot would decrease radiative heat transfer to the combustor walls.

No decrease in heat-loaded electrode temperature was noted for the premixed step-

stabilized flame. Some displacement of the flowfield was noted in both the shadowgraphs and photographs. A distinct disturbance is observed near the surface of the negatively charged upper electrode and may be a result of ion stream flow through the thin layer of cool reactants.

A geometry unsuited to field-induced bulk flowfield displacement is partially responsible for the lack of heat transfer reduction for the step-stabilized combustor. No large flowfield alteration is seen. This may be a result to some extent of electric field distortion caused by the geometry. Flame contact with both electrodes produces an ion stream which flows somewhat parallel to the bulk flow. Body forces, therefore, do not act to displace flow away from the heat-loaded electrode which would increase the boundary layer thickness and decrease heat transfer. Another contributor is the smaller number of soot or carbon particles in a premixed flame as compared to a diffusion flame. They act to increase attainable body forces. Also, any displacement of the reaction zone upstream, although limited, may act to increase heat transfer by increasing gas temperatures in the combustor.

The differences in observed electric field effects between the two phases of the investigation are attributable to several factors. The premixed flame could not be operated at low velocities because of the danger of flashback. Low velocities are expected to allow more pronounced alteration of the flowfield because of increased residence times and a higher ratio of body force to momentum. Diffusion flames contain higher concentrations of carbon particles than a premixed flame. This acts to increase the attainable body force. Further, the premixed flame was generally in contact with both

electrodes because the entire cross section is reactive. This reduces the maximum attainable applied voltage and may distort the electric field. It was possible to operate the diffusion mode without flame contact with both electrodes.

5.2 Recommendations

Further study of the non-premixed mode is suggested. Increased heat transfer reduction may be attainable if the stabilizer can be located higher in the combustor. A drawback would be that this would cause dual electrode flame impingement and problems with arcing from the injector/stabilizer (typically grounded) to the charged electrode. A larger combustor and modifications allowing electrical isolation of the stabilizer would allow it to be moved upward. Premixed rod-stabilized flames may also be of interest if analyzed using this combustor modified as such.

Although the geometry is not as accommodating to field-induced heat transfer reduction as that of the rod-stabilized diffusion flame, further study of the effect of an applied electric field is suggested for the step-stabilized premixed flame. Careful consideration should be taken to allow testing without flame contact with both electrodes and at low velocities. The study of fuel-rich conditions should also allow favorable results because of increased soot production which can increase attainable body force strength.

The convective cooling of the lower electrode is difficult or impossible to control. In addition, it requires significant warm-up periods and high peak-temperature operation.

A controlled forced-convection system would increase complexity but allow more experimental control and repeatability.

The shadowgraphs are effective in analyzing flame front progression and other flowfield attributes. They are however limited because of the number of images required to make useful observations of the randomly fluctuating turbulent flowfield. Long duration shadowgraphs can give highly time-averaged data, but high-contrast images are difficult to attain and interpret. Shadowgraph movies using a video system could prove quite informative.

Measurement of heat flow would benefit from non-intrusive temperature measurement of the electrode surface exposed to the flame. This could be combined with lower surface temperature data to determine local heat flux rates and flame convective heat transfer coefficients. Also, a heat flux microsensor such as that developed by Hager et al. [16] might prove helpful if problems associated with high applied voltages and temperature survivability can be overcome.

Improved visualization, heat flow quantification, and a forced-convection cooling system would all be beneficial to the acquisition of good data, but are not absolute necessities. These things are limited by additional complexity and cost. Modification of the combustor geometry is the best next step in the investigation of heat transfer amelioration by application of electric fields.

References

1. Lawton, J. and F. J. Weinberg, Electrical Aspects of Combustion, Clarendon Press, Oxford, 1969.

2. Lawton, J., P. J. Mayo, and F. J. Weinberg, "Electrical Control of Gas Flows in Combustion Processes," Proc. Roy. Soc., A303, pp. 275-298, 1968.

3. Salamandra, G. D., and N. I. Maiorov, "Instability of a Flame Front in an Electrical Field," Comb. Expl. and Shock Waves, v14, n3, pp. 90-96, 1978.

4. Payne, K. G., and F. J. Weinberg, "A Preliminary Investigation of Field-induced Ion Movement in Flame Gases and Its Applications," Proc. R. Soc., A250, pp. 316-336, 1959.

5. Sandhu, S. S., and F. J. Weinberg, "Laser Interferometric Studies of the Control of Heat Transfer from Flame Gases by Electric Fields," Comb. and Flame, v25, pp. 321-334, 1975.

6. Clements, R. M., and P. R. Smy, "The Effect of Electrohydrodynamic Boundary Layers on Heat Transfer from Flame Gases," Comb. and Flame, v29, pp. 33-41, 1977.

7. Oakes, B. K.,"Reduction of Convective Heat Transfer to a Flat Plate by Application of an Electric Field," Undergraduate Research Paper, VPI&SU, 1991.

8. Calcote, H. F., and R. N. Pease, "Electrical Properties of Flames," Ind. Engng Chem. ind. Edn., v43, pp. 2726-2731, 1951.

9. Mitchell, J. E., and F. J. Wright, "Effects in Diffusion Flames By Radial Electric Fields," Comb. and Flame, v13, pp. 413-418, 1969.

10. Heinsohn, R. J., C. F. Wilhelm, Jr., and P. M. Becker, "Effect of Electric Fields on Ducted Diffusion Flames," Comb. and Flame, v14, pp. 341-349, 1970.

11. Place, E. R., and F. J. Weinberg, "Electrical Control of Flame Carbon," Proc. R. Soc., A289, pp. 192-205, 1965.

12. Mayo, P. J., L. A. Watermeier, and F. J. Weinberg, "Electrical Control of Solid Propellant Burning," Proc. R. Soc., A284, pp. 488-498, 1965.

13. Noorani, R. I., and R. E. Holmes, "Effects of Electric Fields on the Flame Propagation Velocity of Methane-Air Flame," AIAA Journal, v24, n1, pp. 190-192, 1986.

14. Kishi, T., L. Xie, and M. Kono, "Effects of DC Electric Fields on Laminar Burning Velocity by Using Different Types of Premixed Gas Burners," Presented at Poster Session P201 in B-5 at the 24th International Symposium on Combustion, July 5-10, 1992.

15. Ganji, A. R., and R. F. Sawyer, "Experimental Study of the Flowfield of a Two-Dimensional Premixed Turbulent Flame," AIAA Journal, v18, n7, pp. 817-824, 1980.

16. Hager, J. M., S. Simmons, D. Smith, S. Onishi, L. W. Langley, and T. E. Diller, "Experimental Performance of a Heat Flux Microsensor," ASME Paper 90-GT-256, 1990.

Appendix A: Computer Programs

The computer programs used to reduce, average, and normalize data are given on the following pages. All programs were written in FORTRAN 77 on an IBM Personal Computer.

```
      PROGRAM HEXTEM
C     Written by Brian K. Oakes, Summer 1992
C     This program converts temperatures coded in hexadecimal form into decimal
C     values.  It also adds a nondimensional coordinate (x/D or x/H) representing the
C     distance downstream of the stabilizer (step or rod).
      CHARACTER*1 FB(16), SB(16)
      REAL RFB(16), RSB(16), TEMP, HIGH, LOW, STEP, SHIFT, X
      X = 0.0
C     Opem source file containing hexadecimal temperature data
      OPEN (UNIT=19,FILE='RUNA.304')
C     Open target files for converted data
      OPEN (UNIT=1,FILE='tempA1.304')
      OPEN (UNIT=2,FILE='tempA2.304')
      OPEN (UNIT=3,FILE='tempA3.304')
      OPEN (UNIT=4,FILE='tempA4.304')
      OPEN (UNIT=5,FILE='tempA5.304')
      OPEN (UNIT=6,FILE='tempA6.304')
      OPEN (UNIT=7,FILE='tempA7.304')
      OPEN (UNIT=8,FILE='tempA8.304')
      OPEN (UNIT=9,FILE='tempA9.304')
      OPEN (UNIT=10,FILE='tempA10.304')
      OPEN (UNIT=11,FILE='tempA11.304')
      OPEN (UNIT=12,FILE='tempA12.304')
      OPEN (UNIT=13,FILE='tempA13.304')
      OPEN (UNIT=14,FILE='tempA14.304')
      OPEN (UNIT=15,FILE='tempA15.304')
      OPEN (UNIT=16,FILE='tempA16.304')
      OPEN (UNIT=17,FILE='tempA17.304')
      OPEN (UNIT=18,FILE='tempA18.304')
      DO 30 J = 1,18
C     Read high and low values of imaging system scale (added to data files after
C     acquisition)
      READ (19,*) HIGH,LOW
      PIXEL = 0
C     Read temperatures coded in hexadecimal form
      DO 20 COUNT = 1,16
      READ (19,100) FB(1),SB(1),FB(2),SB(2),FB(3),SB(3),FB(4),SB(4),FB(5
     *),SB(5),FB(6),SB(6),FB(7),SB(7),FB(8),SB(8),FB(9),SB(9),FB(10),SB(
     *10),FB(11),SB(11),FB(12),SB(12),FB(13),SB(13),FB(14),SB(14),FB(15)
     *,SB(15),FB(16),SB(16)
  100 FORMAT (1A,1A,1X,1A,1A,1X,1A,1A,1X,1A,1A,1X,1A,1A,1X,1A,1A,1X,1A,1
     *A,1X,1A,1A,1X,1A,1A,1X,1A,1A,1X,1A,1A,1X,1A,1A,1X,1A,1A,1X,1A,1A,1
     *X,1A,1A,1X,1A,1A,1X)
C     Convert to decimal temperatures
```

```
      DO 10 I = 1,16
      IF (FB(I).EQ.'1') RFB(I) = 1.0
      IF (SB(I).EQ.'1') RSB(I) = 1.0
      IF (FB(I).EQ.'2') RFB(I) = 2.0
      IF (SB(I).EQ.'2') RSB(I) = 2.0
      IF (FB(I).EQ.'3') RFB(I) = 3.0
      IF (SB(I).EQ.'3') RSB(I) = 3.0
      IF (FB(I).EQ.'4') RFB(I) = 4.0
      IF (SB(I).EQ.'4') RSB(I) = 4.0
      IF (FB(I).EQ.'5') RFB(I) = 5.0
      IF (SB(I).EQ.'5') RSB(I) = 5.0
      IF (FB(I).EQ.'6') RFB(I) = 6.0
      IF (SB(I).EQ.'6') RSB(I) = 6.0
      IF (FB(I).EQ.'7') RFB(I) = 7.0
      IF (SB(I).EQ.'7') RSB(I) = 7.0
      IF (FB(I).EQ.'8') RFB(I) = 8.0
      IF (SB(I).EQ.'8') RSB(I) = 8.0
      IF (FB(I).EQ.'9') RFB(I) = 9.0
      IF (SB(I).EQ.'9') RSB(I) = 9.0
      IF (FB(I).EQ.'A') RFB(I) = 10.0
      IF (SB(I).EQ.'A') RSB(I) = 10.0
      IF (FB(I).EQ.'B') RFB(I) = 11.0
      IF (SB(I).EQ.'B') RSB(I) = 11.0
      IF (FB(I).EQ.'C') RFB(I) = 12.0
      IF (SB(I).EQ.'C') RSB(I) = 12.0
      IF (FB(I).EQ.'D') RFB(I) = 13.0
      IF (SB(I).EQ.'D') RSB(I) = 13.0
      IF (FB(I).EQ.'E') RFB(I) = 14.0
      IF (SB(I).EQ.'E') RSB(I) = 14.0
      IF (FB(I).EQ.'F') RFB(I) = 15.0
      IF (SB(I).EQ.'F') RSB(I) = 15.0
      IF (FB(I).EQ.'0') RFB(I) = 0.0
      IF (SB(I).EQ.'0') RSB(I) = 0.0
      TEMP = (RFB(I) * 16.0 + RSB(I)) / 255.0 * (HIGH-LOW) + LOW
C     Add nondimensional coordinate and write values to files
      SHIFT = 15.94 * (1-X)
      STEP = ((213.6-SHIFT)-real(pixel))*0.0819
      WRITE (J,*) STEP,TEMP
      PIXEL = PIXEL + 1
 10   CONTINUE
 20   CONTINUE
      CLOSE (UNIT=J)
 30   CONTINUE
      END
```

```
      PROGRAM AVER
C     Written by Brian K. Oakes, Spring 1993
C     This program averages temperature files (decimal form).
      REAL FFILE(256), TFILE(256), AFILE(256), STEP(256)
      INTEGER COUNT, NUMBER
C     Open temperature files to be averaged
      OPEN (UNIT=1,FILE='TEMPB1.303')
      OPEN (UNIT=2,FILE='TEMPB3.303')
      OPEN (UNIT=3,FILE='TEMPB4.303')
      OPEN (UNIT=4,FILE='TEMPB9.303')
      OPEN (UNIT=5,FILE='TEMPB10.303')
      OPEN (UNIT=6,FILE='TEMPB11.303')
      OPEN (UNIT=7,FILE='TEMPB12.303')
C     Open new file for averaged temperatures
      OPEN (UNIT=9,FILE='NVLTSAVB.303')
      DO 5 COUNT= 1,256
      TFILE(COUNT) = 0.0
 5    CONTINUE
C     Read and sum temperature values from files
      DO 10 NUMBER = 1,7
      DO 20 COUNT = 1,256
      READ (NUMBER,*) STEP(COUNT),FFILE(COUNT)
      TFILE(COUNT) = TFILE(COUNT) + FFILE(COUNT)
 20   CONTINUE
      CLOSE (UNIT=NUMBER)
 10   CONTINUE
C     Average temperature values
      DO 30 COUNT = 1,256
      AFILE(COUNT) = TFILE(COUNT)/7.0
 30   CONTINUE
C     Write averaged values to file
      DO 40 COUNT = 1,256
      WRITE (9,*) STEP(COUNT),AFILE(COUNT)
 40   CONTINUE
      CLOSE (UNIT=NUMBER)
      END
```

```
      PROGRAM NORM
C     Written by Brian K. Oakes, Spring 1993
C     This program determines the peak temperature in a file and normalizes (divides)
C     all temperatures in the file by this value.
      REAL FFILE(256,4), HIGH(4), STEP(256)
      INTEGER COUNT, NUMBER
      HIGH(1) = 0.0
      HIGH(2) = 0.0
      HIGH(3) = 0.0
      HIGH(4) = 0.0
C     Open temperature files
      OPEN (UNIT=1,FILE='TEMP6.926')
      OPEN (UNIT=2,FILE='TEMP2B.926')
      OPEN (UNIT=3,FILE='TEMP3B.926')
      OPEN (UNIT=4,FILE='TEMP4B.926')
      OPEN (UNIT=5,FILE='NTEMP6.926')
      OPEN (UNIT=6,FILE='NTEMP2B.926')
      OPEN (UNIT=7,FILE='NTEMP3B.926')
      OPEN (UNIT=8,FILE='NTEMP4B.926')
C     Determine highest temperature
      DO 10 NUMBER = 1,4
      DO 20 COUNT = 1,256
      READ (NUMBER,*) STEP(COUNT),FFILE(COUNT,NUMBER)
 20   CONTINUE
      DO 30 COUNT = 1,256
      IF (FFILE(COUNT,NUMBER).GT.HIGH(NUMBER))
      *HIGH(NUMBER) = FFILE(COUNT,NUMBER)
 30   CONTINUE
      CLOSE (UNIT=NUMBER)
C     Normalize all temperatures using the highest value
      DO 40 COUNT = 1,256
      FFILE(COUNT,NUMBER) = (FFILE(COUNT,NUMBER)-73.0)
      */ (HIGH(NUMBER) - 73.0)
 40   CONTINUE
C     Write values to files
      DO 50 COUNT = 1,256
      WRITE (NUMBER+4,*) STEP(COUNT),FFILE(COUNT,NUMBER)
 50   CONTINUE
      CLOSE (UNIT=NUMBER+4)
 10   CONTINUE
      END
```

Appendix B: Additional Diffusion Mode Data

Additional shadowgraphs made for the rod-stabilized diffusion flame are given on the following pages.

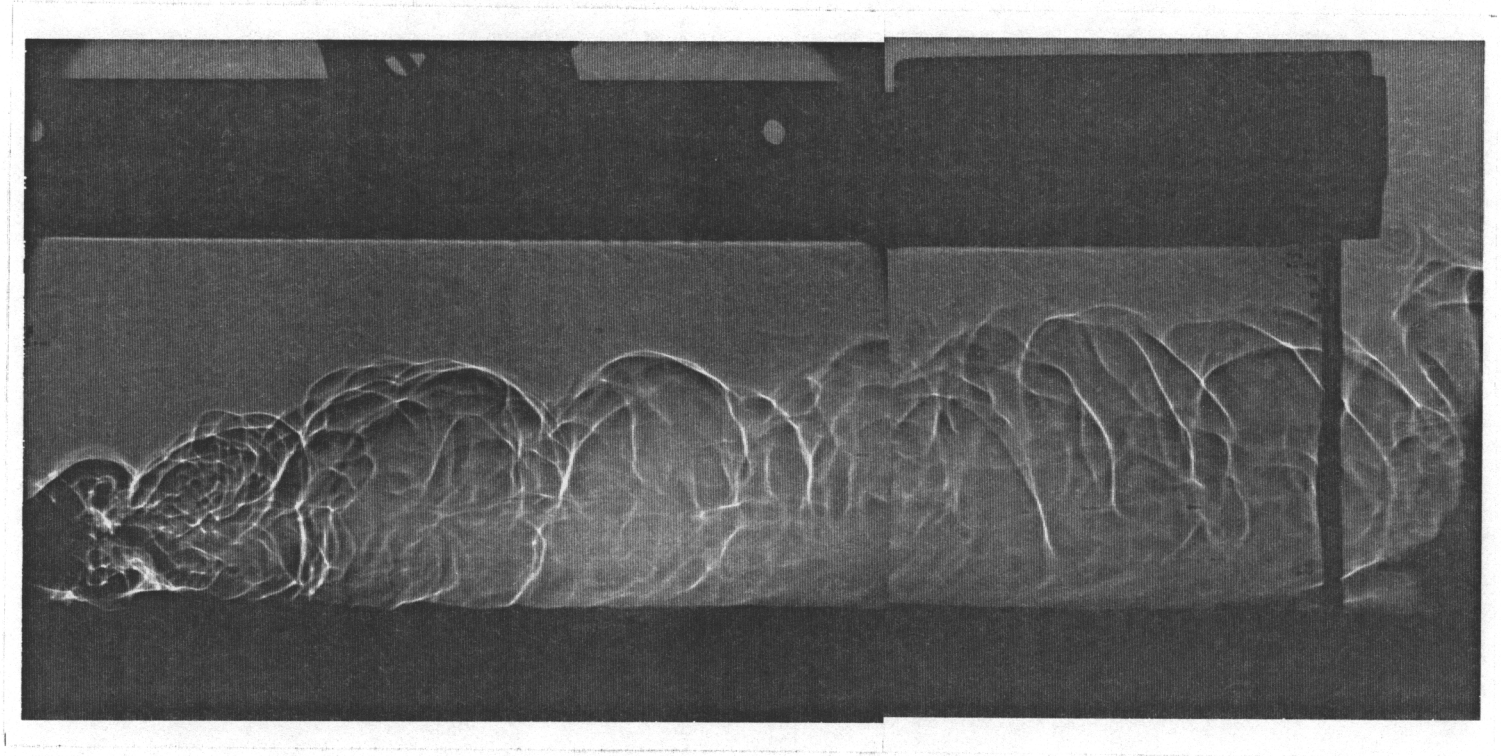

Figure 34. **Composite Shadowgraph, A/F = 320/330, U_a = 3.4/3.5 m/s, V = 0.0 kVDC**

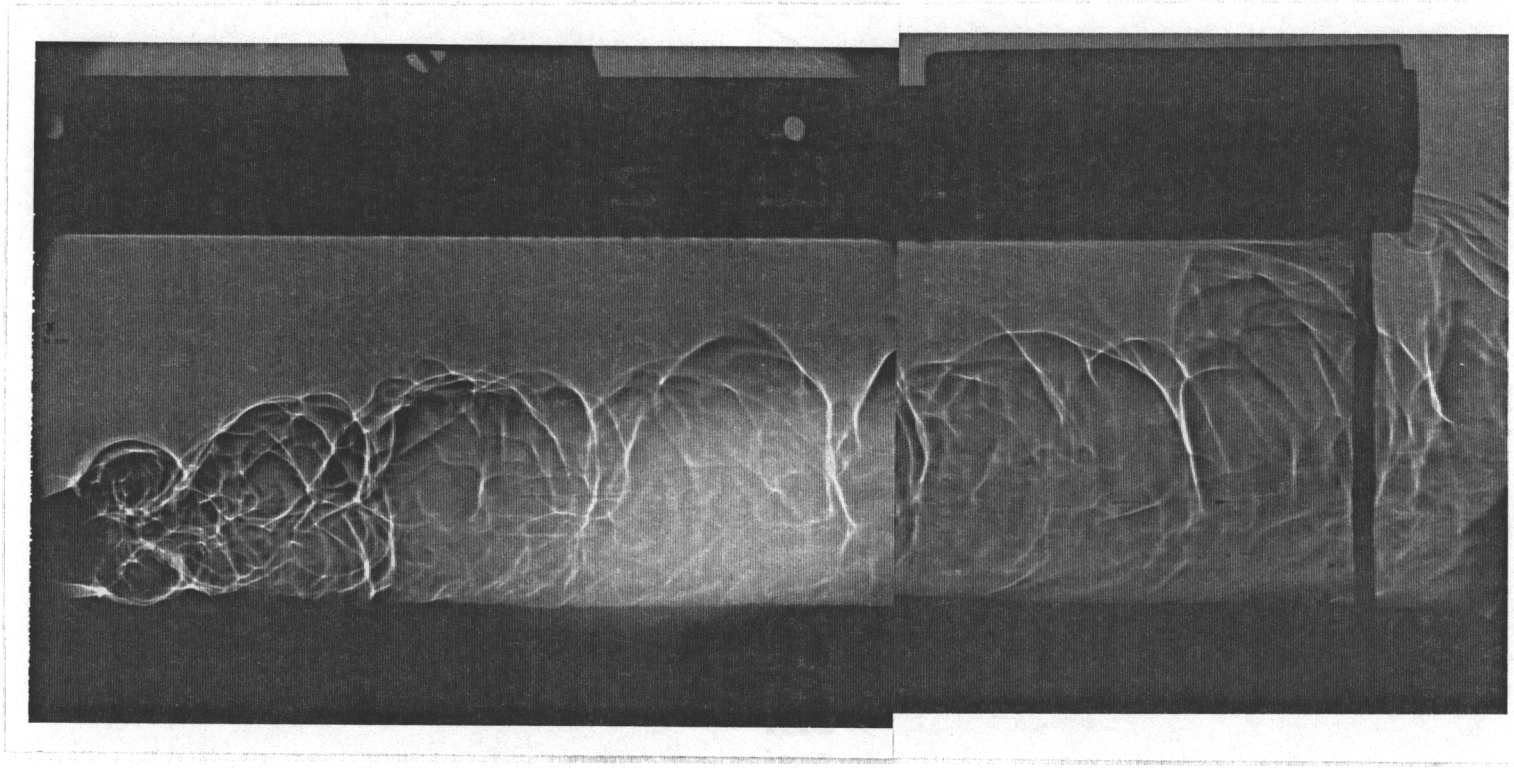

Figure 35. **Composite Shadowgraph, A/F = 320/330, U_a = 3.4/3.5 m/s, V = 4.0 kVDC**

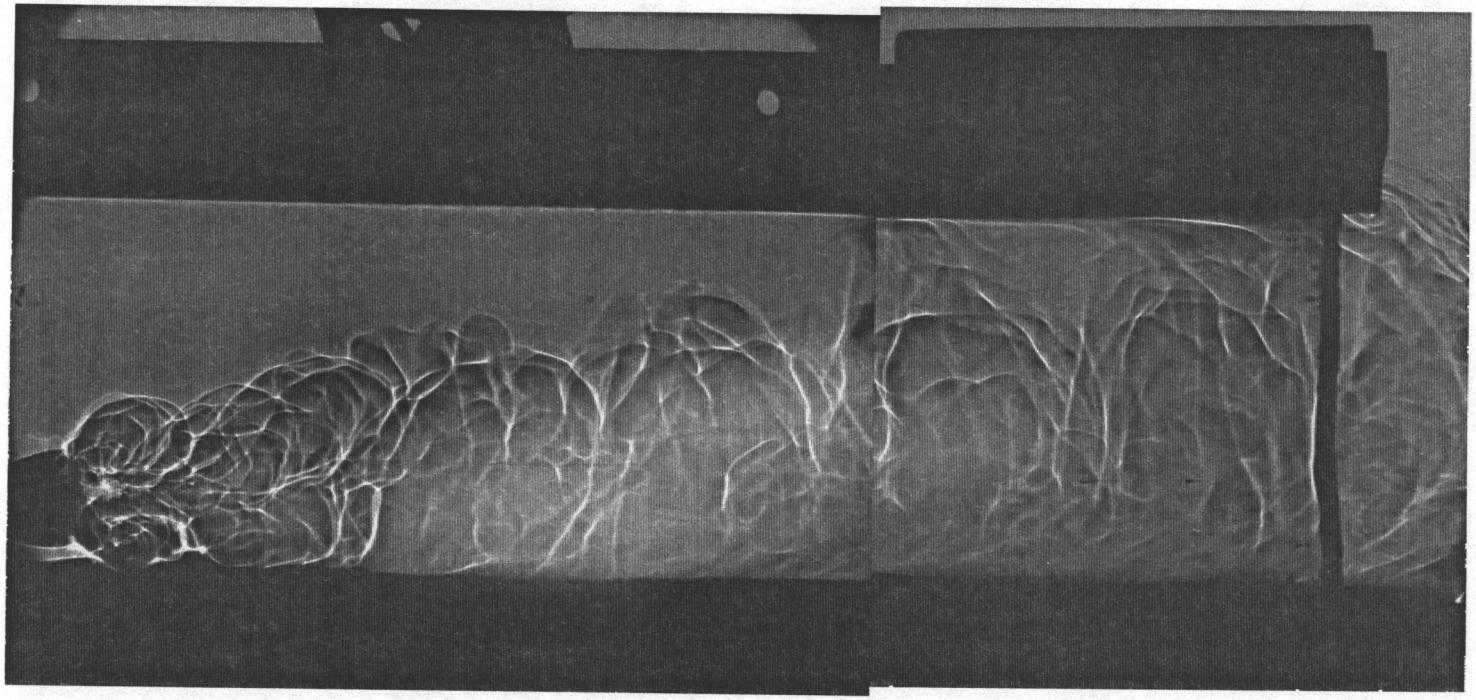

Figure 36. **Composite Shadowgraph, A/F = 320/330, U_a = 3.4/3.5 m/s, V = 8.0 kVDC**

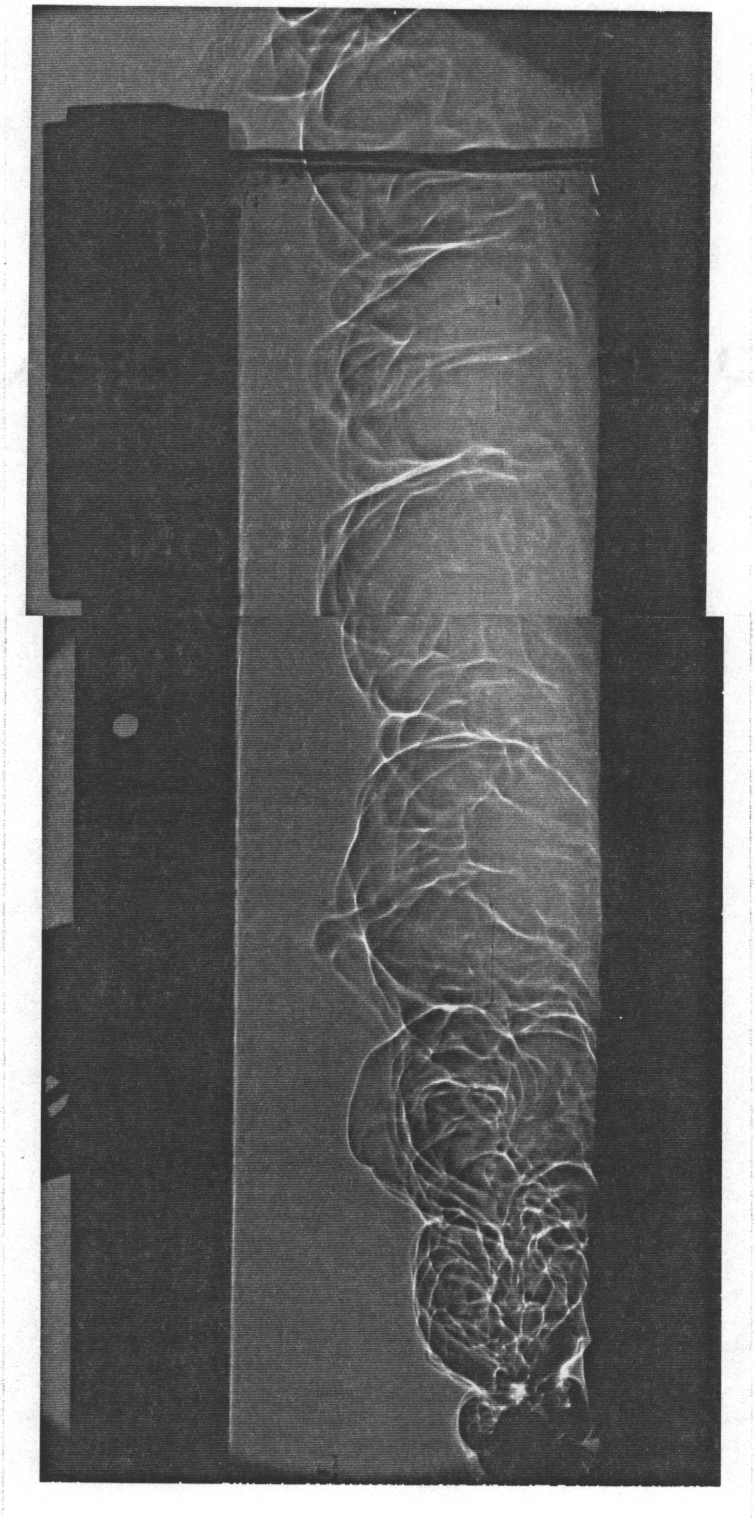

Figure 37. Composite Shadowgraph, A/F = 270/290, U_a = 3.4/3.6 m/s, V = 0.0 kVDC

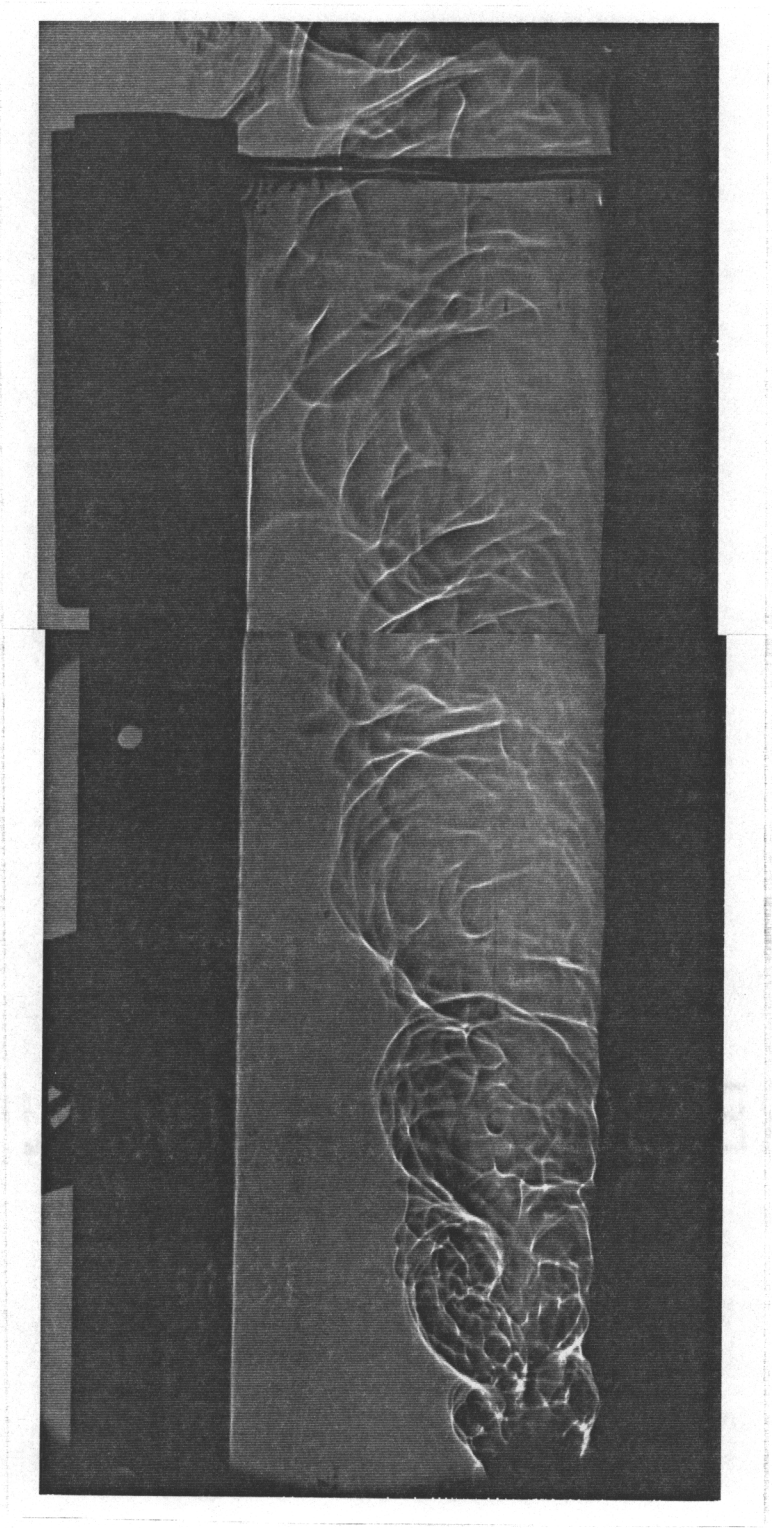

Figure 38. Composite Shadowgraph, A/F = 270/290, U_a = 3.4/3.6 m/s, V = 4.0 kVDC

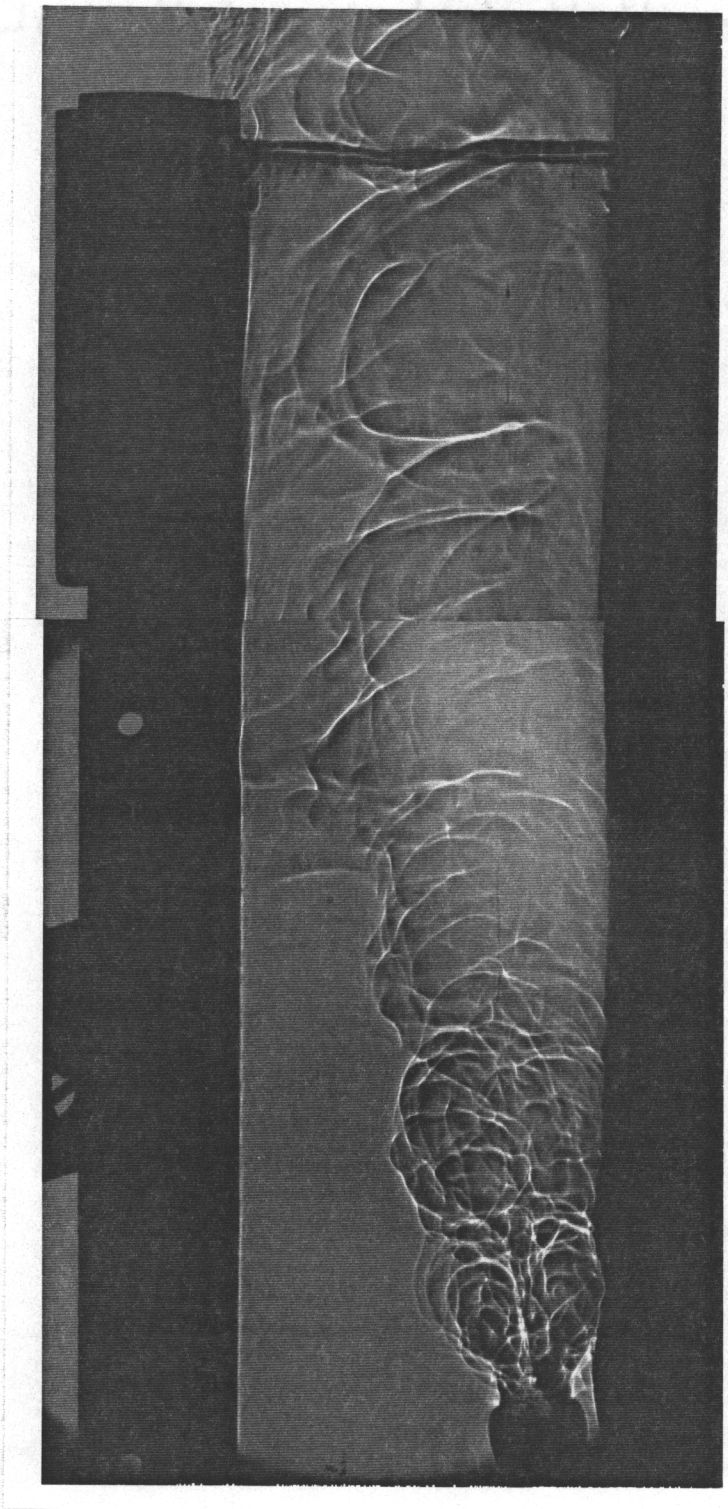

Figure 39. Composite Shadowgraph, A/F = 270/290, U_a = 3.4/3.6 m/s, V = 8.0 kVDC

Appendix C: Additional Premixed Mode Data

Additional shadowgraphs and photographs made for the step-stabilized premixed flame are given on the following pages.

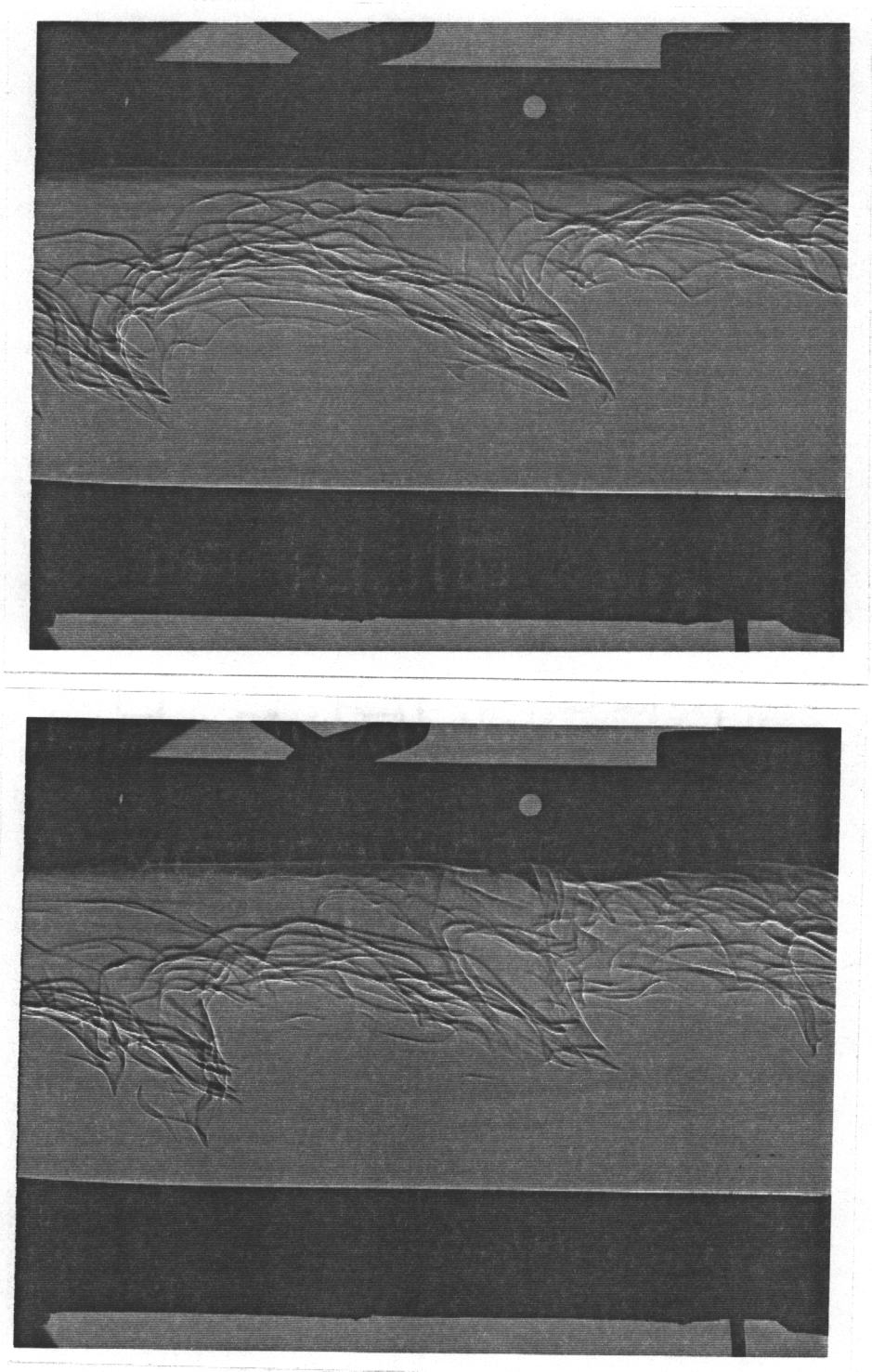

Figure 40. **Shadowgraphs, ϕ = 0.95, U = 4.8 m/s: (Top) V = 0.0 kVDC, (Bottom) V = 2.4 kVDC**

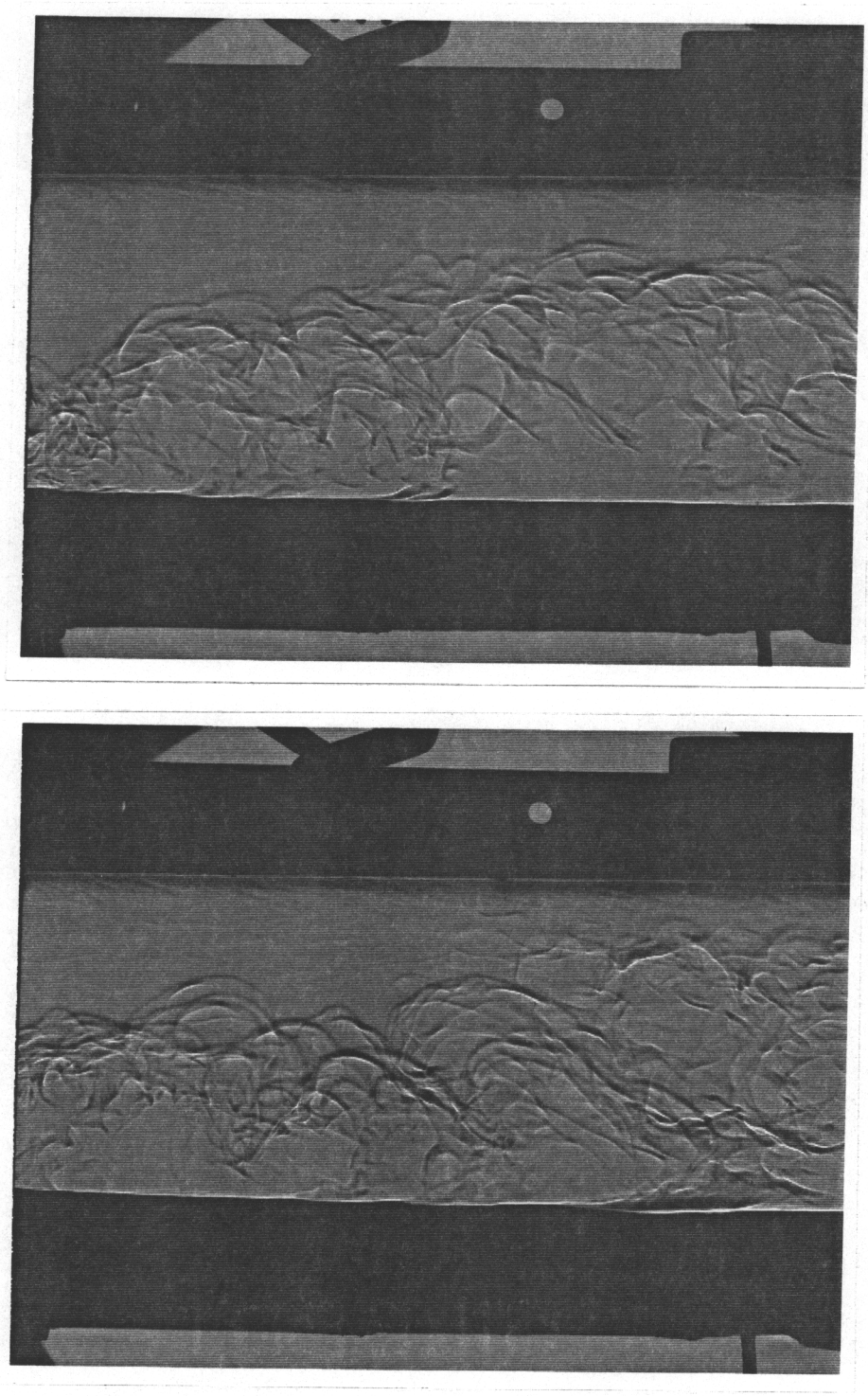

Figure 41. **Shadowgraphs, ϕ = 0.66/0.67, U = 6.7 m/s: (Top) V = 0.0 kVDC, (Bottom) V = 6.6 kVDC**

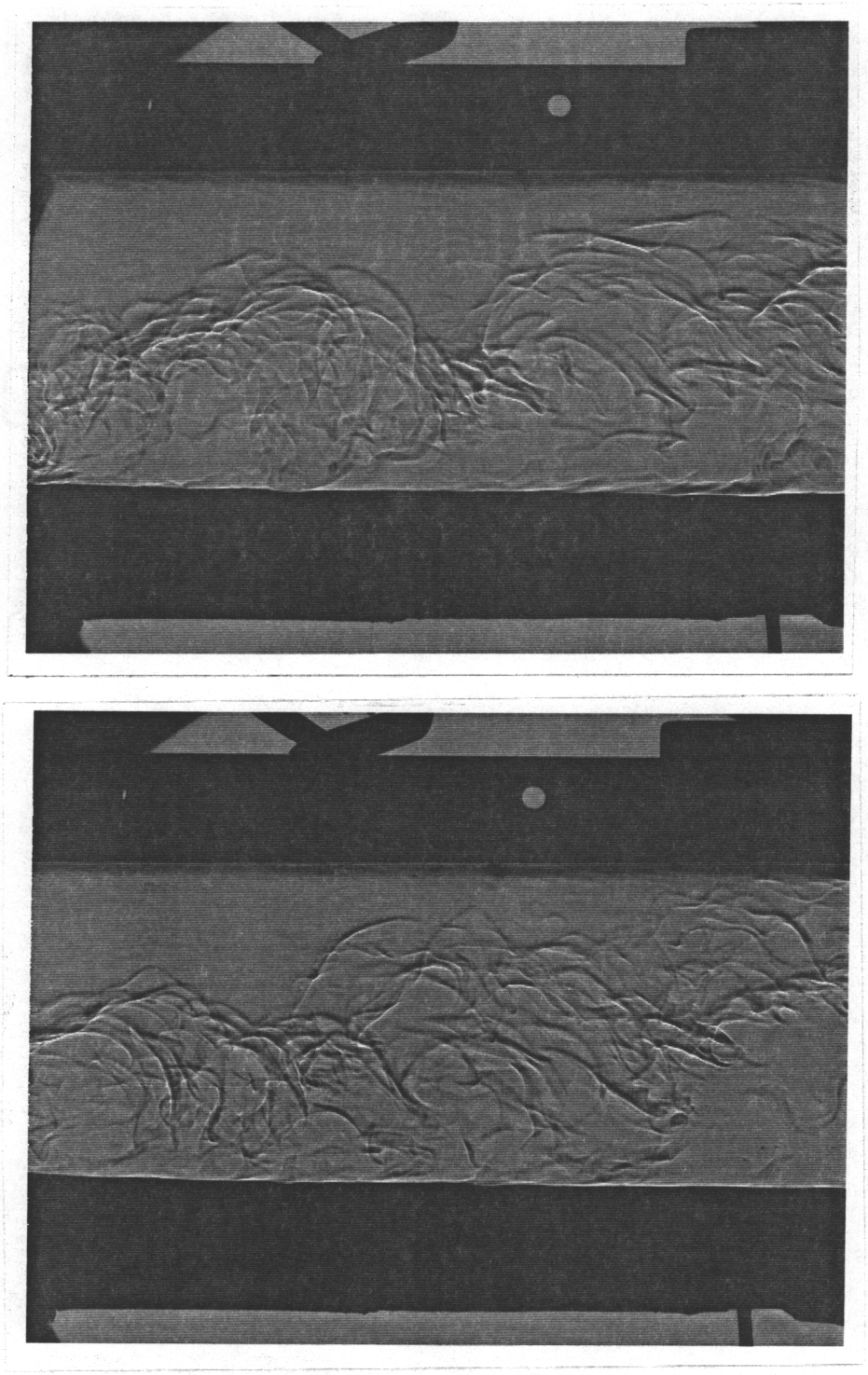

Figure 42. **Shadowgraphs, ϕ = 0.66, U = 6.8/6.7 m/s: (Top) V = 0.0 kVDC, (Bottom) V = 5.6 kVDC**

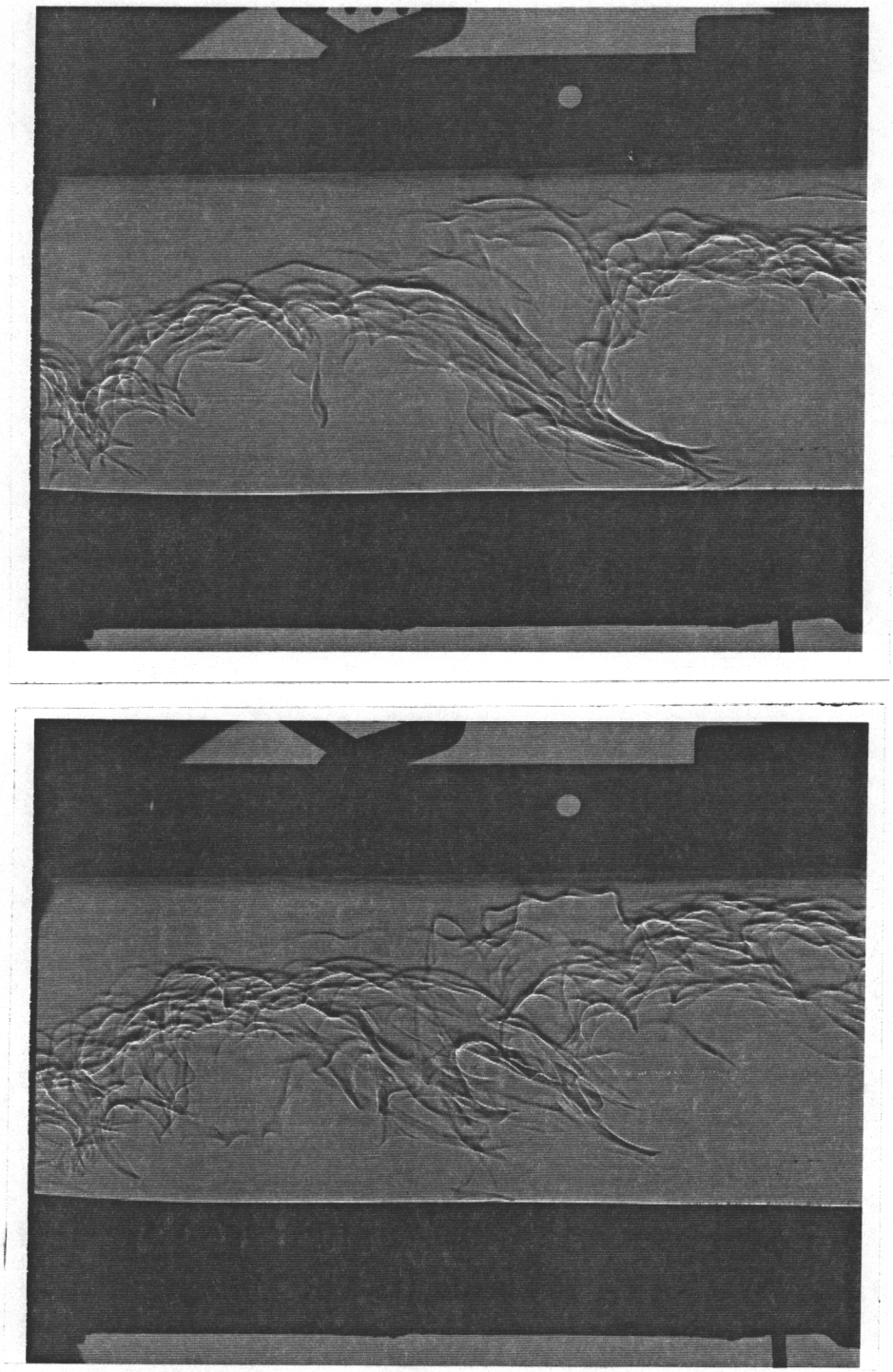

Figure 43. **Shadowgraphs, ϕ = 0.81/0.80, U = 6.6/6.7 m/s: (Top) V = 0.0 kVDC, (Bottom) V = 3.2 kVDC**

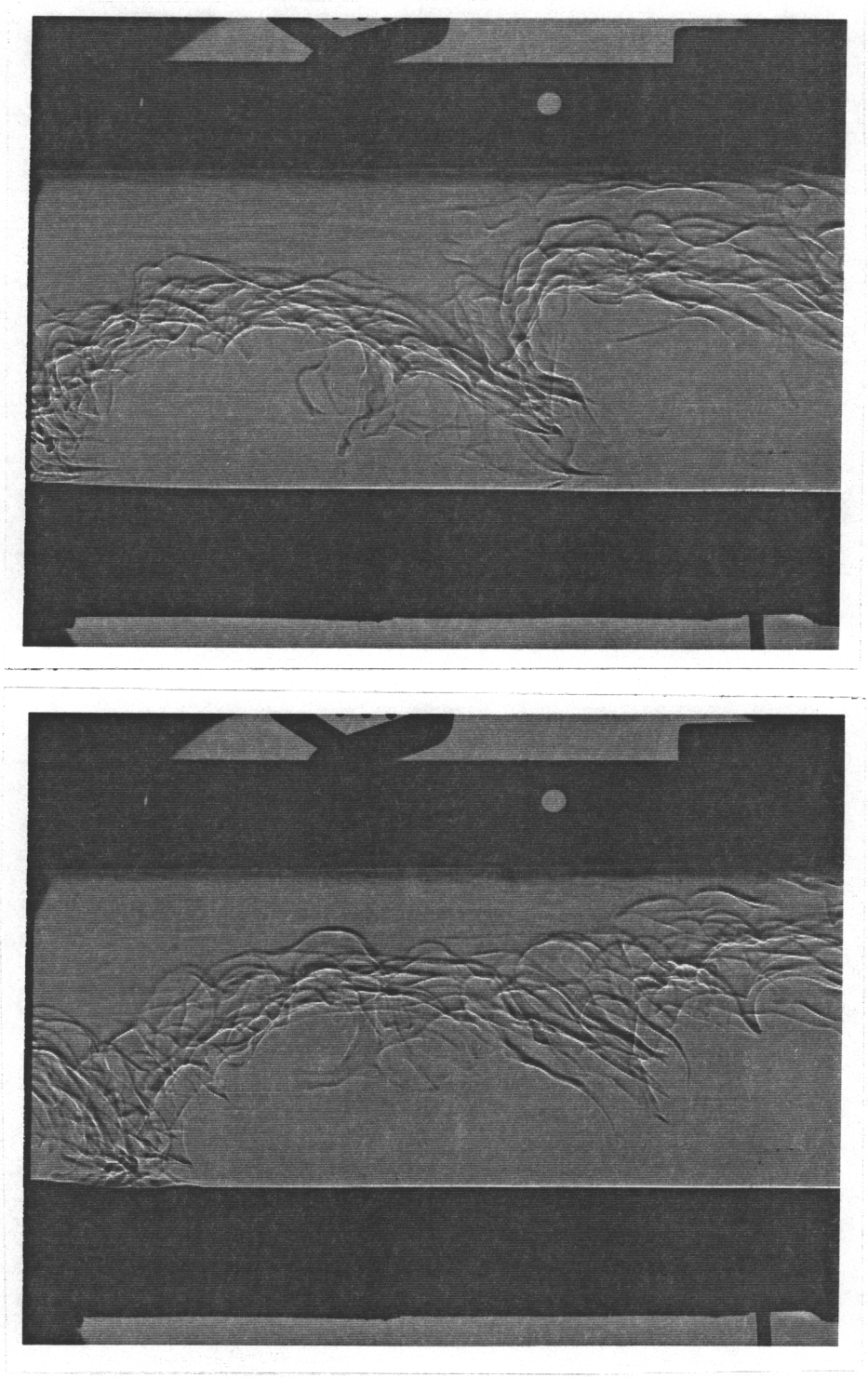

Figure 44. **Shadowgraphs, ϕ = 0.80/0.79, U = 6.7 m/s: (Top) V = 0.0 kVDC, (Bottom) V = 3.6 kVDC**

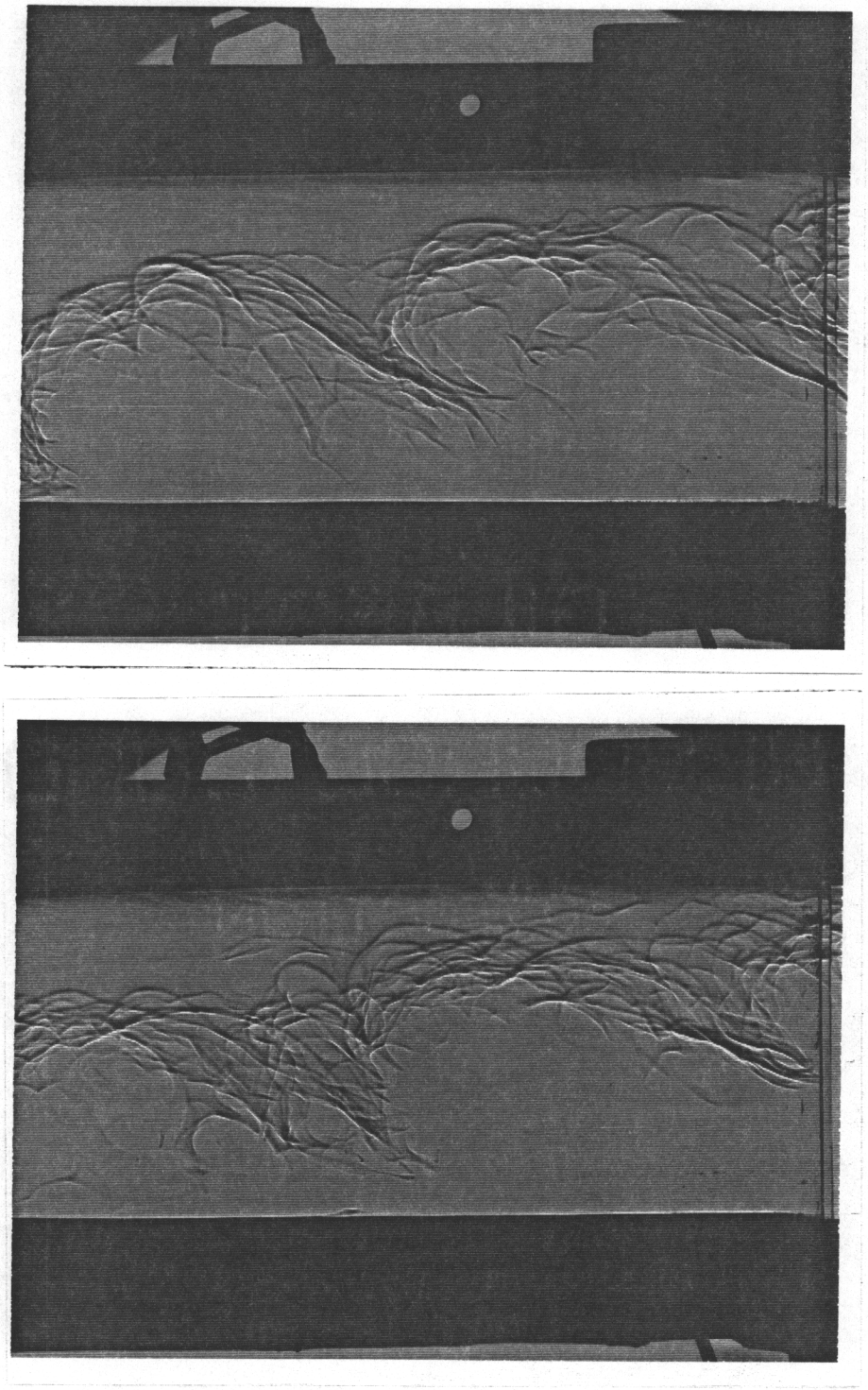

Figure 45. **Shadowgraphs, ϕ = 0.77, U = 5.8 m/s: (Top) V = 0.0 kVDC, (Bottom) V = 4.0 kVDC**

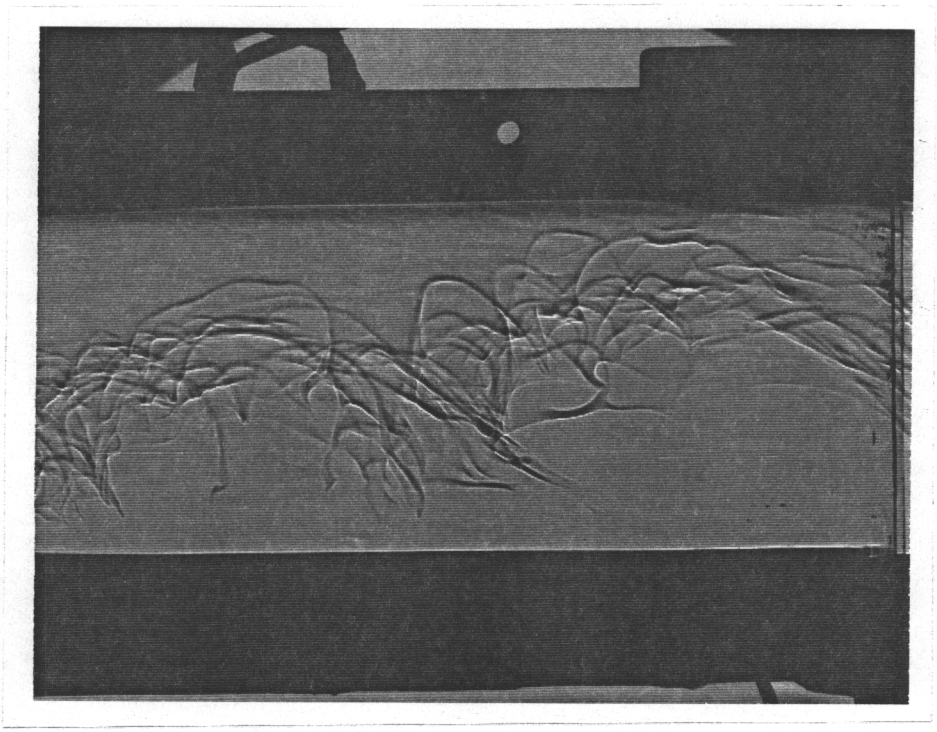

Figure 46. Shadowgraph, ϕ = 0.74, U = 6.0 m/s, V = 4.0 kVDC

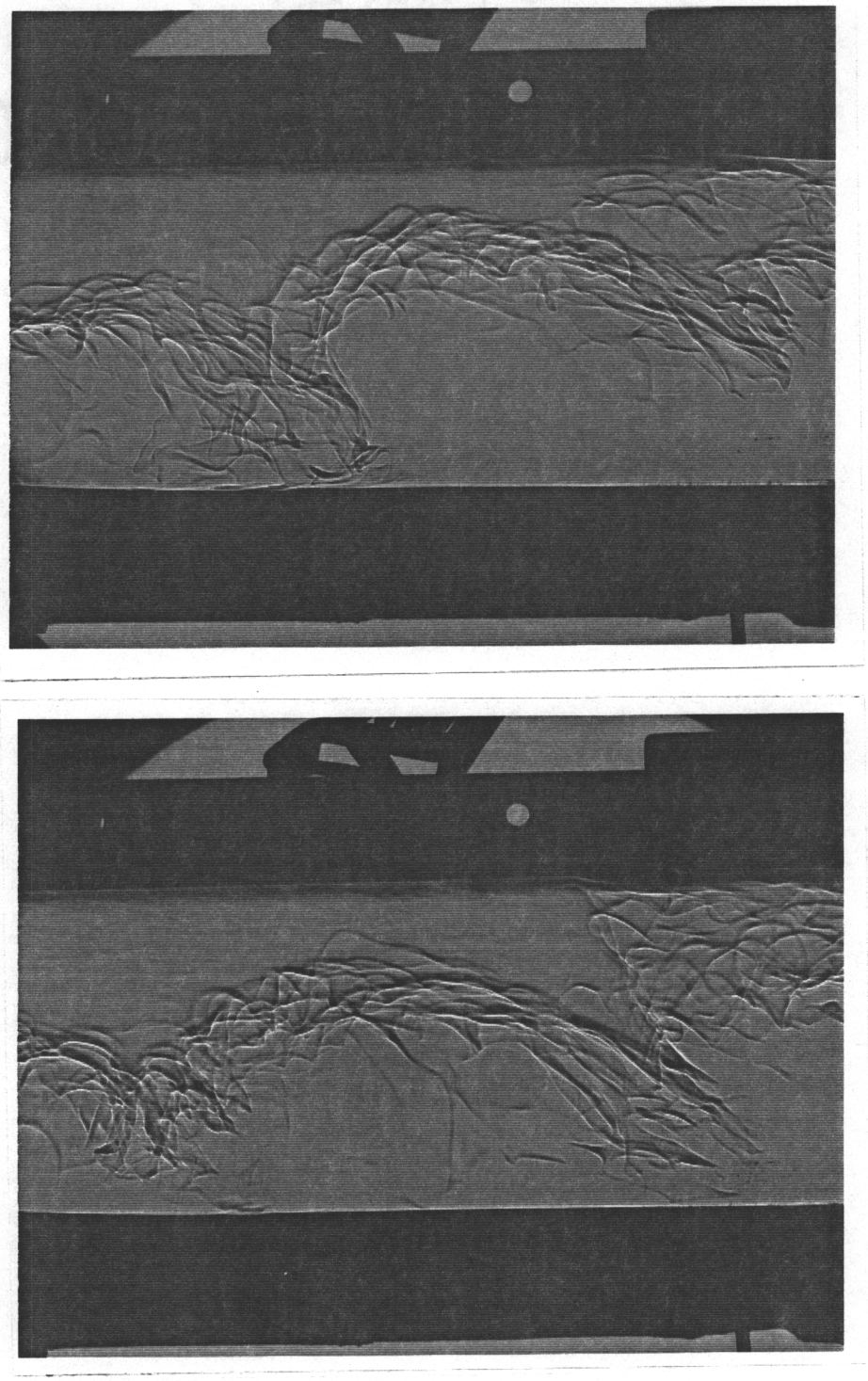

Figure 47. Shadowgraphs, ϕ = 0.77, U = 6.8 m/s: (Top) V = 0.0 kVDC, (Bottom) V = 3.4 kVDC

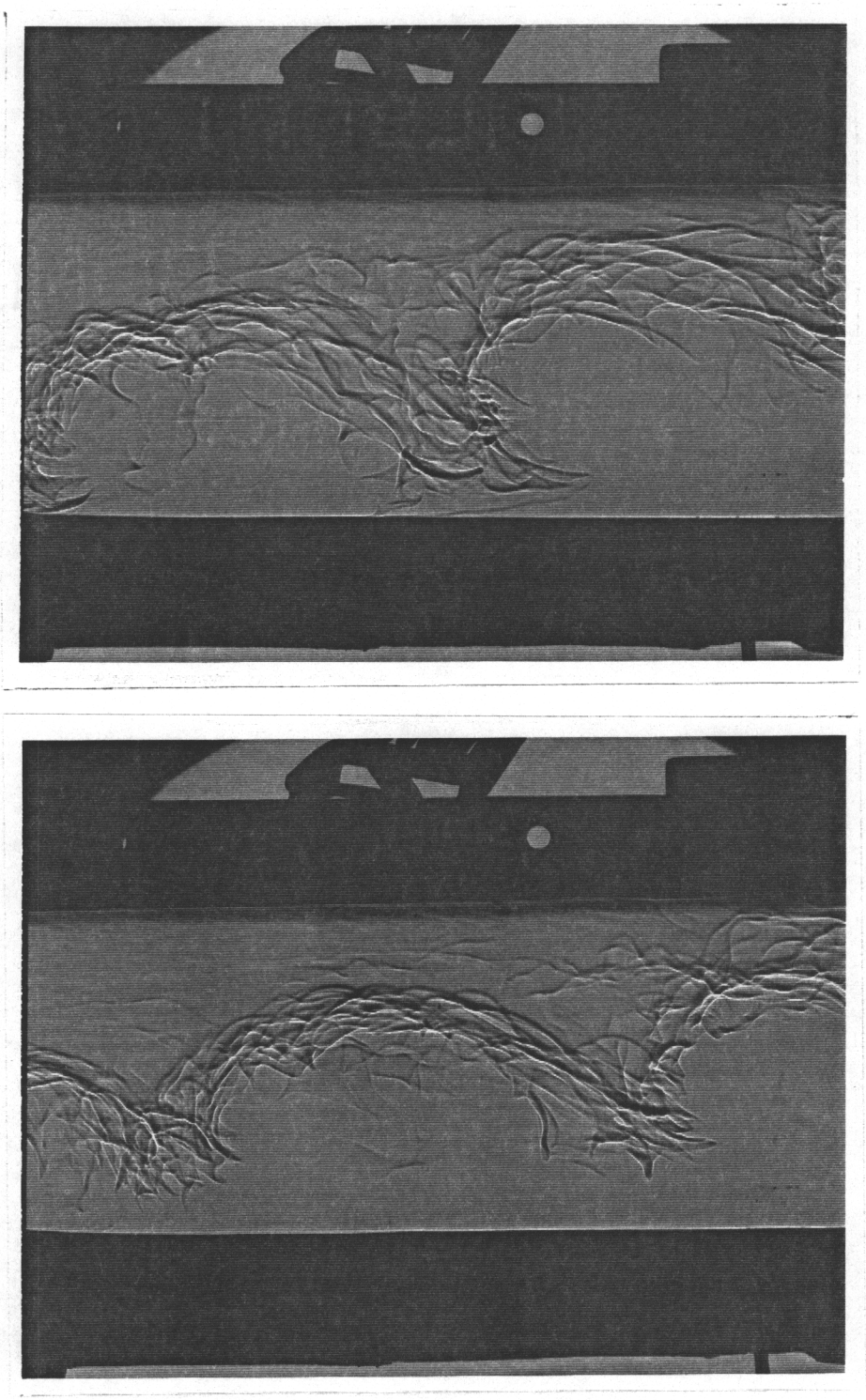

Figure 48. Shadowgraphs, ϕ = 0.77/0.76, U = 6.8/6.9 m/s: (Top) V = 0.0 kVDC, (Bottom) V = 3.2 kVDC

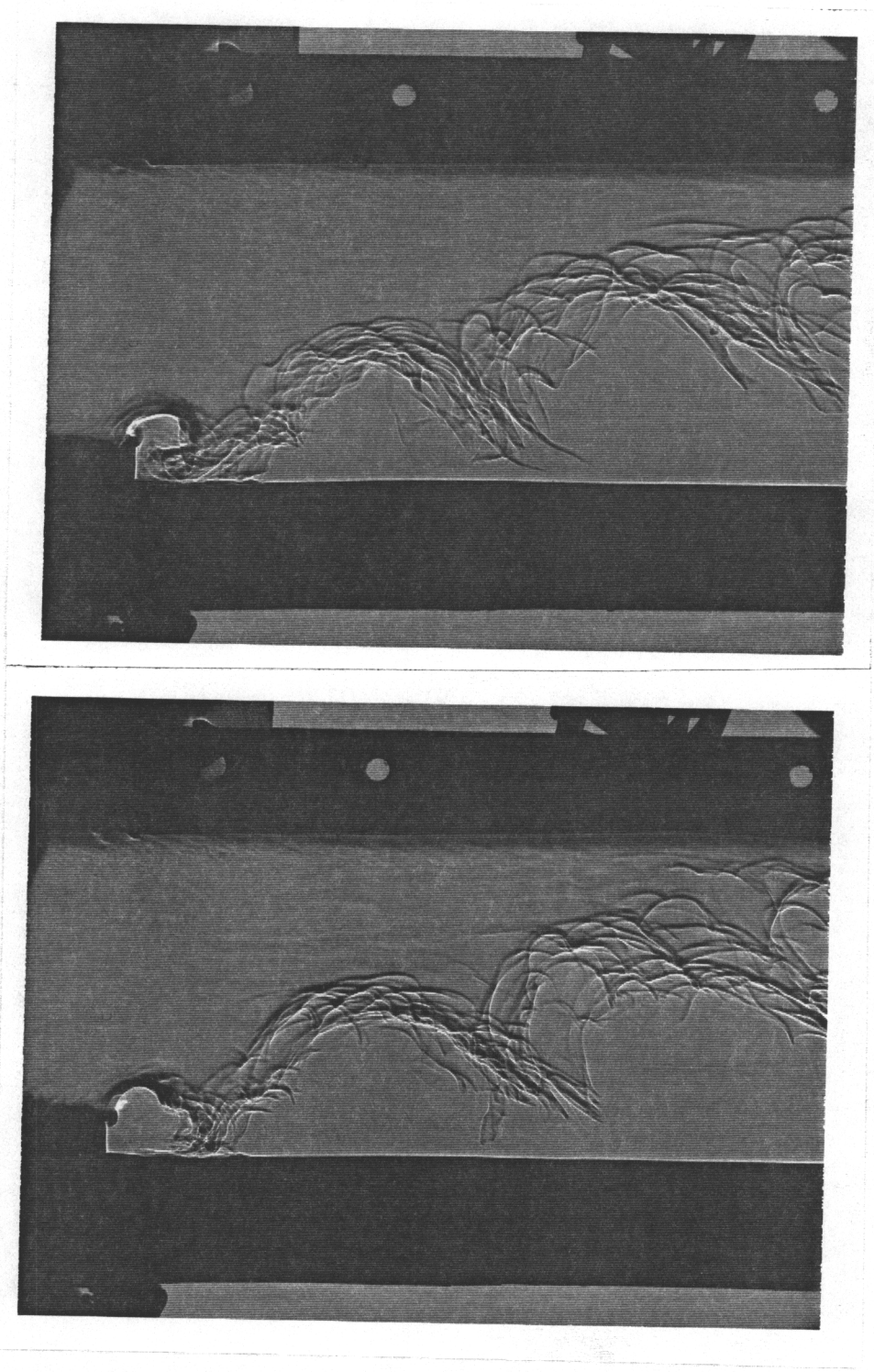

Figure 49. **Upstream Shadowgraphs: (Top) ϕ = 0.83, U = 6.1 m/s, (Bottom) ϕ = 0.96, U = 6.1 m/s**

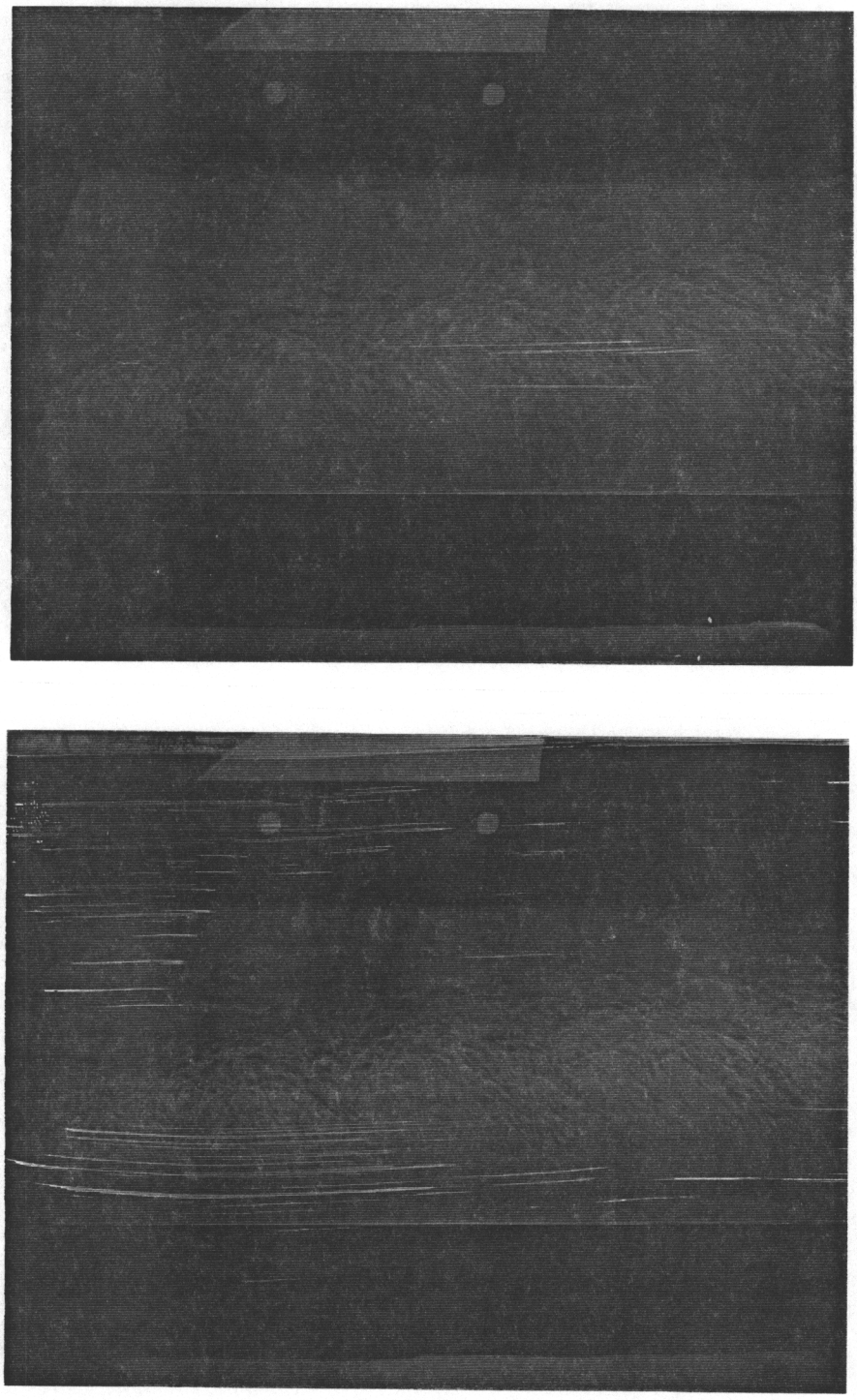

Figure 50. **Multi-exposure Shadowgraphs, ϕ = 0.61/0.62, U = 8.1 m/s: (Top) V = 0.0 kVDC, (Bottom) V = 5.2 kVDC**

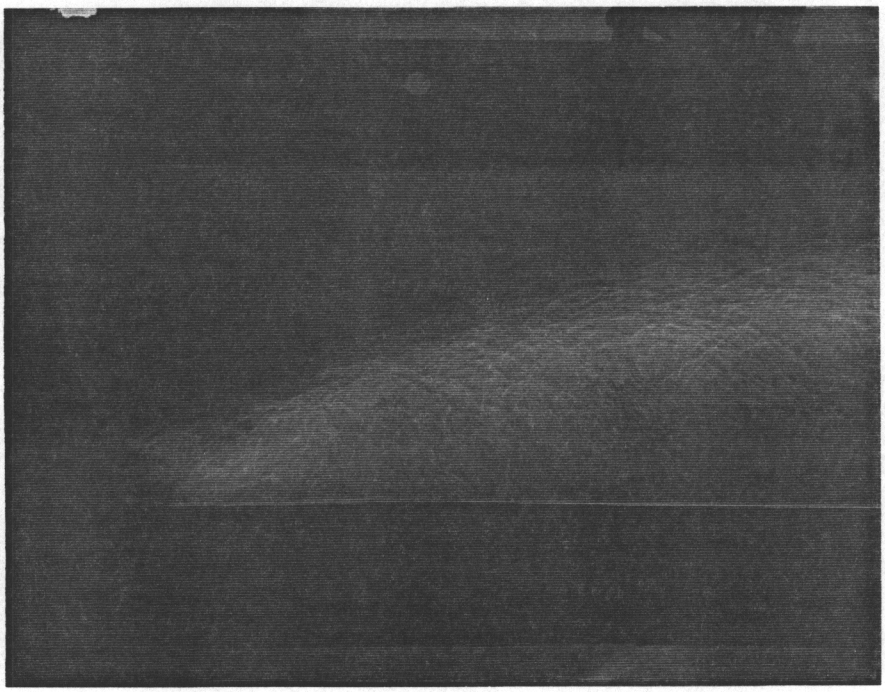

Figure 51. Upstream Multi-exposure Shadowgraph, ϕ = 0.74, U = 5.8 m/s

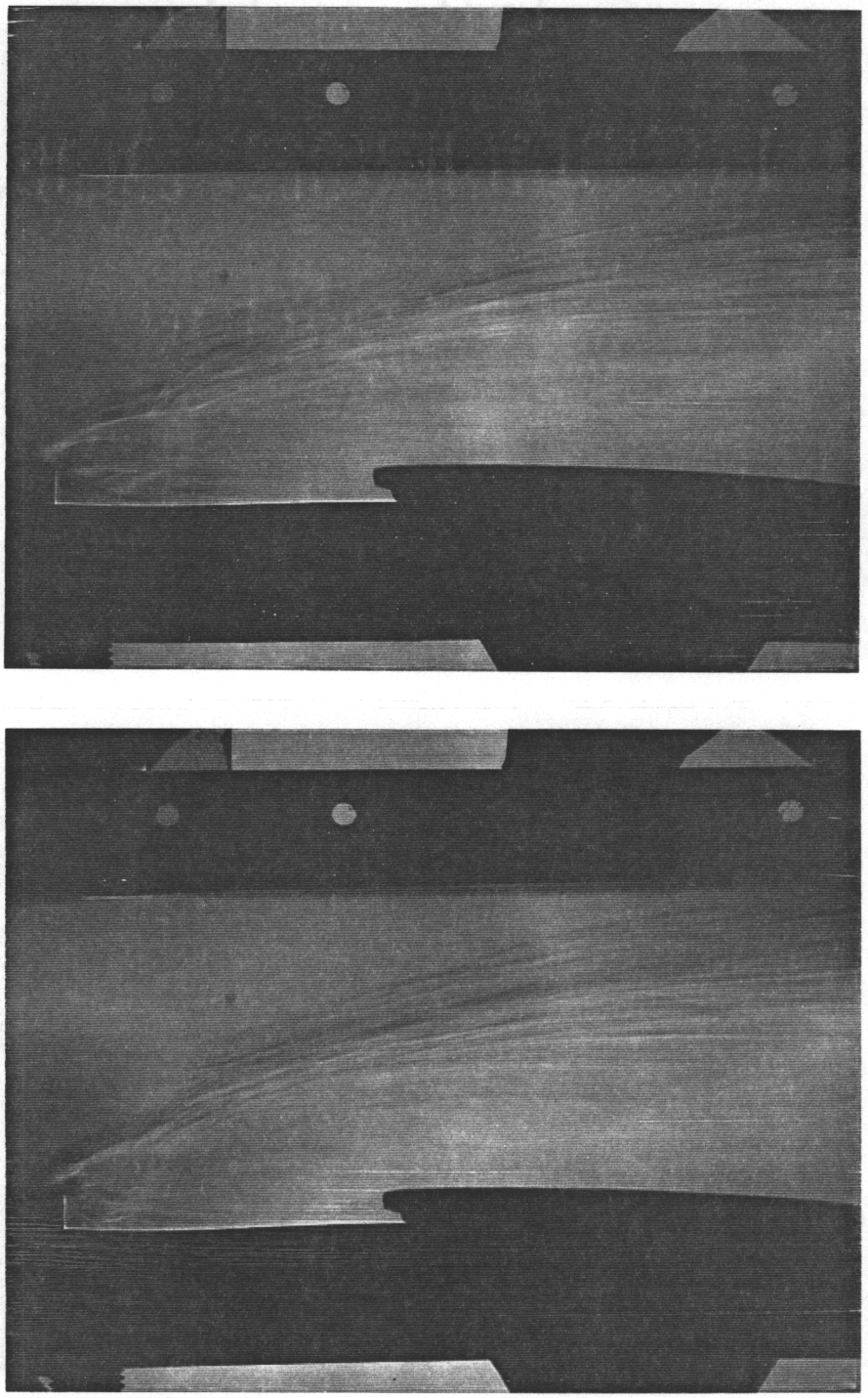

Figure 52. Long Duration Shadowgraphs (1/400 second): (Top) ϕ = 0.87, U = 4.9 m/s, (Bottom) ϕ = 0.86, U = 5.0 m/s

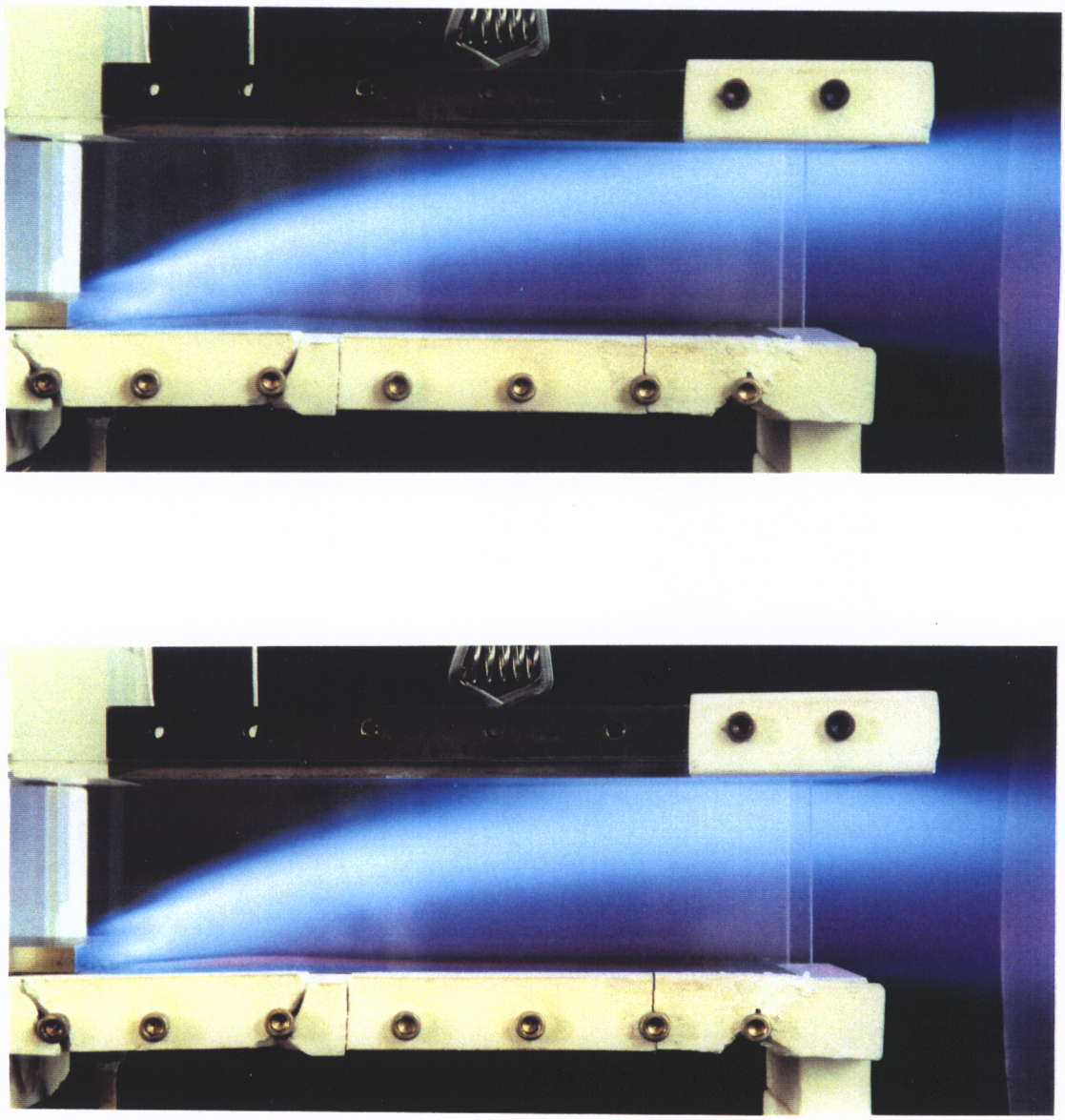

Figure 53. **Photographs, ϕ = 0.84, U = 4.7 m/s: (Top) V = 0.0 kVDC, (Bottom) V = 2.6 kVDC**

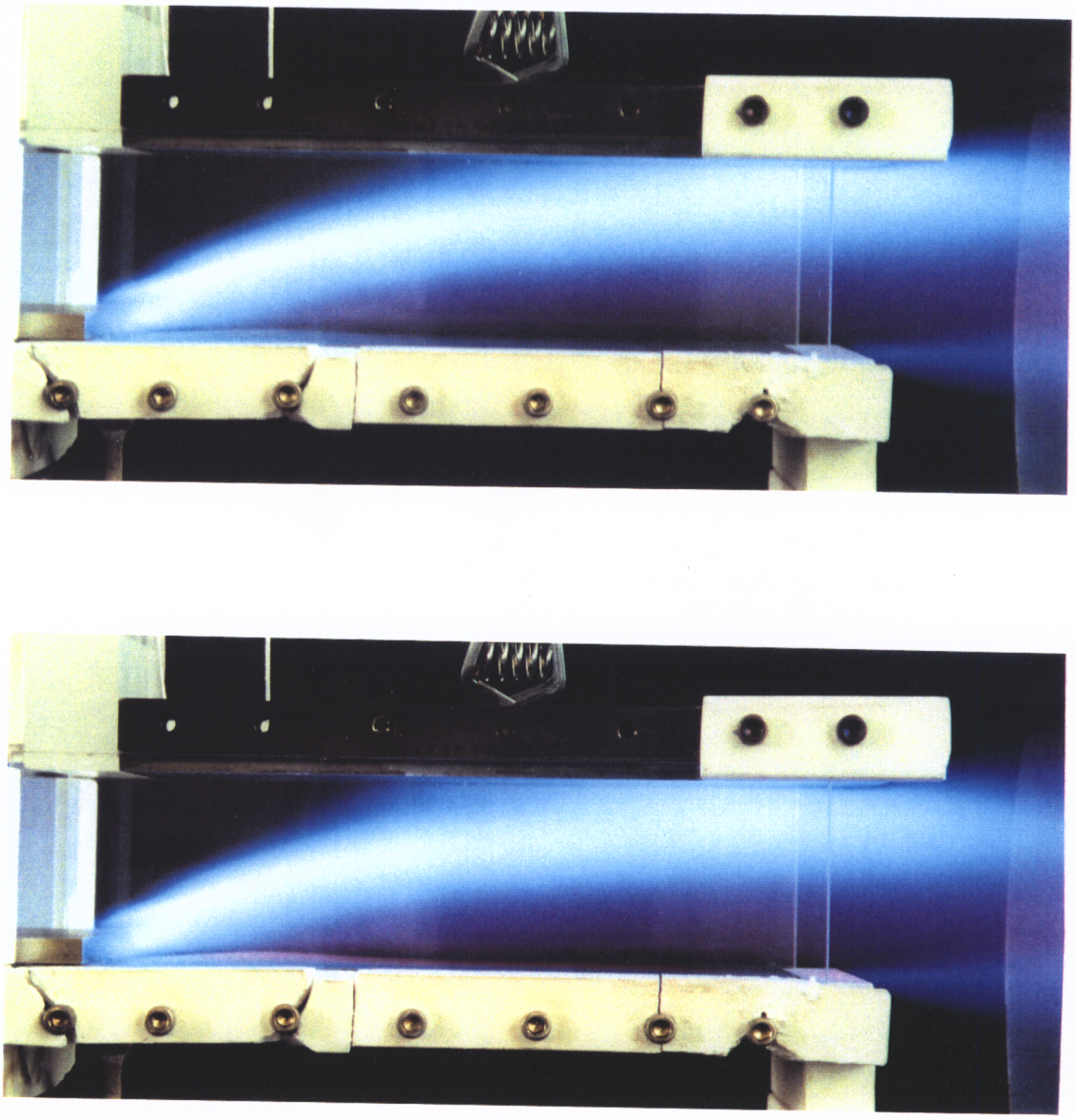

Figure 54. Photographs, ϕ = 0.92/0.91, U = 4.9 m/s: (Top) V = 0.0 kVDC, (Bottom) V = 2.3 kVDC

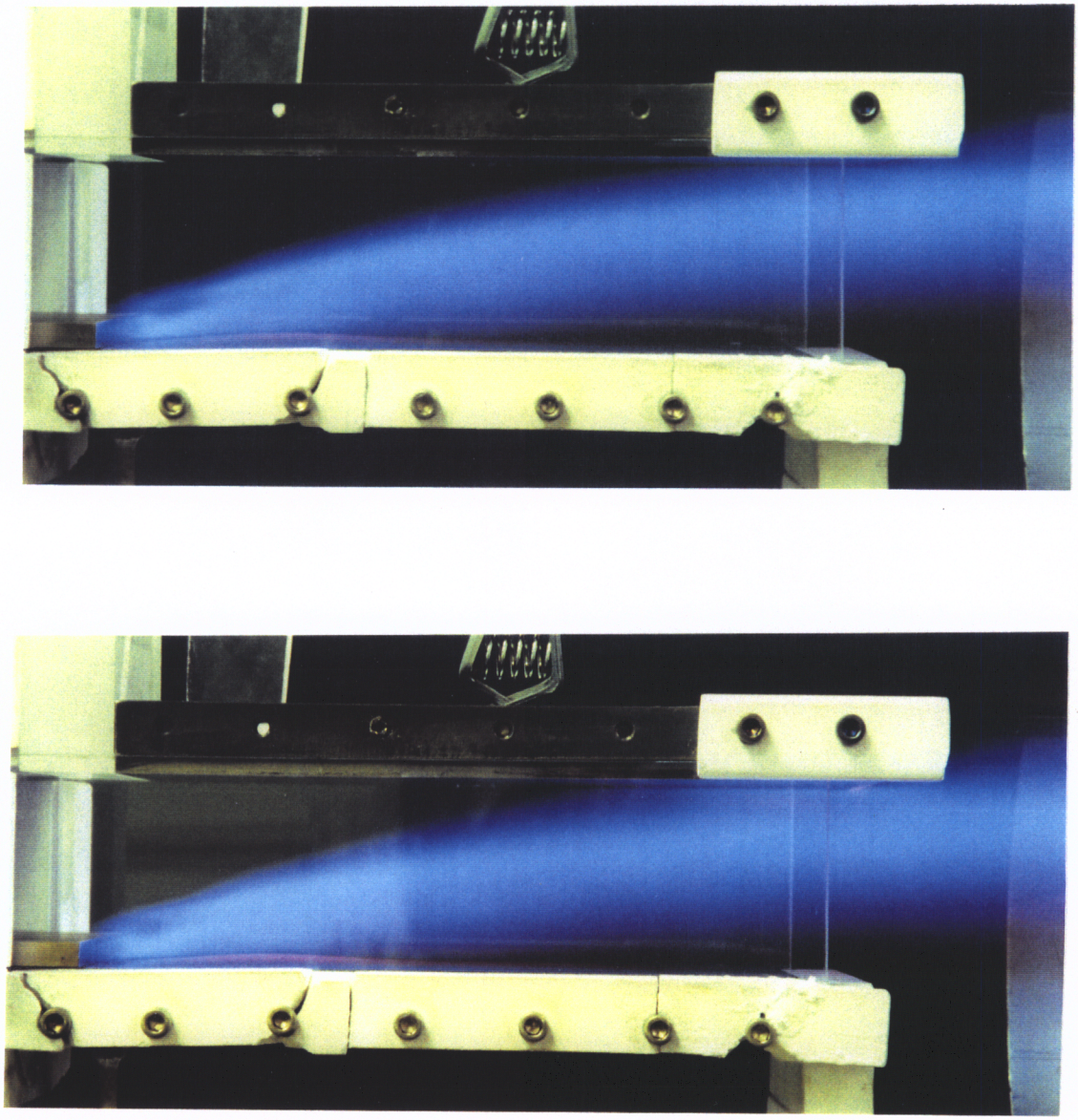

Figure 55. **Photographs, ϕ = 0.74/0.75, U = 5.9 m/s: (Top) V = 0.0 kVDC, (Bottom) V = 3.6 kVDC**

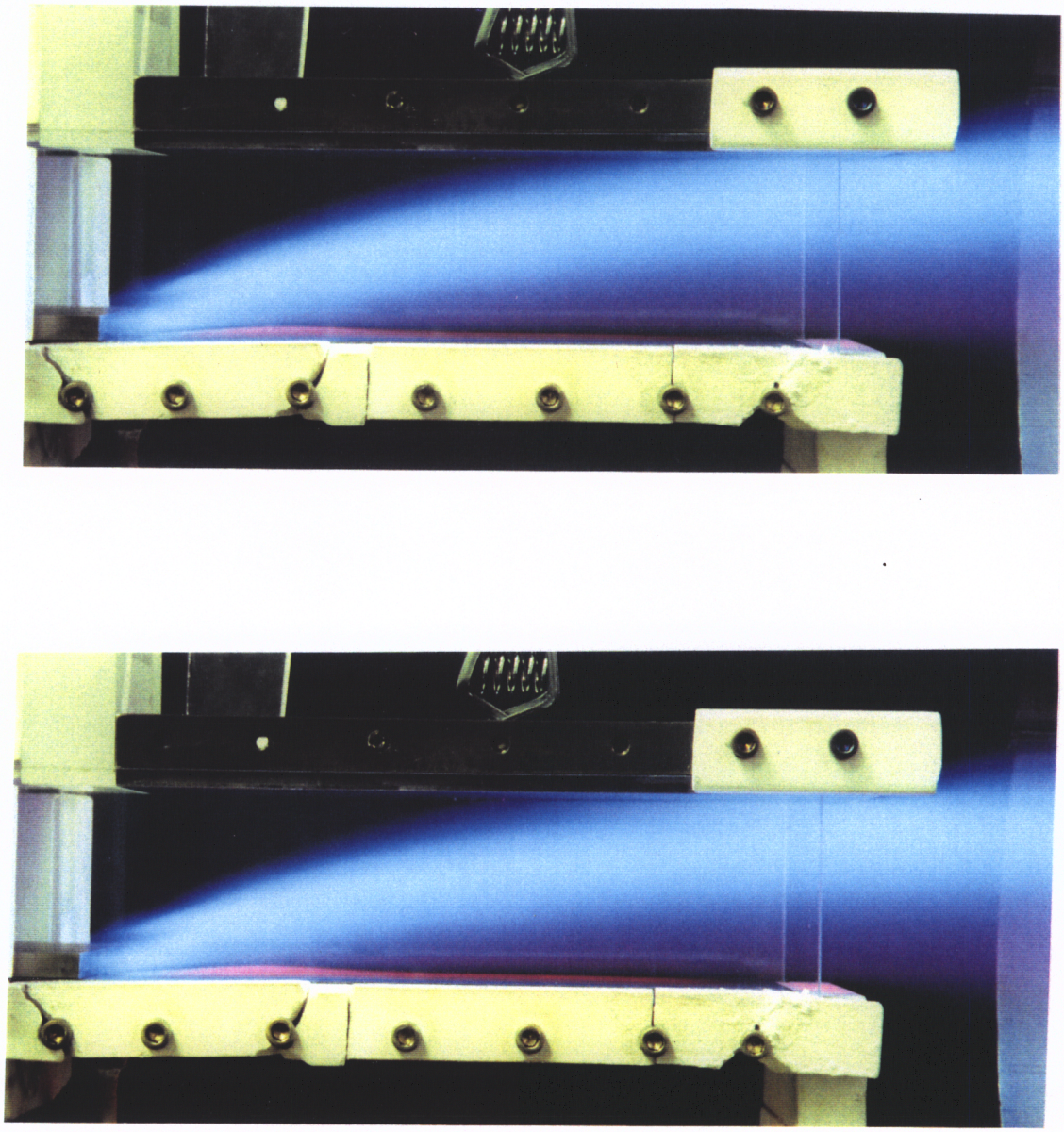

Figure 56. **Photographs, ϕ = 0.86, U = 6.1 m/s: (Top) V = 0.0 kVDC, (Bottom) V = 2.4 kVDC**

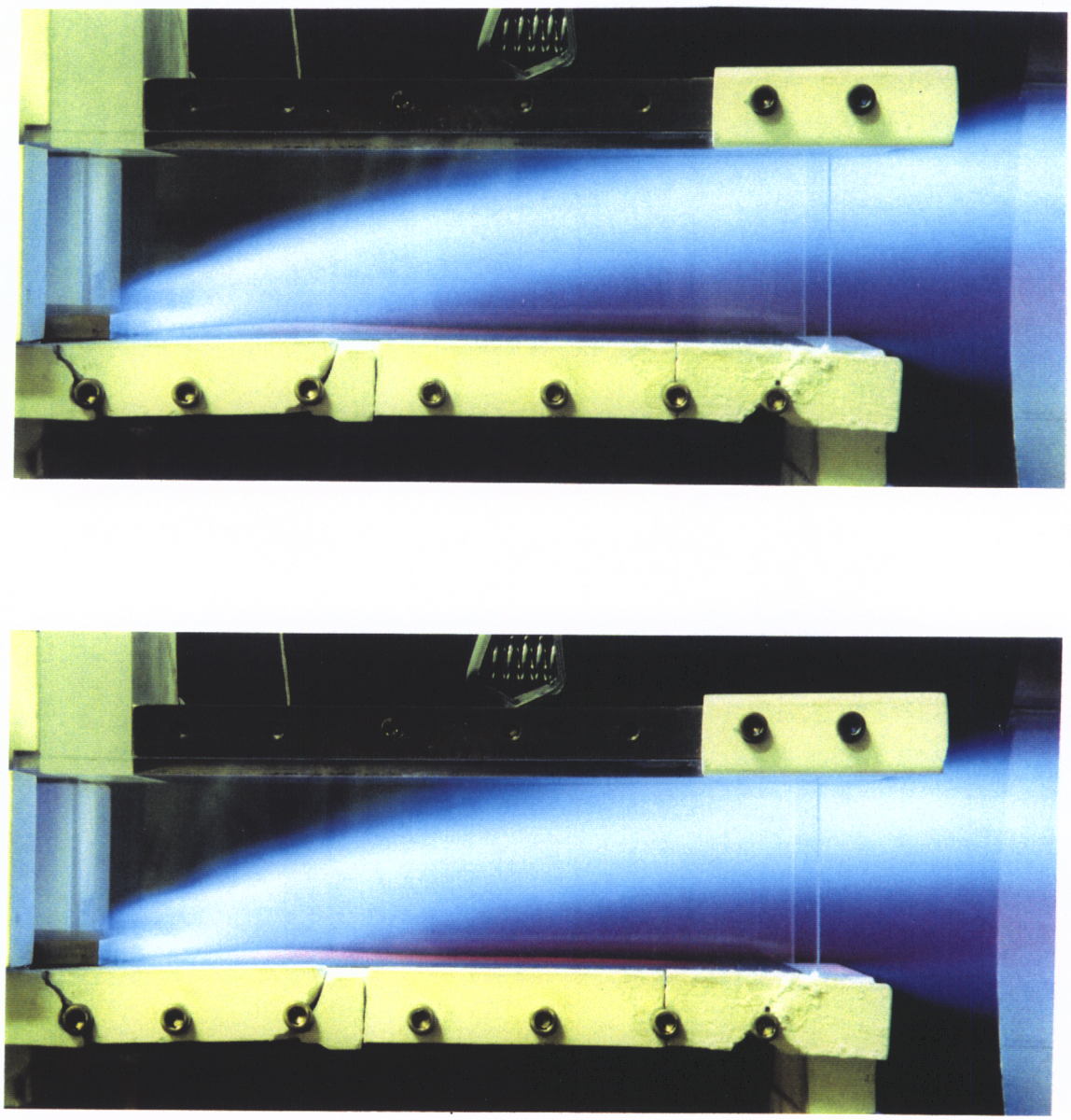

Figure 57. Photographs, ϕ = 1.03/1.01, U = 5.9/6.1 m/s: (Top) V = 0.0 kVDC, (Bottom) V = 2.1 kVDC

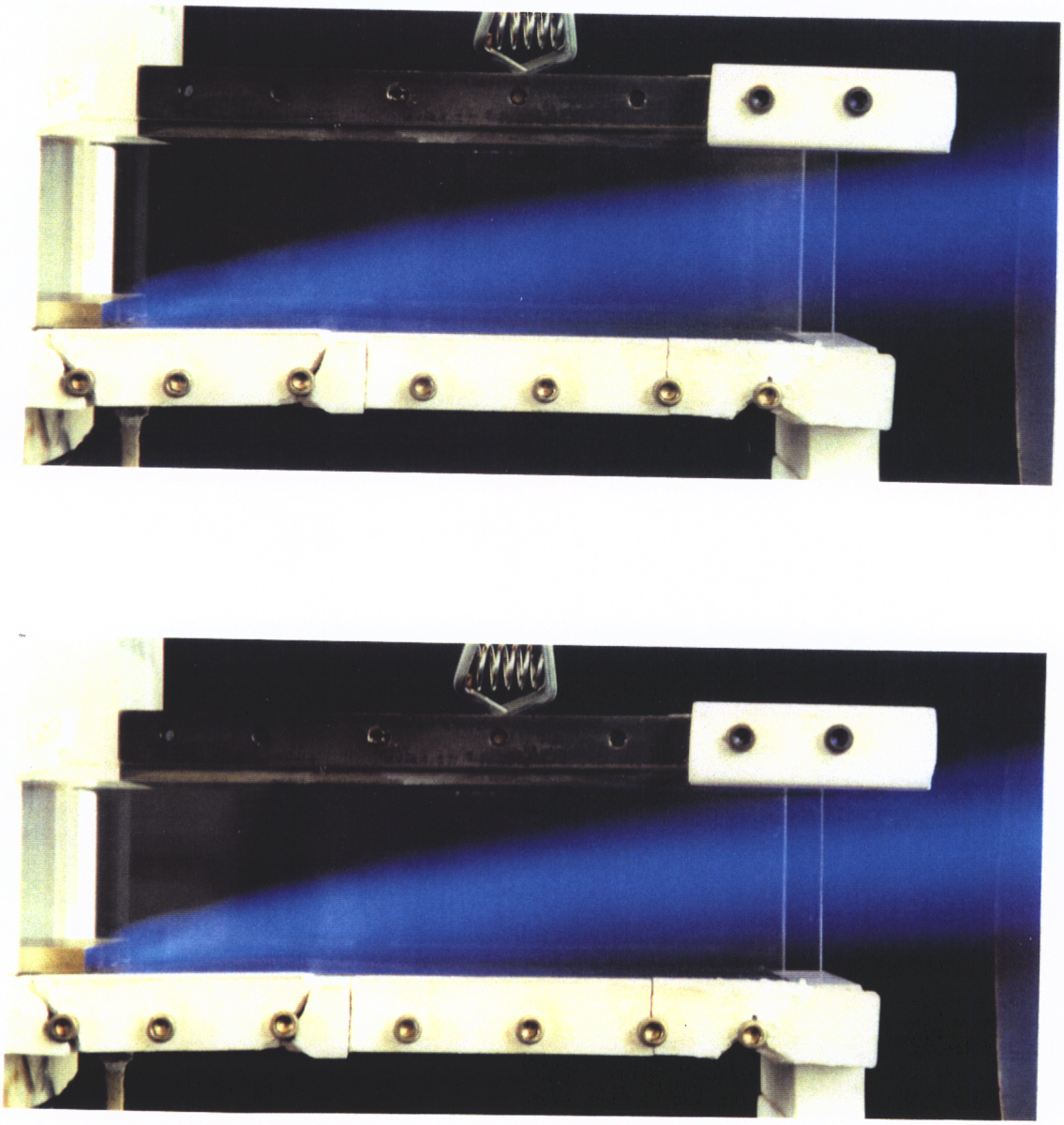

Figure 58. **Photographs, ϕ = 0.65, U = 6.8 m/s: (Top) V = 0.0 kVDC, (Bottom) V = 4.6 kVDC**

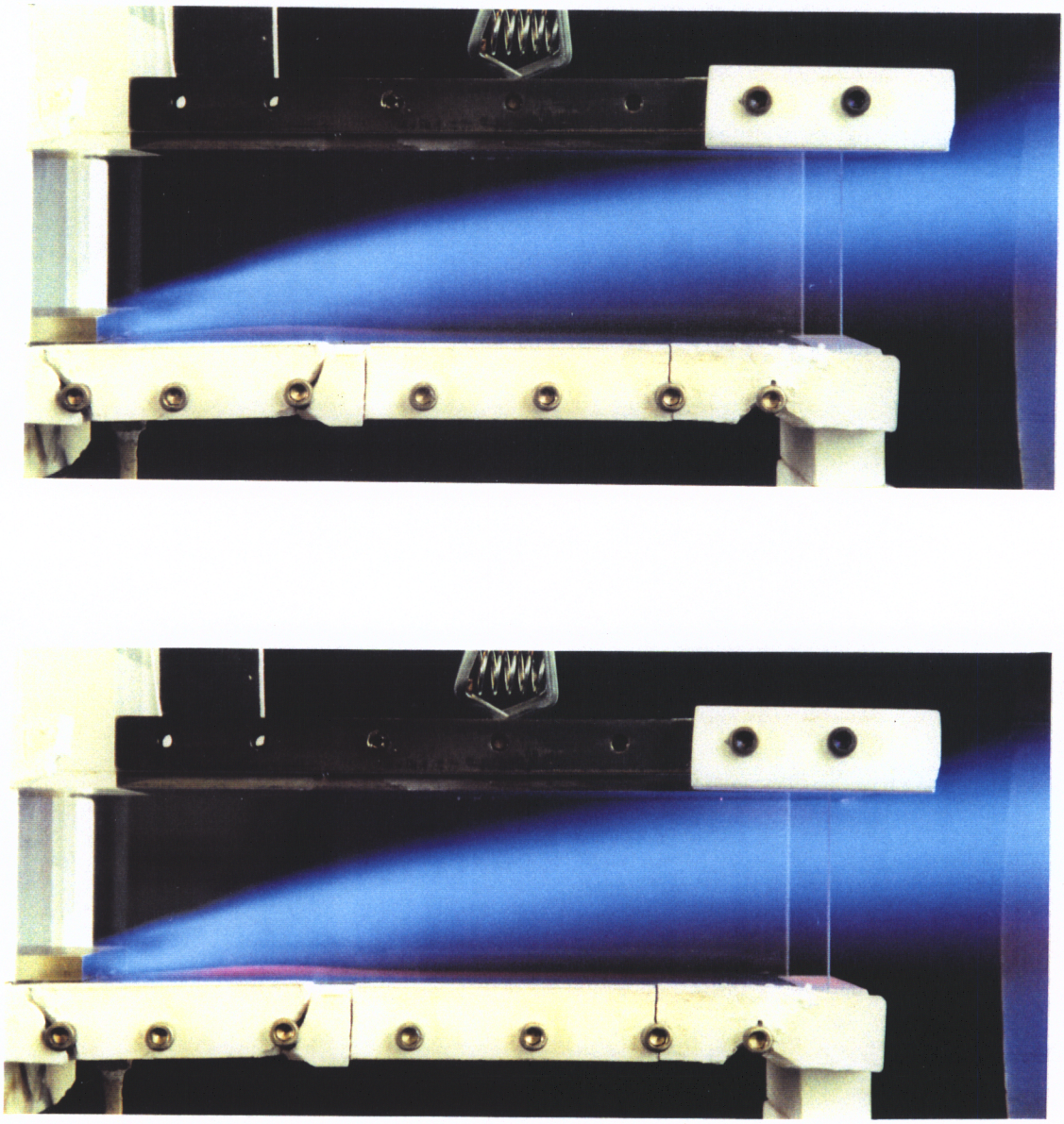

Figure 59. Photographs, ϕ = 0.76/0.77, U = 6.8 m/s: (Top) V = 0.0 kVDC, (Bottom) V = 2.8 kVDC

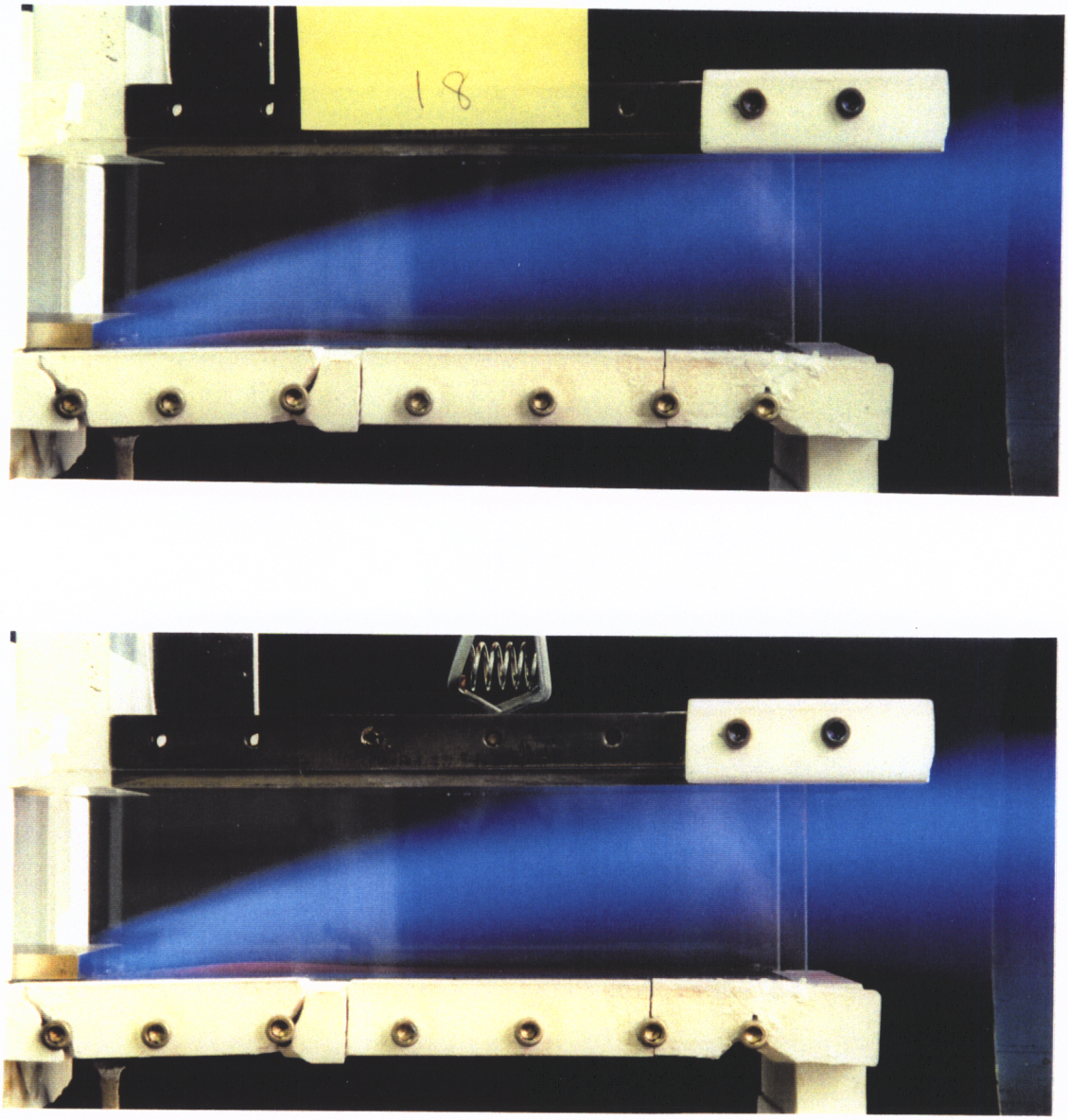

Figure 60. **Photographs, ϕ = 0.88, U = 7.1 m/s: (Top) V = 0.0 kVDC, (Bottom) V = 2.4 kVDC**

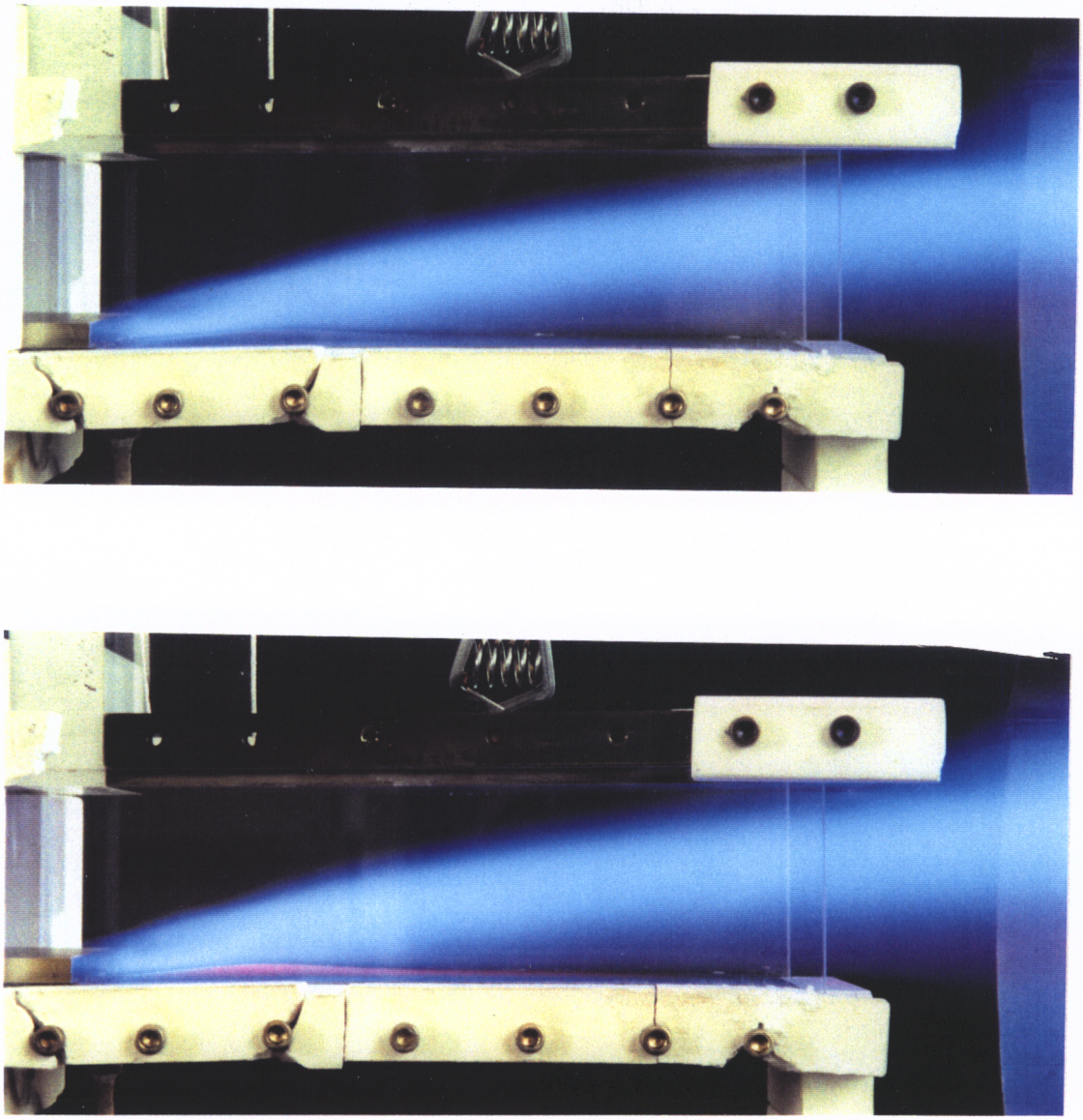

Figure 61. Photographs, ϕ = 0.82, U = 9.9 m/s: (Top) V = 0.0 kVDC, (Bottom) V = 3.2 kVDC

Vita

The author was born on News Year's Day in 1969. He lived and grew up in Danville, Virginia until leaving, September, 1987, to attend college at Virginia Polytechnic Institute and State University. There he pursued a Bachelor's degree in Mechanical Engineering. Four hard years later, he decided to be a real masochist and pursue a Master's Degree in the same field at the same school. Two more difficult years later, he emerged.

He plans to begin work immediately for AMP Inc. in Harrisburg, Pennsylvania as a machine design engineer. He will, after nine months of rotational training, relocate to Greensboro, North Carolina to begin his permanent assignment.

